Investigations on the stability of poly(phenylene vinylene)-based organic light-emitting diodes

Zur Erlangung des akademischen Grades Doktor-Ingenieur (Dr.-Ing.)
genehmigte Dissertation von diplomi-insinööri Oili Pekkola aus Helsinki
Juli 2017 — Darmstadt — D 17

TECHNISCHE
UNIVERSITÄT
DARMSTADT

Fachbereich Material- und Geowissenschaften
Elektronische Materialeigenschaften

Investigations on the stability of poly(phenylene vinylene)-based organic light-emitting diodes

Genehmigte Dissertation von diplomi-insinööri Oili Pekkola aus Helsinki

1. Gutachten: Prof. Dr.-Ing. Heinz von Seggern
2. Gutachten: Prof. Dr. Matthias Rehahn

Tag der Einreichung: 05.12.2016
Tag der Prüfung: 25.04.2017

Darmstadt — D 17

Erklärung zur Dissertation

Hiermit versichere ich, die vorliegende Dissertation ohne Hilfe Dritter nur mit den angegebenen Quellen und Hilfsmitteln angefertigt zu haben. Alle Stellen, die aus Quellen entnommen wurden, sind als solche kenntlich gemacht. Diese Arbeit hat in gleicher oder ähnlicher Form noch keiner Prüfungsbehörde vorgelegen.

Darmstadt, den 25.04.2017

_____

(Oili Pekkola)

Contents

1 Introduction **5**

2 Theoretical background **9**

2.1 Organic semiconductors 9

2.1.1 Physical properties 10

2.1.2 Optical processes 11

2.2 Organic light-emitting diodes 14

2.2.1 Device physics 14

2.2.2 Electrical degradation of organic light-emitting diodes 24

3 Experimental **27**

3.1 Materials 27

3.2 Sample preparation 30

3.3 Methods 32

3.3.1 Standard methods for material and device characterization 32

3.3.2 Electrical stressing 33

3.3.3 Carrier extraction by linearly increasing voltage 33

3.3.4 Photoinduced absorption 36

3.3.5 Secondary ion mass spectrometry 38

3.3.6 Infrared thermography 38

4 Experimental techniques for the investigation of PPV-based devices **39**

4.1 Removing the cathode 39

4.2 Electrical stressing in accelerated conditions 41

5 Dark-CELIV investigations on OC_3C_8-PPV **45**

5.1 Previous investigations with dark-CELIV 45

5.2 Origin of equilibrium charge in OC_3C_8-PPV 45

5.3 Oxygen doping of OC_3C_8-PPV 51

5.3.1 Gradual increase of extraction current in present devices 51

5.3.2 Dynamics of charges in oxygen-doped OC_3C_8-PPV 54

5.4 Summary 56

6 Influence of triplet excitons on device lifetime **59**

6.1 Background 59

6.2 Singlet-to-triplet conversion in layers 61
6.3 Increased triplet exciton concentration in OLED devices 67
6.3.1 Bipolar devices 67
6.3.2 Unipolar devices 71
6.3.3 Consequences of a higher concentration of triplet excitons 78
6.4 Summary 90

7 Summary and outlook **91**

List of Figures **95**

Bibliography **97**

Curriculum Vitae **110**

1 Introduction

In late 1980s, Tang and Van Slyke presented an efficient two-layer organic light-emitting diode (OLED) [1]. This device was based on small molecule organic semiconductors and started the development of organic thin-film electroluminescence [2]. A few years later, in 1990, Burroughes and co-workers introduced the first light-emitting diodes that were based on a conjugated polymer, a poly(p-phenylene vinylene) (PPV) [3]. This first polymer-based OLED was realized with precursor-based PPV, but soon afterwards different groups were able to use solution-processed polymers [4]. This enabled an easy processing of the active materials by wet chemical deposition.

Since these early findings, the development of OLEDs has been fast. OLEDs reached the market in 1997, as Pioneer Corporation released the first commercial OLED product, a passive matrix display for car audio devices [5]. Nowadays the probably best-known OLED application, an active matrix OLED (AMOLED) mobile phone display, was first released by Samsung Mobile Display in 2007 [6]. Nowadays Samsung uses OLEDs in all their high-end smartphones and many other companies have AMOLED displays in their flagship models, too. OLED TVs reached the market in 2013, and LG is the leading player in the field. In general, OLED display technology has in recent years become a real alternative for LCD displays. Unlike LCDs, OLEDs emit light themselves and do therefore not need a backlight, which enables the realization of extremely thin and light-weight devices. The contrast of OLED displays is generally superior to that of LCDs, and their emission is independent of the viewing angle. In addition to displays, lighting is another area for OLED technology. OSRAM Opto Semiconductors was the first company to announce a commercial OLED white lighting panel in 2010 [7]. Due to their large-area, diffuse emission and the possibility for the realization of very thin, planar and flexible light sources, OLEDs offer plenty of possibilities for new kinds of illumination solutions. OSRAM OLED is currently working intensively with automobile industry, focusing on rear lights as well as interior lighting.

Of course, OLEDs do not have only advantages. Up to date, they are more expensive than LCDs. Additionally, blue emitter materials suffer from lifetime issues: their lifetime is significantly lower than that of green and red emitters [8], which leads to changes in color balance. Due to the emissive nature of OLED displays, they are often difficult to use in direct sunlight [7].

The vast majority of the OLED products currently in market are based on small molecules. Small molecules are typically processed by evaporation, which enables the use of multilayered structures. Polymers are deposited by wet chemical methods like inkjet printing or spin coating, and the realization of several-layer structures is in general not possible due to the damaging of the underlying layers with the solvents. Additionally, in comparison to their small molecule-based counterparts, polymer-based OLEDs suffer from issues related to their lifetime and efficiency [7], which limits

their application in commercial products. Despite the dominance of small molecules in the OLED market, there are ongoing efforts on the development of polymer-based OLED devices for commercial use, and they are a lucrative alternative especially for low-cost, printed devices owned by their easy wet chemical processing. Although the intensive research during the last 30 years has already provided the field with extensive knowledge in topics related to the materials as well as device physics, and OLEDs have developed from small-scale laboratory prototypes to a mature, commercially available technology, especially polymer-based diodes are still in need of research in order to increase their lifetime to the level of small molecules. The aim of this thesis is to contribute to this research, increasing the knowledge of light-emitting diodes based on conjugated polymers.

This work focuses on one of the most important conjugated polymers, poly(p-phenylene vinylene) and aims to gain new insights into the fatigue of PPV-based devices. The thesis begins with the introduction of the relevant theoretical background in the material class of organic semiconductors as well as of organic light-emitting diodes and their functional principles in Chapter 2. After this, special attention is paid to the electrical degradation of OLEDs in form of a short literature review on the most important degradation mechanisms.

Chapter 3 focuses on the experimental side of the work. It begins with the introduction of the materials that were used in this thesis and continues with the sample preparation procedure. Finally, the utilized methods are introduced.

The results of the thesis are divided into three main topics. First, two methods that were developed for the general investigation of PPV-based diodes are introduced in Chapter 4. Fatigue studies often require access to the active polymer layer after the operation of the device in order to detect possible morphological changes, for example. For this, it is necessary to remove the cathode from the device. Chapter 4 introduces a removal process in which the calcium cathode is etched away with acetic acid. The other topic of this chapter is the aging of OC_3C_8-PPV-based diodes under accelerated conditions. A scaling law for the operation at different current densities is determined, enabling the operation of the diodes at higher current densities that lead to faster degradation.

Chapter 5 concentrates on the stability of OC_3C_8-PPV during storage in inert atmosphere. Many conjugated polymers are very sensitive towards oxygen, which is why careful encapsulation of the devices is necessary. The chapter focuses on the interaction between oxygen and OC_3C_8-PPV and shows that residual oxygen is found to diffuse in the polymer even during storage in the glovebox, leading to unintentional p-doping of the active material. The evolution of doping and the dynamics of the hole diffusion in the form of temporal establishment of steady-state conditions in a doped system are investigated with dark-CELIV. The findings suggest that even an unencapsulated storage in inert atmosphere with a low concentration of residual oxygen can lead to reactions in the sensitive polymers.

Chapter 6 investigates the other main topic of the thesis, the influence of triplet excitons on device lifetime. In fluorescent OLEDs, only singlet excitons participate in emission. This leaves the

triplet excitons - statistically the majority of all formed excitons - to dissipate their energy non-radiatively. The impact of a large density of triplet excitons on the stability of the OLEDs has not been extensively investigated until now. In the present work, the concentration of triplet excitons in the active polymer is increased through the incorporation of a triplet sensitizer material into the polymer. The influence of the increased triplet exciton concentration on the performance and stability of the devices is then investigated; the triplet excitons are found to shorten the lifetime of the diodes significantly. The chapter then continues with the discussion of phenomena that influence the accelerated degradation.

Finally, the results and conclusions of the thesis as well as an outlook for futher research are summarized in Chapter 7.

2 Theoretical background

This chapter provides theoretical background on topics that are essential for the understanding of the results presented in this thesis. First, organic semiconductors are introduced, focusing on the general properties of this material class. The chapter then continues with organic light-emitting diodes, describing the physical processes that take place during operation and the different operation schemes with the help of energy diagrams. Finally, special attention is payed to the electrical fatigue of the OLEDs.

2.1 Organic semiconductors

Organic semiconductors are commonly divided into two material classes, low-molecular weight *small molecules* and *conjugated polymers*. Examples of both types are presented in Fig. 2.1. An important difference between small molecules and conjugated polymers lies in the processability. Small molecules are typically deposited from the gas phase via physical vapour deposition (PVD), which enables the preparation of multilayer structures of desired layer order and thickness. In contrast to this, the thermal stability of conjugated polymers is limited and they are processed out of solution by spin-coating, dip-coating or printing, for example. The advantage of solution-processing is the simple and cheap layer preparation. However, the deposition of multiple layers is challenging as the underlying layers are easily dissolved by the solvent if orthogonal solvents are not available. This limits the use of conjugated polymers to simple device structures. The commercially available OLEDs are therefore typically based on small molecules. In this work, only polymers were used and the focus of this chapter is thus set on those materials.

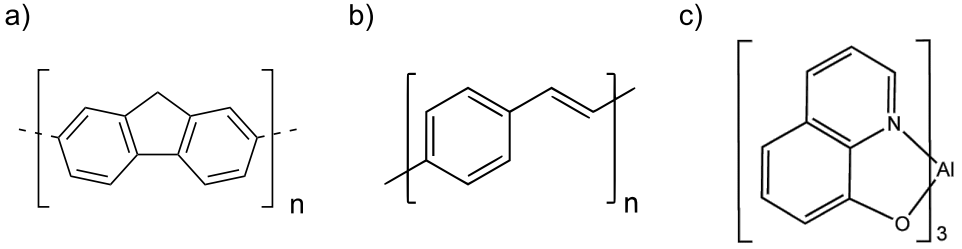

Figure 2.1: *Examples of organic semiconductors: polymers a) polyfluorene, b) poly(p-phenylene vinylene) and the small molecule c) tris-(8-hydroxyquinoline) aluminum.*

2.1.1 Physical properties

Organic semiconductors are carbon-based materials with a conjugated π electron system, where single and double bonds alternate. Fig. 2.2 a) shows a schematic picture of the formation of a double bond. The carbon atoms are sp^2 hybridized and the three sp^2 hybrid orbitals lie planarly with an angle of 120° between them, leaving one unhybridized p_z orbital perpendicular to the plane. The sp^2 orbitals of adjacent carbon atoms form σ bonds that build the backbone of the material. During the bond formation, the hybrid orbitals split into one occupied, bonding σ and one unoccupied, antibonding σ^* molecular orbital. Additionally, the unhybridized $p_z$orbitals form a π bond with the p orbital of a neighboring atom. Similar to the formation of the σ bond, also the $p_z$orbitals split into a bonding π and antibonding π^* molecular orbitals. The σ bond is strong and the energetic difference between the σ and σ^* molecular orbitals is high, whereas the weaker interaction between the $p_z$orbitals leads to a significantly smaller splitting of the π and π^* orbitals.

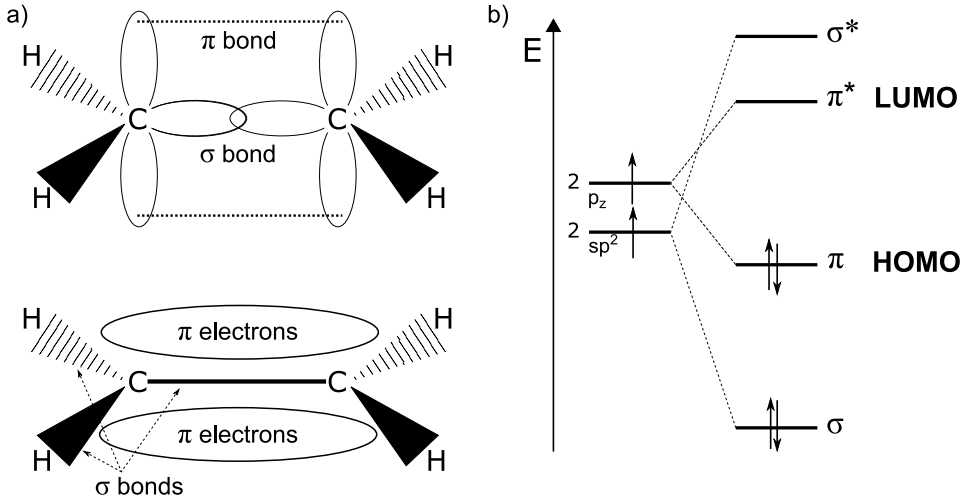

Figure 2.2: *a) Formation of a double bond in ethene, the simplest conjugated π system. The π bonds are formed between p_z orbitals whereas the sp^2 orbitals form the σ bond. b) Energy diagram of the bonding and anti-bonding σ and π molecular orbitals. The antibonding molecular orbitals are denoted with an asterisk. HOMO and LUMO are formed by the π orbitals.*

When several carbon atoms with alternating single and double bonds are joined together in a molecule, their $p_z$orbitals interact, forming new molecular orbitals. They are filled with the $p_z$electrons starting from the lowest energy so that the bonding π molecular orbitals are completely filled and the antibonding π^* molecular orbitals completely empty. The π electrons delocalize over the complete conjugation length and a delocalized π electron system is formed. The bonding π orbital with the highest energy is called *the highest occupied molecular orbital* (HOMO) and the antibonding π^* orbital with the lowest energy *the lowest unoccupied molecular orbital* (LUMO). The energy gap between HOMO and LUMO in conjugated molecules is typically between 1.5 and

3 eV [9], which leads to absorption and emission in the visible range. The energy gap decreases with increasing conjugation length. This offers possibilities to synthetize materials with desired optoelectronic properties by tuning the conjugation length.

In polymers, the conjugation length does not cover the complete chain length. Because the overlap of the π orbitals is dependent on the geometry of the macromolecule, defects and distortions in the chain geometry limit the extend of the conjugation. For example, an effective conjugation length of 5-10 monomer units has been reported for MEH-PPV [10]. In addition to the structure of the polymer, the effective conjugation length is affected by synthesis and processing of the material [11].

The interaction between single molecules is van der Waals type and is therefore much weaker than between covalently bonded inorganic semiconductors. As a consequence, the optical and energetic properties of isolated molecules do not differ greatly from molecules in the solid. The weak bonding between molecules also results in lower melting points and reduced hardness. Due to the weak interaction between molecules, the electronic wavefunction is not as extended as in inorganic semiconductors. In polycrystalline and amorphous systems, the charge carriers are localized and no band transport takes place [12]. These systems are characterized by local differences in the conformation and morphology. Due to coulomb interaction, the presence of an excess charge leads to polarization of its environment. Because of the lack of translational symmetry, this polarization will be random, and charges will see different dipole orientations in their environment. This leads to a statistical variation in the energy levels. The energetic distribution of the localized states (the density of states, DOS) is assumed to be Gaussian with a width of approximately 100 meV and was first introduced by Bässler in the Gaussian disorder model [13]:

$$DOS(E) = \frac{N}{\sqrt{2\pi\sigma^2}} \cdot \exp\left(-\frac{{E_{HOMO/LUMO}}^2}{2\sigma^2}\right) \tag{2.1}$$

where N is the density of molecules in a solid, σ the width of the Gaussian density of states (the standard deviation) and $E_{HOMO/LUMO}$ the energetical position of the maximum of the HOMO or LUMO density of states. The Gaussian distribution of HOMO and LUMO is illustrated in Fig. 2.3.

2.1.2 Optical processes

Upon an excitation of a molecule, an electron is lifted to an excited state and a hole is left on the ground state. The exciton, the resulting electron-hole pair, is bound by Coulomb interaction. There are three types of excitons: Wannier, Frenkel and charge transfer (CT) excitons. The excitons in organic semiconductors, especially in organic light-emitting diodes, are typically Frenkel-type. They have a radius on the order of few nanometers and are localized on one molecule. The Frenkel excitons are strongly bound and have a binding energy as high as 0.5 to 1 eV [9]. Frenkel excitons

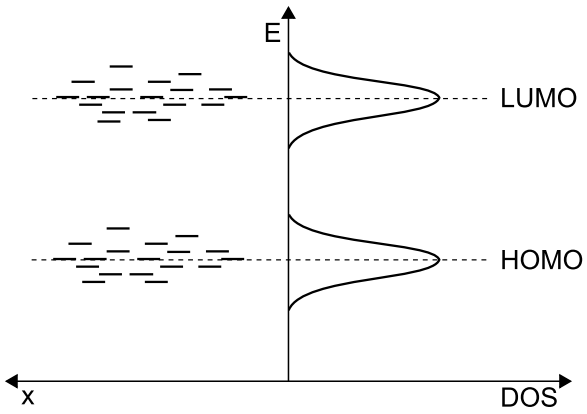

Figure 2.3: *Energetic distribution of electronic states in an organic semiconductor. The distribution of HOMO and LUMO is taken to be Gaussian.*

have well-defined singlet and triplet states. The properties of these states are introduced in the following. Charge transfer excitons, on the other hand, are excitations in which the electron and the hole lie on adjacent molecules. This type of excitons is of importance in organic solar cells, in which the charge separation takes place at a donor-acceptor interface. The third type of excitons, the Wannier exciton, is typically found in inorganic semiconductors.

The basic optical processes in an organic molecule are depicted in Fig. 2.4. The electronic energy levels of the molecule are illustrated with thick horizontal lines. The ground state is the singlet state S_0, whereas S_1 and S_2 represent the first and second excited singlet states. Correspondingly, the first and second excited states of the triplet manifold are denoted with T_1 and T_2. The thin horizontal lines correspond the vibronic sublevels of each energy level. Radiative processes are illustrated with straight vertical arrows and non-radiative with wavy arrows.

Absorption of a photon takes place from the ground state to one of the excited singlet states. There are non-radiative and radiative ways to dissipate the energy that was gained through absorption. Vibrational relaxation and internal conversion (IC) are non-radiative processes. Vibrational relaxation, shown as wavy downward arrows in Fig. 2.4, takes place within vibrational levels of one electronic state. Vibrational relaxation is a very fast process and is thus very likely to take place immediately after absorption. The relaxation is called internal conversion if vibrational levels of two electronic states overlap; in this case the excited electron transfers from the vibrational level of a higher electronic state to a vibrational level of a lower one.

Emission of photons from the first excited singlet state S_1 to the ground state, called fluorescence, is a radiative process. Because of the fast relaxation of excitations to the lowest vibrational S_1 state, fluorescence generally takes place only from this state. Its characteristics do therefore not depend on the excitation wavelength [14]. Transition between singlet and triplet systems involves a spin flip. A nonradiative transition is called intersystem crossing (ISC), whereas a radiative transition from T_1 to the ground state S_0 has the name phosphorescence.

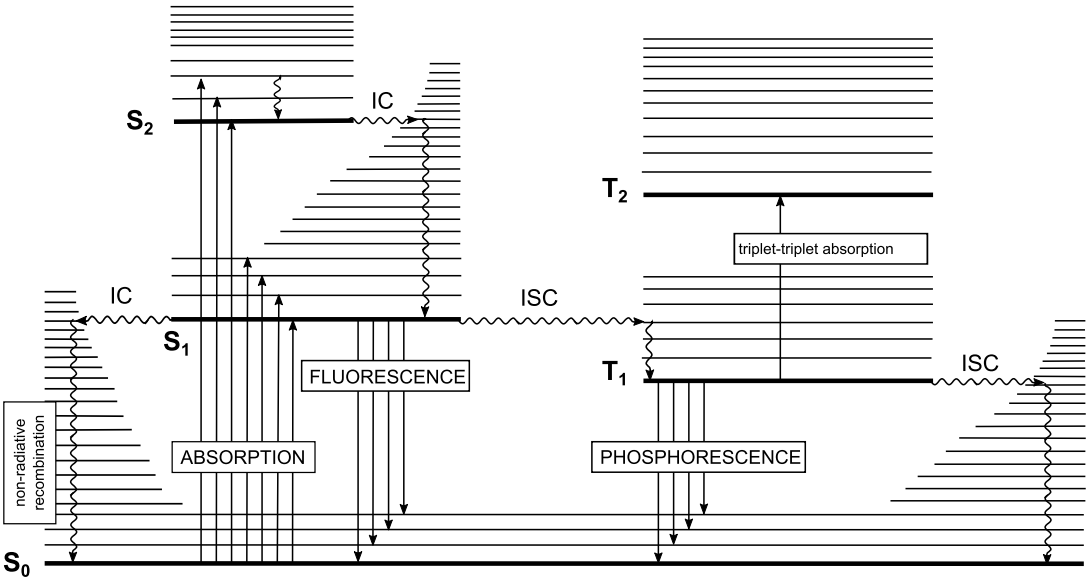

Figure 2.4: *Perrin-Jablonski diagram showing the energetic level scheme of an organic semiconductor, adopted from [9, 12, 14]. IC stands for internal conversion and ISC for intersystem crossing. For details see text.*

The spins of the two electrons that are forming a singlet state are anti-parallel (see Fig. 2.5). The singlet states have a total spin quantum number of $S = 0$. An excited state with parallel spins is called the triplet state. It has a total spin of $S = 1$. As its name denotes, the triplet state is degenerate with three quantum states and a spin multiplicity of 3. The energy of the triplet states is always lower than the corresponding singlet energy.

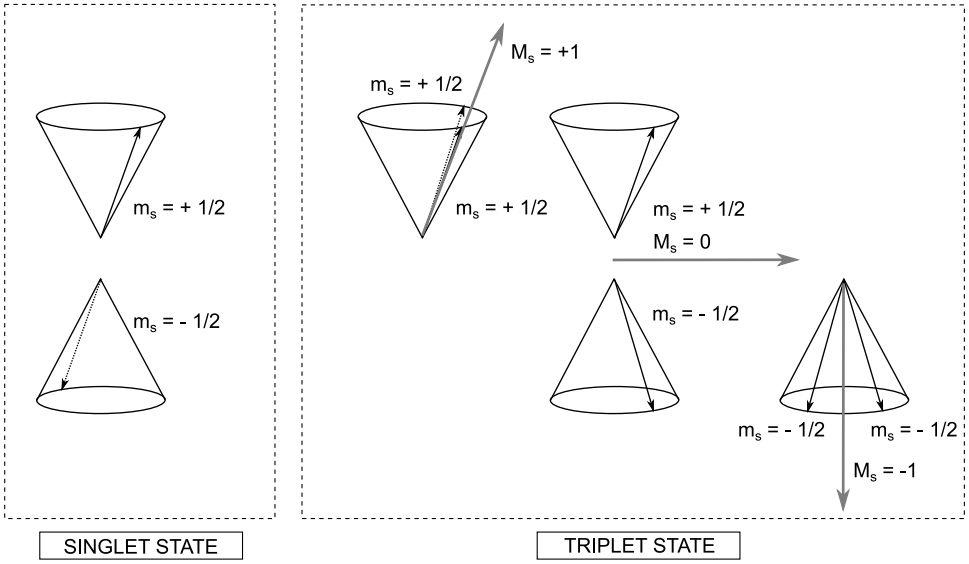

Figure 2.5: *Singlet and triplet states on an organic molecule. The singlet state has a zero total spin, whereas the three-fold degenerate triplet state has a spin of $S = 1$.*

Transitions that involve a change in spin multiplicity are forbidden. However, the quantum mechanical selection rules are weakened by spin-orbit coupling. The coupling is very weak in materials consisting of pure hydrocarbons. In these systems, emission from the triplet state is very weak. However, if heavier atoms like Pt or Ir are involved, the spin-orbit interaction becomes stronger and the spin selection rules that forbid the $S - T$ transition are weakened [12]. Transitions between singlet and triplet states become allowed and the rates for intersystem crossing as well as phosphorescence increase. Molecules with intense emission from the triplet state, called triplet emitters, are often organo-transition metal compounds [15]. They are utilized in phosphorescent OLEDs.

2.2 Organic light-emitting diodes

The following section focuses on the the functional principles of organic light-emitting diodes. The main processes that take place are introduced and explained. The section ends with a short review of the electric fatigue of organic light-emitting diodes.

2.2.1 Device physics

A simple polymer-based organic light-emitting diode consists of a thin (on the order of 100 nm) polymer layer sandwiched between two electrodes. At least one of the electrodes, normally the bottom electrode, is transparent, which allows for light outcoupling. Fig. 2.6 shows a schematic picture of the processes related to the operation of an OLED. The functional principle of OLEDs can be divided into five processes: injection of charge carriers from the contacts into the organic semiconductor (1), their transport in the organic material (2), formation of excitons (3), their diffusion (4), and the (radiative) recombination (5). In the following, the single steps are explained in more detail.

Charge carrier injection

The density of intrinsic charge carriers in organic semiconductors is low. Consider an organic semiconductor with a bandgap of 2.5 eV and an effective density of states $N_0 = 10^{21}\,\mathrm{cm}^{-3}$. The density of charge carriers can be estimated with Boltzmann distribution $n_i = N_0 \exp\left(\frac{-E_G}{2k_B T}\right)$ to be $n_i < 1\,\mathrm{cm}^{-3}$. Such a density of intrisic charge carriers leads to an extremely low conductivity. In order to overcome this limitation, the charge carrier density can be increased by different means. Charge carriers can be created optically, as is done in the photo-CELIV technique (Chapter 3.3.3), by electrochemical doping or injection from the contacts. The latter is the process that enables device operation in organic light-emitting diodes.

During operation, an external voltage is applied and holes are injected from the anode and electrons from the cathode. Fig. 2.7 illustrates the contact formation between a metal and an organic

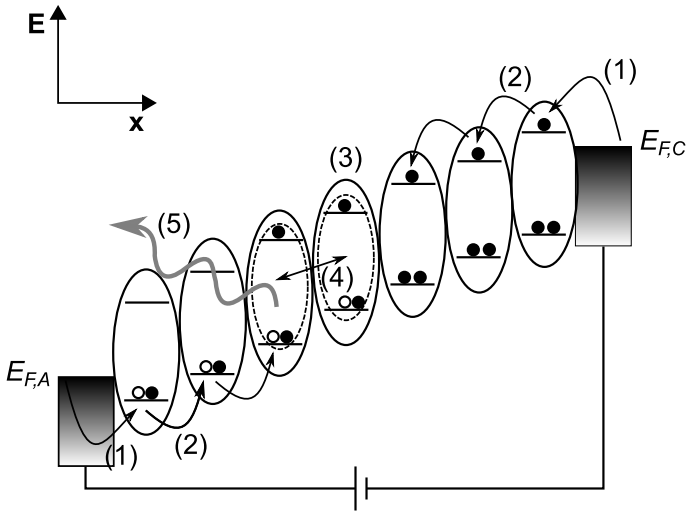

Figure 2.6: *A schematic illustration showing the working principle of an OLED. The individual processes are the injection of charge carriers from the contacts into the organic semiconductor (1), their transport in the organic material (2), formation of excitons (3), their diffusion (4), and the (radiative) recombination (5).*

semiconductor. The energetic states of the metal and the semiconductor are shown in Fig. 2.7a for the case prior to contact. E_{vac} denotes the vacuum level; Φ_M and $E_{F,M}$ are the work function and the Fermi level of the metal, respectively. Correspondingly, the organic semiconductor has the Fermi level $E_{F,SC}$ and the work function Φ_{SC}. E_I is the ionization potential and E_A the electron affinity of the semiconductor. When the metal and the semiconductor are brought into electric contact (Fig. 2.7b), their Fermi levels become equal through diffusion of electrons from the lower work function material into the material with the higher work function. The diffusion over the interface leads to the formation of a charge carrier reservoir that is observed as the bending of the band structures. Due to the high charge carrier density, the reservoir in the metal reaches only few monolayers, whereas its size can exceed 100 nm in the organic semiconductor that has a low intrinsic charge carrier density.

The formation of the space charge caused by the charge carrier reservoir generates an electric field that accounts for a drift current in the opposite direction to the diffusion current. In thermodynamic equilibrium, the drift and diffusion currents compensate each other and the overall current equals zero. If interface effects are neglected, the injection barrier for electrons $\Phi_{B,e}$ is defined as the difference between the work function of the electron injecting contact Φ_M and the electron affinity of the organic semiconductor E_A; for holes, the barrier $\Phi_{B,h}$ equals the energetic difference between the work function of the contact metal Φ_M and the ionization potential of the organic material E_I:

$$\Phi_{B,e} = \Phi_M - E_A \quad \text{and} \quad \Phi_{B,h} = E_I - \Phi_M \tag{2.2}$$

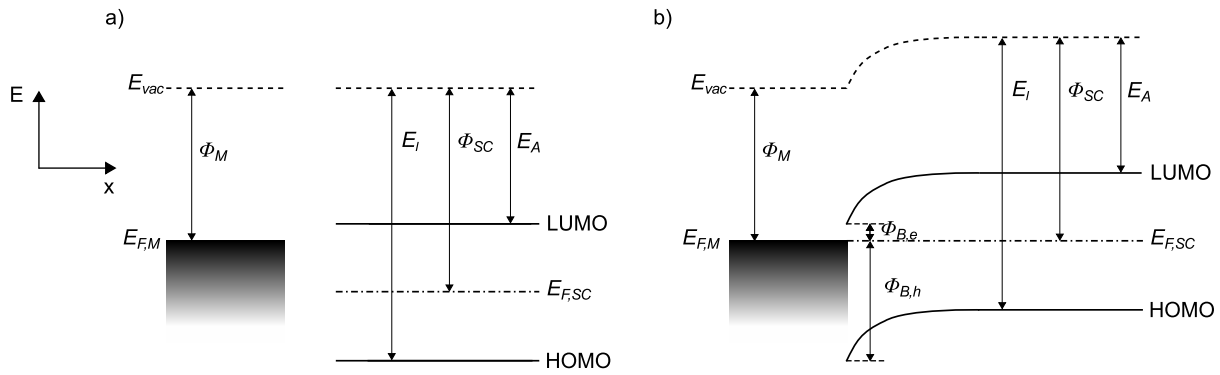

Figure 2.7: *A schematic illustration of contact formation between a metal and an organic semiconductor. The relevant variables are Φ_M and Φ_{SC} for the work functions of the metal and the semiconductor, respectively, $E_{F,M}$ and $E_{F,SC}$ for the Fermi levels of the metal and the semiconductor, E_A the electron affinity and E_I the ionization potential of the semiconductor and E_{vac} the vacuum level. a) The situation prior to electric contact. b) In electric contact, the Fermi levels of both materials become equal through a charge transfer between the materials; in this case, electrons are transferred from the metal into the semiconductor. The band bending in the organic semiconductor is induced by the formation of a space charge region. Injection barriers for electrons and holes are denoted with $\Phi_{B,e}$ and $\Phi_{B,h}$.*

For an optimal injection, the injection barriers for both charge carrier types (denoted with $\Phi_{B,e}$ and $\Phi_{B,h}$ for electrons and holes, respectively) should be kept as low as possible. This requirement influences the choice of the electrodes. As the work function of the cathode should match the LUMO of the organic material, low work function materials such as calcium or barium are often used as negative electrodes in OLEDs. Due to the high reactivity of these materials, however, more stable systems like LiF/Al [16, 17] or Ag have gained importance as cathode materials. The anode, on the other hand, is a high work function material in order to obtain a good energetical alignment with the HOMO of the semiconductor. Since one of the electrodes has to be transparent to ensure efficient light outcoupling from the OLED, transparent conductive oxides (TCO), most often ITO (indium tin oxide), are typically used as anodes. Due to the nearly endless possibilities for tailoring the energetic positions of HOMO and LUMO levels of the organic materials as well as choosing suitable contacts for both anode and cathode side of the device, injection barriers can often be optimized to a large extent. However, the actual barrier height can vary significantly from the value that would be expected from the alignment of vacuum levels at the interface [18, 19] and is strongly dependent on processing conditions like deposition sequence and morphology [19].

In ohmic metal-semiconductor contacts, the energetical alignment between the contact and the semiconductor is good and the injection barrier is so small that charge carriers are injected into the semiconductor already without an applied voltage. The injection is a diffusion process, and the charge carriers build a reservoir close to the contact. The inner electric field in the semiconductor, caused by the asymmetric contacts, prevents the carriers from drifting out of the reservoir until an external voltage high enough is applied to turn the direction of the electric field.

Unfortunately, it is not possible to find suitable electrode materials for all semiconductor systems. In such case, an ohmic contact cannot be established and the charge carriers must overcome an injection barrier. The effective barrier height is affected by the so-called Schottky effect [12, 20] that is illustrated in Fig. 2.8 for the case of the injection of electrons from a metal into a semiconductor. An injected charge carrier in the semiconducor at the distance x from the electrode surface induces an image charge of opposite sign in the metal at $-x$. There is an Coulomb interaction between the injected charge and its image charge. The field of the image charge gives rise to an attractive force, the so called image force, and its potential is called the image potential Φ_{image}:.

$$\Phi_{image} = -\frac{e^2}{16\pi\epsilon_r\epsilon_0 x} \tag{2.3}$$

where e is the elementar charge, ϵ_r the relative permittivity, ϵ_0 the vacuum permittivity and x the distance of the charges from the metal surface. Now, if an external bias is applied, an electric field F is induced in the semiconductor, leading to a potential Φ_{field}:

$$\Phi_{field} = -eFx \tag{2.4}$$

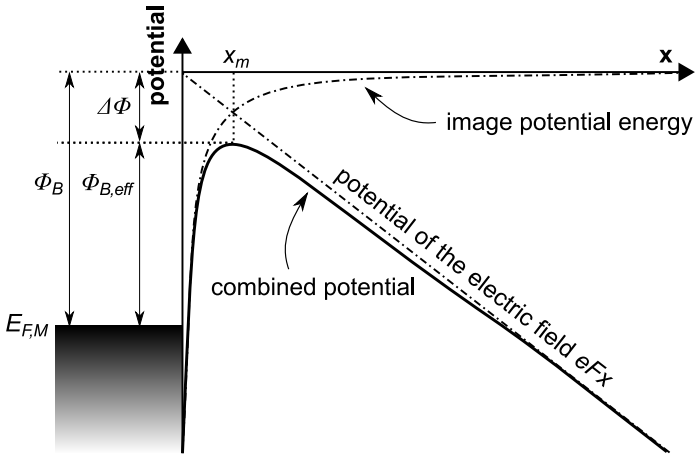

Figure 2.8: *A schematic illustration of the Schottky effect for the injection of an electron from a metal into a semiconductor at an applied electic field F. The injection barrier Φ_B is reduced to an effective barrier $\Phi_{B,eff}$ due to the influence of image charge. x_m is the distance of the barrier maximum from the metal-semiconductor interface.*

The electric potential of the applied field is superpositioned with the image potential. This leads to the lowering of the injection barrier Φ_B by the amount $\Delta\Phi$:

$$\Delta\Phi = \sqrt{\frac{e^3 F}{4\pi\epsilon_r\epsilon_0}} \tag{2.5}$$

Additionally, the maximum of the barrier is shifted from the metal-semiconductor interface into the semiconductor to the distance x_m as illustrated in Fig. 2.8.

Models that describe the injection of charge carriers into a semiconductor over an existing injection barrier are illustrated schematically in Fig. 2.9. The charge carriers can overcome the injection barrier by thermionic emission, field emission and thermionic field emission, a combination of the two.

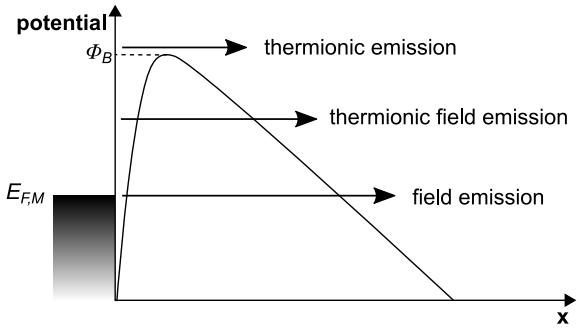

Figure 2.9: *A schematic illustration of different models to describe the injection of charge carriers into a semiconductor in the case of an existing injection barrier.*

In thermionic emission, the charge carrier is excited thermally to overcome the injection barrier. It is assumed that the injection barrier Φ_B is much smaller than the thermal energy $k_B T$. The model was originally calculated by Richardson for the emission of electrons from a metal into vacuum. Taking the Schottky effect into account, the current density is given by the Richardson-Dushman equation [12]:

$$j_{RD} = -A^* T^2 \exp\left(-\frac{\Phi_{B,eff}}{k_B T}\right) \tag{2.6}$$

$A^* = 4\pi e m^* k^2/h^3$ is the effective Richardson constant that is proportional to the effective mass m^*.

If the applied electric field F is high enough, the triangular injection barrier $\Phi_{B,eff}$ is thin enough for the charge carriers to tunnel through it. This injection process is called field emission. The tunneling current was calculated by Fowler and Nordheim [21] as follows:

$$j \propto F^2 \cdot \exp\left(\frac{2\alpha(\Phi_B)^{3/2}}{3eF}\right) \tag{2.7}$$

where $\alpha = 4\pi\sqrt{2m^2}/h$, F is the electric field and Φ_B the height of the injection barrier.

In reality, both thermionic emission and field emission are borderline cases that do not occur separately. Injection of charge carriers is therefore a mixture of both processes, thermionic field emission. The injection barrier is partly overcome by thermal activation and partly by tunneling. The dominating process is determined by the injection barrier, temperature and electric field.

Charge transport

After the charge carriers are injected from the contact into the active material, they are driven through the active layer by the electric field that is applied to the diode. Depending on the degree of order, there are two possible mechanisms for charge transport in organic materials. In highly purified molecular crystals, band transport is observed [9]. It should be noted that the bands are narrow due to the weak electronic delocalization. In polycrystalline and amorphous organic materials, on the other hand, the charges are transferred from one site to another via a hopping mechanism. Because the focus of this thesis is on amorphous polymers, only hopping transport will be discussed. It can essentially be described as a sequence of redox reactions. In case of electron transport, the electron moves from a donating molecule, which is a radical ion, to a receiving one, where a new radical ion is created. During electron transfer, the molecule that receives the electron is reduced to a singly charged anion, whereas the donating molecule is oxidized. Similarly, a molecule that receives a hole during hole transport is oxidized to a singly charged cation, while the hole donating molecule is reduced.

In a hopping process, the charges tunnel between localized states. The frequency of the jumps between states i and j $\nu_{i,j}$ can be described in a simplified form with the Miller-Abrahams model [22]:

$$\nu_{i,j} = \nu_0 \cdot \exp\left(-2\alpha r_{i,j}\right) \cdot \begin{cases} \exp\left(\frac{E_i - E_j}{k_B T}\right) & \text{for} \quad E_i > E_j \\ 1 & \text{for} \quad E_i \leq E_j \end{cases} \tag{2.8}$$

where ν_0 is the so called attempt-to-escape frequency (in other words the maximum hopping rate), α the inverse localization radius or the spatial decline of the electronic wavefunction, expressing how well the charge carriers can tunnel between states i and j, r_{ij} the distance between the states i and j, E_i and E_j their energies, k_B the Boltzmann factor and T the temperature.

Tunneling is an isoenergetic process. Jumps from state i to state j require therefore an additional absorption or emission of a phonon. The tunneling probability is expressed with the second term in Eq. 2.8. The third term corresponds to the probability of the absorption or emission of a phonon. Thermal activation is required for upward jumps. The charge carrier must move to a higher energy by absorbing a phonon prior to tunneling. The probability for an upward jump is of Arrhenius type. Downward jumps ($E_i \leq E_j$) are independent of temperature and their probability is considered to be one.

Hopping between localized states results in low mobilitiy of the charge carriers. Charge carrier mobility is defined as the proportionality factor between the mean drift velocity v and the electric field F;

$$v = \mu F \tag{2.9}$$

Charge carrier mobility is dependent on the electric field. The mobility at a certain electric field F follows the Poole-Frenkel type dependence [23]

$$\mu(E) = \mu^* \exp\left(\gamma\sqrt{F}\right) \tag{2.10}$$

where μ^* is the so-called zero field mobility, the mobility in the abscence of an electric field. γ, the field strength factor, is a material constant that depends on the electric disorder of the environment and increases with the broadening of the Gaussian DOS, which is manifested with an increasing width σ. At best, amorphous organic semiconductors reach mobilities on the order of $10^{-3}\ cm^2/\mathrm{Vs}$ [9], but in many cases the values are much lower. The mobilities are therefore orders of magnitude lower than those of inorganic semiconductors.

The transport of charge carriers is affected by electronic traps. They are energetic sites that lie within the band gap of the material. Trapped charge carriers are not available for charge transport without thermal activation. An activation energy E_A is needed to free a trapped charge carrier. The depth of traps and thus the activation energy is defined as the energetic difference between the trap energy and the corresponding transport level. Based on their energetic position, traps are divided into shallow and deep traps. If a trap lies energetically below the Fermi level E_F, one speaks of a deep trap. Shallow traps lie above the Fermi level and have activation energies of the same magnitude than the thermal energy ($E_A \leq k_B T$). Owing to their low energy, charge carriers in shallow traps are easily released, whereas carriers in deep traps are nearly immobilized once trapped [24].

Traps can be created by impurities or structural defects, for example [25]. Impurities are molecules with HOMO or LUMO (or both) located whithin the energy gap of the host, whereas structural defects in the material lead to fluctuation in the surroundings or the molecule and the conjugation length. These fluctuations create tail states below the transport level that act as traps [26].

When the holes and electrons approach each other, they form an exciton, an excited state on a single molecule. The area in which the charge carriers meet to form excitons is called the recombination zone. Its position depends on the injection, transport and recombination properties of the material. As an example, the PPVs are hole conductors. Hole mobilities are thus some orders of magnitude higher than electron mobilities and provided that the injection properties are similar on both contacts, the recombination zone lies close to the cathode rather than in the middle of the active layer.

Once formed, the excitons can migrate in the active layer by diffusion. The migration of an exciton can take place by three transfer mechanisms [27]: radiative energy transfer, Förster transfer and Dexter transfer. The radiative energy transfer, also called re-absorption, involves an emission and a subsequent absorption of a photon. It is a relevant process only if the absorption and emission spectra of the material overlap. The non-radiative transfer mechanisms, Förster and Dexter energy transfer, are presented in Fig. 2.10. Förster energy transfer [28] is a non-radiative long-range (up to 10 nm) transfer process that takes place via resonant energy transfer of neighboring molecules. A spectral overlap between the emission of the donor and absorption of the acceptor molecule is required. Here, donor and acceptor do not necessarily have to refer to different materials. In the case of exciton migration in a single material, donor and acceptor are adjacent molecules of the same type. For Förster-type transfer, the transition between ground and excited states have to be allowed for both donor and acceptor molecule. The Förster mechanism is therefore limited to singlet excitons.

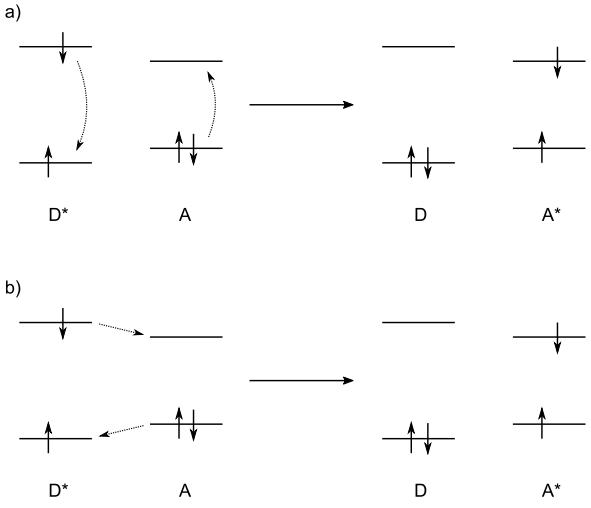

Figure 2.10: *Exciton energy transfer mechanisms. a) Förster energy transfer. The transitions on both donor and acceptor molecules have to be spin-allowed, which limits the Förster transfer to singlet excitons only. b) Dexter energy transfer. The mechanism allows the transfer of both singlet and triplet excitons.*

The Dexter energy transfer [29] involves a direct exchange of electrons and requires an overlap of the electronic wavefunctions of the involved molecules. The Dexter transfer is therefore a short-distance process with a typical range of 0.1 - 1 nm [27]. The mechanism allows the transfer of both singlet and triplet excitons and is considered to be the main transfer mechanism for triplets [30].

Recombination

The radiative decay of an exciton leads to an emission of a photon. The energy of the photon and therefore the wavelength of the emitted light depends on the energetic difference between the LUMO and the HOMO of the organic semiconductor reduced by the exciton binding energy. The emission color can therefore be manipulated by tuning the energetic positions of the HOMO and LUMO of the emitter material. However, not all excitons decay radiatively, leading to electroluminescence. Statistically, singlet and triplet excitons are formed with a ratio of 1:3 [2, 31]. As discussed in Section 2.1.2, the radiative transition from the excited triplet to the ground singlet state is forbidden by the spin selection rules. This leads to low efficiencies in fluorescent OLEDs, because the majority of the excitons does not participate in electroluminescence. Additionally, there are also non-radiative recombination pathways for singlet excitons. For example, in cases where charge transport is strongly unbalanced and the recombination zone lies near one of the contacts, the excitons can be quenched at the contact [32]. Excitons can also be quenched through exciton-exciton annihilation at high exciton densities [33–35] or be dissociated into a geminate pair of charge carriers by deep traps or other non-radiative recombination centers [9, 36]. The quenching of excitons can be reduced by the use of multilayer OLED stack structures: with the use of electron and hole blocking layers, the recombination zone can be confined to the desired position away from possible quenchers like the electrodes.

Device Operation

Fig. 2.11 shows the energetic schemes of a prototypical, single-layer OLED during different stages of operation. For clarity, the localized energetic states of the organic semiconductor are presented as straight lines and band bending is omitted. The situation prior to electric contact is depicted on top left (1). The rectifying behavior of an OLED is provided through the choice of different contact materials. They are characterized by the work function ϕ, the difference between the Fermi level of the electrode material and the vacuum level. As the electrodes are contacted (2), their Fermi levels equalize due to diffusion of charge carriers. The potential difference between the anode and the cathode, called built-in potential eU_{BI}, causes an internal field in the device. This field causes a drift current in the opposite direction to the diffusion. The drift and diffusion currents compensate each other and there is no net flow of charge carriers.

If a negative voltage $U < 0$ is applied (3), meaning the anode is negative with respect to the cathode, the inner field caused by the difference in the Fermi levels of the contact materials is increased by the

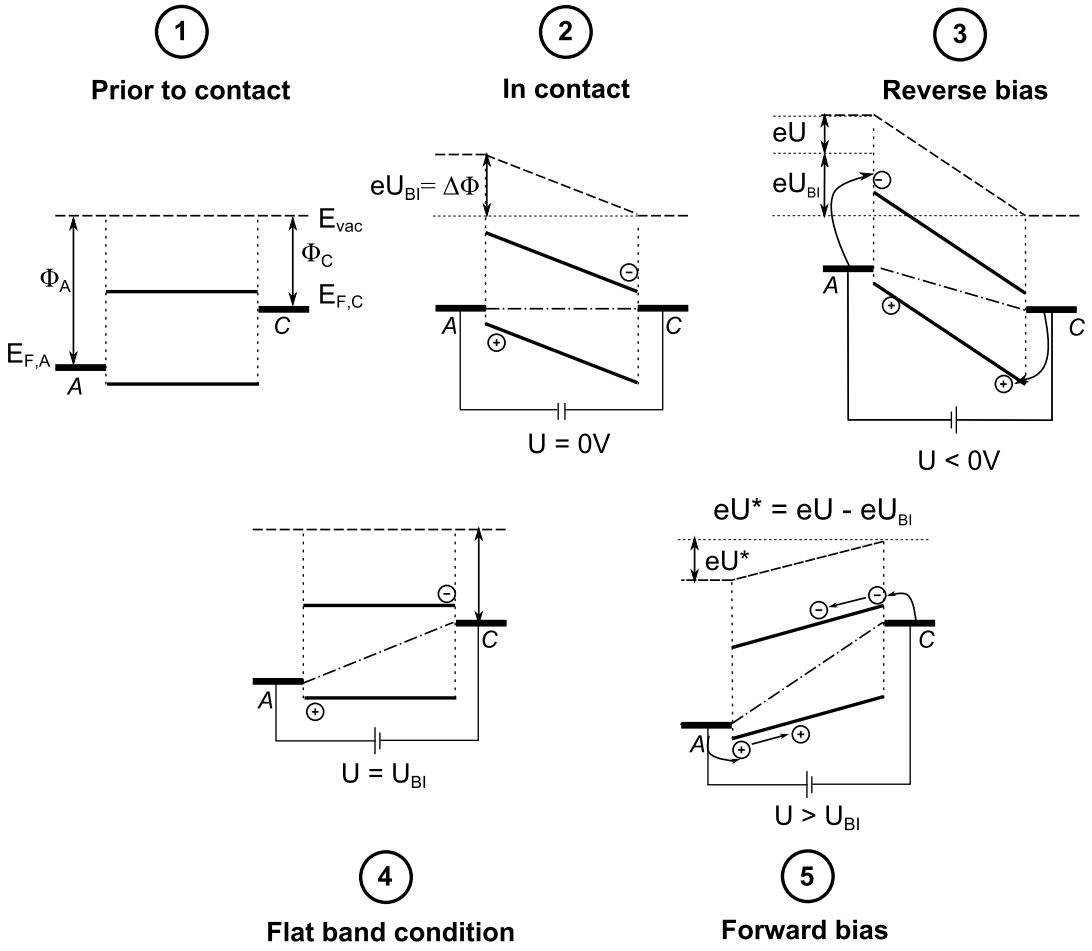

Figure 2.11: *Operation schemes for an OLED. (1) Situation prior to electric contact of the electrodes. (2) As the electrodes are contacted, the Fermi levels equalize and an inner field develops within the organic semiconductor. The potential difference between the electrodes is called built-in voltage U_{BI}. (3) Reverse bias leads to large injection barriers for both charge carrier types. (4) If the applied voltage equals the built-in voltage, the inner field in the diode is compensated by the external bias and a flat-band condition is reached. (5) Increasing the voltage further in forward direction leads to the injection of charge carriers and a net drift current.*

applied bias. The voltage U^* across the organic layer is now expressed as $U^* = U + U_{BI}$. Electrons are now injected from the anode and holes from cathode; due to the high injection barriers the resulting current is very small. This situation is called reverse bias and the contacts are reffered to as blocking contacts.

In order to facilitate net drift current in the device, a voltage is applied in forward direction so that the anode is positive with respect to the cathode, $U > 0$. With voltages smaller than the built-in voltage ($U < U_{BI}$), there is no current flow. If the applied voltage U equals U_{BI}, the so-called flat band condition (4) is reached and the inner field in the diode is compensated by the external

bias. Applied voltages higher than U_{BI} (5) result in charge injection from the contacts into the semiconductor layer and a rapid increase in current density.

2.2.2 Electrical degradation of organic light-emitting diodes

This section offers a short overwiev on the relevant processes that are related to the electrical fatigue of polymer-based OLEDs. During continuous electrical operation, the performance of OLEDs deteriorates. The devices are often operated at a constant current; during driving, a decrease in luminance intensity is observed. It is mostly accompanied by a simultaneous increase in impedance that is manifested by an increasing operating voltage. An example of such a temporal evolution is presented in Fig. 2.12. The diode with the structure ITO / PEDOT:PSS / OC_3C_8-PPV/ Ca / Al was operated at a constant current density of 50 $^{mA}/_{cm^2}$. At the beginning of the operation, the luminance decreases rather steeply before leveling off to a more moderate decay. The increasing driving voltage results from the increasing impedance of the device. As for this exemplary device, in many cases the luminance decay is more or less a mirror reflection of the voltage rise in polymer-based OLEDs [37]. The lifetime of a diode is generally defined as the half-life t_{50}, which means the time it takes for the luminance to decrease to half of its initial intensity. The t_{50} of the exemplary diode in Fig. 2.12 is approximately 150 h.

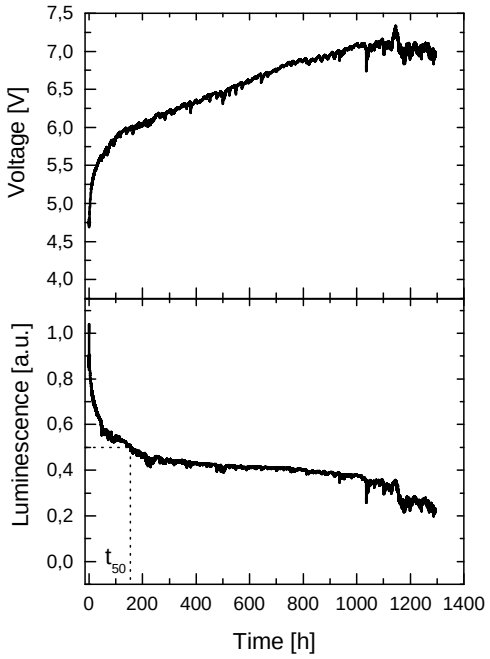

Figure 2.12: *Exemplary lifetime measurement of an OLED with a structure ITO / PEDOT:PSS / OC_3C_8-PPV/ Ca /Al and a PPV layer thickess of 120 nm. The device was driven at a constant current density of 50 $^{mA}/_{cm^2}$. The t_{50} lifetime of the device is approximately 150 h.*

The degradation of OLEDs is a complex topic and it is by no means possible to assign the deteriation to a single process. Today, some topics that were seriously problematic for the first OLEDs have lost

their importance owing to the technological progress in the field. Dark spots are a typical example. The first OLEDs were not encapsulated, which lead to problems regarding the stability of the low work function cathodes. Exposing the devices to ambient atmosphere leads to degradation of the cathode that manifests itself as non-emissive areas that were investigated in numerous publications in 1990s and 2000s [38–42]. Dark spots have been generally attributed to localized delamination of the cathode on areas with pre-existing particle defects on the substrate [37].

Another degradation process that is largely irrelevant in the state-of-the-art OLEDs is the catastrophic failure of the devices, also called the sudden death. It is related to the development of electrical shorts in the device and leads to a sudden, often complete loss of luminance. Catastrophic failure has been connected to pre-existing morphological defects in the organic semiconductor or in the electrodes that lead to the formation of microscopic conduction paths in the organic material and to short cuts between the electrodes [43, 44]. Like dark spots, also the catastrophic failure can be prohibited to a large extent with the present know-how. It is essential to control the film formation and morphology of the materials as well as the preparation processes.

In contrast to the two degradation mechanisms introduced above that are related to fabrication conditions and exposure to ambient atmosphere and can be avoided by controlling of these factors, intrinsic degradation is a far more complex issue. It is defined as the progressive and uniform decrease of luminance without any obvious change in device appearance that takes place over time during operation [37, 38, 45–47]. The processes leading to intrinsic degradation are manifold. One way of classifying them is to divide them into the morphological stability of the organic layer, the formation of traps and luminescence quenchers, interface degradation and electrode instability [37].

The thermal and morphological stability of the organic layer has been subject to discussion especially with low T_g materials; hole transport materials, particularly TPD, have mostly been in focus of attention [45, 48–50]. Crystallization of the active material has been linked to shorter device lifetimes and defect formation [51–53]. The formation of traps affects both the luminance and the operating voltage. Firstly, traps can act as non-radiative recombination centers [25, 54, 55] that decrease luminance intensity [36, 56, 57]. Secondly, the formation of traps increases the operating voltage by decreasing the effective mobility of the charge carriers [37]. Furthermore, the change in the effective mobility of one charge carrier type influences the balance of charge carriers. Polymer-based light emitting diodes are simple, single- or double-layer devices in which the confinement of excitons within the desired recombination zone by charge blocking layers is not possible. A strongly unbalanced transport of electrons and holes moves the recombination zone close to the electrodes and increases the quenching of excitons at the contacts, limiting the device efficiency.

Degradation products of the organic materials as well as defects that originate from synthesis act as traps and non-radiative recombination centers [25, 46, 58]. The chemical degradation in the bulk of efficient state-of-the art OLEDs is often charge carrier induced [46]. In this type of degradation, the radical cations or anions of the organic materials are not stable and the degradation is caused by

the transport of charges through the organic material. An example is the instability of the cationic species of the small molecule Alq_3 [45, 58–60]. For PPV, the two most relevant defects that originate from synthesis are the tolane-bisbenzyl defect [61, 62] and the halogene vinyl defect [63, 64].

Owing to the simple structure of polymer-based OLEDs, degradation of organic-organic interfaces is not as critical as in small molecule OLEDs that consist of multiple layers. Here, especially the interface between hole transport layer and emission layer is considered to be of importance [37, 45]. In contrast to this, the instability of the electrode-semiconductor interfaces is an important issue for both small molecule and polymer-based devices. At the cathode-organic interface, diffusion of Ca and Ba into a PPV layer has been observed [65]. The commonly used ITO has been reported to act as the source of both indium and oxygen that diffuse into the organic material [37]. Indium has been detected in the organic layers of stressed devices [66] but it is not considered to be of great importance for the stability of OLEDs [37, 47]. Oxygen seems to be more problematic. Diffusion of oxygen out of the ITO anode has been reported to affect the lifetime of polymer-based OLEDs [67]. The diffusion stems from the surface treatment of ITO with oxygen or UV-ozone plasma that forces oxygen atoms to the ITO surface. The oxygen is not stable on the surface and diffuses readily into the organic layer [37]. Inserting a conducting polymer (mostly PEDOT:PSS) as hole injection layer between ITO and the organic semiconductor has been reported to greatly increase the stability of the diodes [67, 68]. The injection of holes directly from PEDOT:PSS makes the stability of the ITO no longer critical for the lifetime of the device. However, the PEDOT:PSS layer as such has been related to the degradation of polymer-based OLEDs as well. PEDOT:PSS is sensitive to moisture and has been attributed to the formation of dark spots [69].

3 Experimental

This chapter begins with the introduction of the materials used throughout this thesis. After that, the procedures for sample fabrication are described, including the cleaning of the substrates, deposition of the active layers and the electrodes. The chapter then continues with the standard characterization of the samples by spectroscopy, recording of current-voltage-luminance characteristics and electrical stressing of the devices. To finish, the experimental techniques applied for the investigation of charge transport and the influence of the triplet excitons on the devices are described. These methods include charge extraction by linearly increasing voltage (CELIV), photoinduced absorption, secondary ion mass spectrometry and infrared thermography.

3.1 Materials

OC_3C_8-PPV

The active polymer used in this work is poly(2-propoxy-5-(2'-ethylhexyloxy)-phenylene vinylene) (OC_3C_8-PPV). It belongs to the group of poly(phenylene vinylenes), or in short PPVs. PPVs are an important group of organic semiconductors and have been utilized in the field of polymer-based OLEDs from the very beginning: the first polymer-based OLED was prepared with unsubstituted PPV as the active material [3]. The unsubstituted PPV is insoluble and difficult to process due to its strong interchain π - π stacking interactions [70]. Adding side chains to the polymer backbone increases the conformal mobility of the polymer chains and make the material soluble. The side chains are mostly long alkyl chains that are attached to the benzene ring of the polymer. The molecular structures of the unsubsituted PPV as well as OC_3C_8-PPV are shown in Fig. 3.1. OC_3C_8-PPV has unsymmetric alkoxy side chains and dissolves in common organic solvents such as toluene.

The OC_3C_8-PPV used in this work was synthetized by Dr. Nicole Vilbrandt from the group of Prof. Matthias Rehahn in the Ernst-Berl-Institut für Technische und Makromolekulare Chemie at the Technische Universität Darmstadt. The synthesis was performed using the Gilch route [71] that is out of scope of this work; for details of the synthesis, the interested reader is referred to the thesis of Dr. Nicole Vilbrandt [72].

The absorption and electroluminescence spectra of OC_3C_8-PPV are plotted in Fig. 3.2. OC_3C_8-PPV has an absorbance maximum at 506 nm within the broad fundamental absorption. The electroluminescence spectrum has three peaks that correspond to the 0-0, 0-1 and 0-2 transitions. The emission peaks are connected to the formation of aggregates during the annealing of the polymer

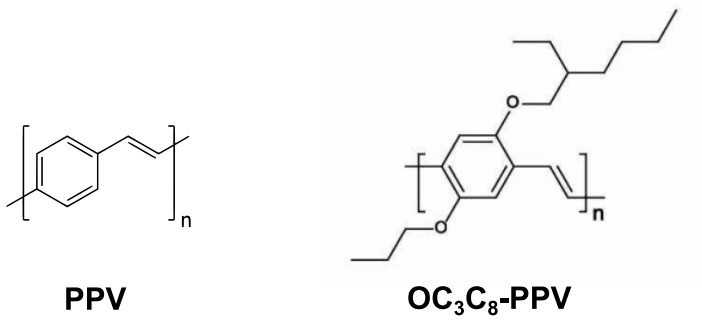

Figure 3.1: *Molecular structures of unsubstituted PPV (left) and OC_3C_8-PPV (right).*

films. The highest-energy 0-0 transition is thought to originate from the single-chain chromophore, whereas the other peaks are caused by aggregated parts [72]. A high degree of chain aggregates enhances the intensity of the 0-1 peak with respect to the 0-0 electronic transition [73, 74]. The orange-colored emission of OC_3C_8-PPV is red-shifted with respect to the absorption; this is due to the Stokes shift. The positions of the HOMO and LUMO levels of OC_3C_8-PPV were obtained by cyclovoltammetry measurements performed by Dr. Nicole Vilbrandt. The HOMO and LUMO lie at 5.2 and 2.6 eV, respectively.

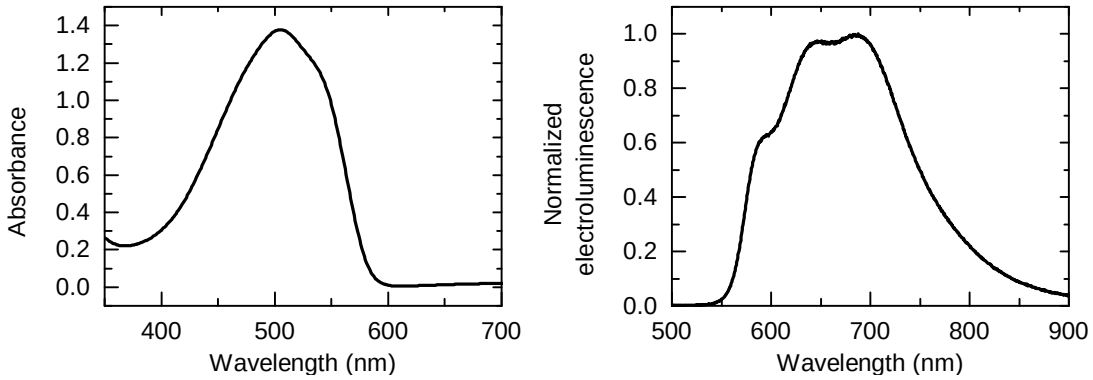

Figure 3.2: *Left: Absorption spectrum of a 140 nm thick OC_3C_8-PPV film. Right: Electroluminescence spectrum of a device with the structure ITO / PEDOT:PSS / OC_3C_8-PPV/ Ca / Al (right).*

PtOEPK

Platinum (II) octaethylporphyrine ketone (PtOEPK) belongs to the group of metalloporphyrines and is often used as an oxygen sensor [75]. In this work, it was applied as the triplet sensitizer for OC_3C_8-PPV. The molecular structure of PtOEPK is shown in Fig. 3.3. Due to the strong spin-orbit coupling caused by the presence of the central platinum atom, PtOEPK has a high intersystem crossing efficiency. It is a phosphorescent material; no fluorescence emission from the material has been detected [75].

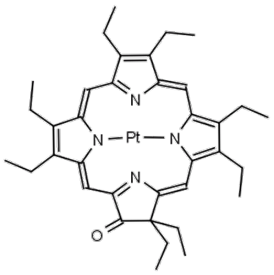

Figure 3.3: *Molecular structure of PtOEPK.*

The absorbance and emission spectra of PtOEPK are plotted in Fig. 3.4. The absorption spectrum is typical for porphyrines [76] and has two distinct peaks. The transition to the second excited state at 403 nm is called the Soret band; the Q band at 599 nm originates from the transition to the first excited state. The phosphorescence peaks at 758 nm. The HOMO and LUMO values of PtOEPK are not known in literature. As orientation, the HOMO and LUMO of PtOEP, a very similar molecule, lie at 2.8 - 3.2 eV and 5.3 - 5.6 eV [77–79]. Based on the optical spectra, the energy gap of PtOEP is approximately 0.2 - 0.3 eV larger than that of PtOEPK.

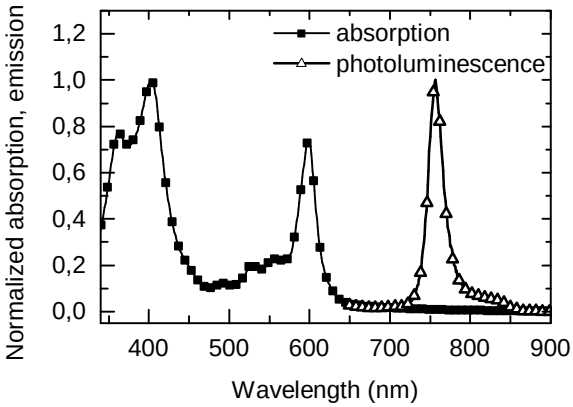

Figure 3.4: *Absorption and photoluminescence spectra of PtOEPK.*

Contact materials

Indium doped tin oxide (ITO) is a standard choice for the anode in OLEDs. ITO-coated glass substrates were obtained from VisionTek Systems. In order to prevent the diffusion of alkali metal ions from the glass into the ITO layer, an SiO_2 barrier layer had been deposited between the substrate and ITO. After purification, the ITO substrates were treated with ozone in order to remove carbon contaminations from the surface and to increase the work function of ITO. After the treatment, the work function has been reported to be 4.75 - 4.8 eV [80, 81].

A layer of poly(3,4-ethylenedioxythiophene):polystyrene sulfonate (PEDOT:PSS) between ITO and the active polymer has been observed to improve the diode performance. PEDOT:PSS smooths the

ITO surface and improves the hole injection. The work function of PEDOT:PSS is 5.2 eV [82] and is therefore well matched with the HOMO of OC_3C_8-PPV. The PEDOT:PSS was obtained from Heraeus as an aqueous dispersion with the product name Clevios^{TM} P VP Al 4083. The PEDOT:PSS ratio was 1:6 by weight.

Alternatively to ITO / PEDOT:PSS, holes can also be injected from a gold electrode. In this thesis, Au was used as the top electrode in hole-only devices. The work function of Au has been reported to vary depending on the deposition method and the degree of contamination on the surface [83, 84]; values between 4.8 and 5.4 eV have often been reported [19, 84–86].

For an efficient injection of electrons, low work function electrodes are required. Calcium has a work function of 2.9 eV and matches the OC_3C_8-PPV LUMO well. Calcium is highly reactive and oxidizes fast in contact with oxygen. It was therefore routinely protected with a capping aluminum layer in the devices used in this work. In cases like electron-only devices where a low work function bottom electrode is needed, the significantly more inert LiF / Al is a good alternative to Ca. This electrode consists of a thick aluminum layer and a thin lithium fluoride interlayer with a thickness of 0.7 nm. The work function of LiF / Al is 2.9 eV [87].

3.2 Sample preparation

The sample layout is illustrated in Fig. 3.5. The ITO anode was structured by photolithography and it consisted of four L-shaped areas. The PEDOT:PSS as well as the PPV layers were spin-coated on top of the ITO. The stripe-formed cathode was deposited via physical vapor deposition. The diodes were the areas on which anode and cathode overlap. There were four diodes on each substrate, each with an area of 10 mm^2. The use of multiple small diodes instead of one large one had two benefits. Firstly, it increased the yield through the smaller probability of both short cuts caused by dust particles and uneven emission due to variations in the quality of the spin-coated polymer layer. Secondly, the simultaneous preparation of multiple diodes enabled the direct comparison of the devices without unwanted changes in preparation parameters and conditions.

For the diodes, it is crucial to have clean and dustfree substrates. Due to the thin films with a thickness on the order of some hundred nm, even smallest dust particles can cause short cuts. In order to compensate the lack of clean room environment, the sample preparation that took place outside the glovebox was performed in a flow box, in which a continuous flow of filtered air guaranteed dust-free conditions. The standard cleaning procedure of the ITO substrates was as follows:

1. Rinsing with deionized water, drying with nitrogen flow
2. 15 min ultrasonic bath at 60 °C in 5 % deconex (an alkaline cleaning concentrate)
3. Rinsing with deionized water, drying with nitrogen flow
4. 15 min ultrasonic bath at room temperature in acetone

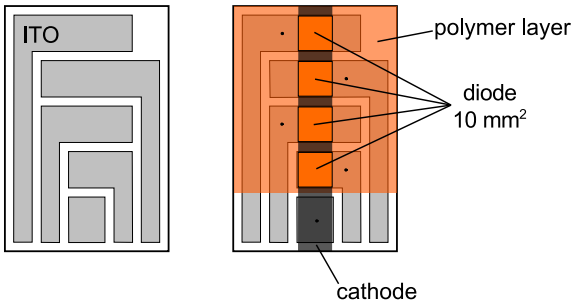

Figure 3.5: *The sample layout consists of an L-formed anode structure (left), the active polymer layer covering the substrate homogeneously and a stripe-formed cathode (right). Due to the L-formed anode structure, there are four diodes on one substrate. The anodes are contacted separately with pins (denoted with dots) and the cathode contact is shared between all diodes (the dark square in the middle at the bottom).*

5. Rinsing with deionized water, drying with nitrogen flow
6. 15 min ultrasonic bath at room temperature in isopropanol
7. Rinsing with deionized water, drying with nitrogen flow
8. 15 min UV-ozone treatment in a UV-ozone photoreactor UVP100 from Ultra-violet Products Ltd.

Both PEDOT:PSS and PPV layers were deposited on the substrate via spin coating. PEDOT:PSS is delivered as an aqueous solution and must therefore be spin coated outside the glovebox. Like substrate cleaning, also the spin coating took place in a flow box in order to avoid the contamination of substrate surface by dust particles. In order to obtain as homogeneous films as possible, the PEDOT:PSS solution was mixed with isopropanol with a ratio of 2:1. The mixture was filtered with a 0.45 μm polyvinylidene fluoride (PVDF) filter prior to spin coating to avoid having dry or agglomerated particles on the substrate. The PEDOT:PSS films were spin coated at 3000 RPM for 30 s, resulting in a layer thickness of approximately 30 nm. The substrates were subsequently annealed on a hot plate at 110 °C for 5 min in order to remove residual water from the layer.

The spin coating of the active PPV layer as well as all following preparation steps took place in a glovebox in nitrogen atmosphere with oxygen and air concentrations on the order of 1-3 ppm. OC_3C_8-PPV was dissolved in toluene at a concentration of 7.5 $^{mg}/_{ml}$ for solutions with both pristine OC_3C_8-PPV and OC_3C_8-PPV blended with PtOEPK. After preparing the solutions, they were left stirring overnight and filtered with a 5 μm polytetrafluorethylen (PTFE) filter. The solutions were spin coated at approximately 3000 RPM and annealed on a hot plate for 5 min at 130 ° C. The resulting layer thickness of 130 nm was controlled with a Dektak XT profilometer.

The metal electrodes were deposited by physical vapor deposition in the vacuum deposition system UNIVEX350G from Oerlikon Leybold Vacuum. The evaporation system is integrated in the glovebox. The samples do therefore not need to leave the inert atmosphere during the preparation process.

The deposition setup allows the use of four substrates at once. With four diodes per substrate, alltogether 16 diodes can be prepared simultaneously. In this way unwanted differences between substrates caused by e.g. changes in evaporation parameters can be avoided and a direct comparison of the diodes is possible.

The materials were deposited in vacuum at a pressure on the order of 10^{-6} mbar at typical rates of 2-5 Å/s. As sources, resistively heated tungsten boats (for Au), tungsten spirals (for Al) and molybdenum boats (for Ca and LiF) were used. The form of the evaporated areas was defined by shadow masks. For an even thickness of the deposited material on all substrates, they were rotated at 5 RPM during the evaporation process. The film thickness was controlled by an oscillating crystal.

3.3 Methods

This section introduces all methods used in this thesis. First, the focus is set on the standard material and device characterization and electrical stressing of the OLEDs, one of the fundamental methods that were applied in this work. After this, the section continues with the other applied techniques: carrier extracion by linearly increasing voltage (CELIV), photoinduced absorption, secondary ion mass spectrometry and infrared thermography.

3.3.1 Standard methods for material and device characterization

Optical spectroscopy

Transmission measurements were performed with a UV-VIS spectrometer Lambda 900 from Perkin Elmer. The sample layers were deposited on glass substrates. For each sample, an empty glass substrate was first measured as a reference. Photoluminescence spectra were measured with a Cary Eclipse Fluorescence Spectrophotometer from Varian. For electroluminescence measurements, a Maya 2000 Pro fiber spectrometer from Ocean Optics was used. It enabled the direct measurement of samples inside the glovebox without the need of encapsulation or sealed sample holders with an inert atmosphere.

Current-voltage-luminance characteristics

Each set of prepared diodes was first characterized by recording the current-voltage-luminance characteristics with a HP4515A from Hewlett Packard. The applied voltage was varied and the current density flowing through the device as well as the luminance were measured. The luminance was recorded as the current of a photodiode that was positioned directly over the measured diode. For converting this current to luminance, a photometric measure of the luminous intensity with the unit cd/m^2, each material was calibrated with a spot photometer CS 100 from Minolta.

3.3.2 Electrical stressing

The electrical stressing of the devices was performed with a constant current density as is standard practice in the field. The self-built lifetime measurement setup enabled the simultaneous measurement of six substrates. Because each substrate has four diodes, altogether 24 diodes could thus be measured simultaneously. Each diode was connected to a separately controlled current source and the desired current density was applied. The voltage that was required for the chosen current density as well as the luminance were recorded. The luminance was measured by a photodiode positioned directly over the diode. The diodes were measured sequentially one after each other. In order to be able to record the fast changes in the early stages of device operation, each diode was measured every 30 seconds for the first 60 minutes, every 60 seconds for the next 60 minutes and after that every 120 seconds.

3.3.3 Carrier extraction by linearly increasing voltage

Carrier extraction by linearly increasing voltage was first introduced by Juška et al. in 2000 [88]. The technique was originally developed for the determination of charge carrier mobility and concentration in microcrystalline silicon and doped conjugated polymers, in which thermally generated equilibrium charge carriers can be investigated [88, 89]. For undoped organic semiconductors, which have a very low intrinsic charge carrier density, nonequilibrium charge carriers are created by the absorption of a laser pulse; in this case, the method is referred to as photo-CELIV [90–92]. For the sake of clarity, in this work the investigations with and without optical excitation are referred to as photo-CELIV and dark-CELIV, respectively.

Since its introduction, CELIV has attracted considerable interest. The technique is simple, the data analysis straightforward and, most notably, it can be applied to thin films with a thickness on the order of or below 100 nm. It is therefore possible to investigate charge transport phenomena directly in the actual device geometries. This is of importance especially for solar cells with mixed donor/acceptor blends, in which the morphology of the layers plays a crucial role and cannot be reproduced reliably for large film thicknesses as required for time-of-flight measurements.

A photo-CELIV experiment is illustrated schematically in Fig. 3.6. The basic principle is simple: first, the sample is illuminated by a short laser pulse through a transparent contact. The pulse penetrates the sample and creates (in an ideal case) a homogeneous charge carrier density in the active layer. During the complete measurement, an offset bias corresponding the built-in voltage of the diode is applied to the sample in order to minimize the inner electric field in active layer. The photogenerated charge carriers experience flat band conditions and remain in the semiconductor. After an adjustable delay time t_{del} after the laser pulse, the external bias is increased linearly in reverse direction with the voltage rate $U' = dU/dt$. This voltage ramp leads to the extraction of the

charge carriers. Due to the reverse bias, both contacts are blocking and the injection of new carriers is prohibited.

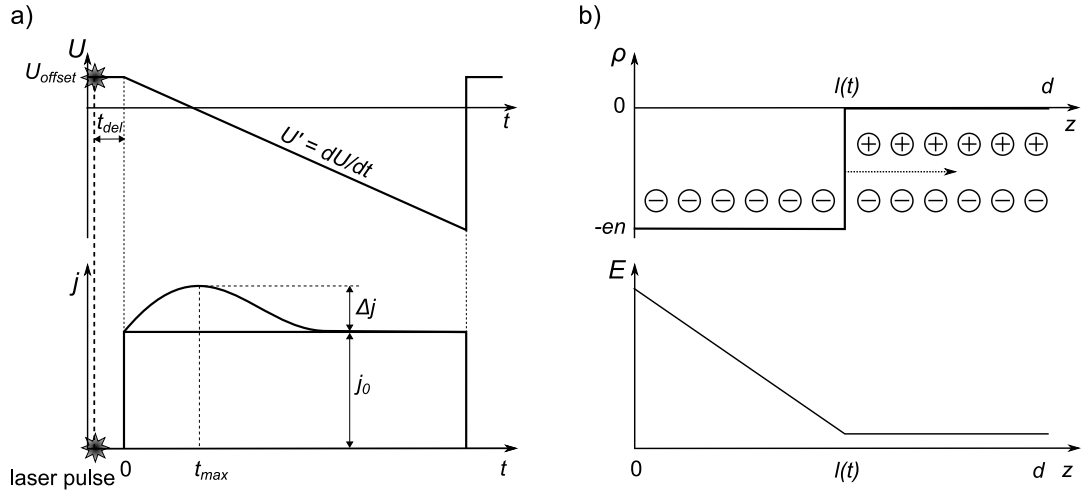

Figure 3.6: *a) Schematic illustration of a photo-CELIV measurement. Top: the applied voltage ramp in reverse direction. The ramp begins after a delay time t_{del} after the laser pulse. During the measurement, an offset voltage is applied to compensate the built-in voltage of the device. Bottom: the current response. j_0 denotes the displacement current that is induced by the linear voltage ramp. If the sample is excited with the laser, an additional photocurrent with the maximum Δj appears. The maximum is reached at a time t_{max}. b) The charge carrier density distribution and electric field in the sample for a hole-dominated device, in which $\mu_h >> \mu_e$, adapted from [93].*

The obtained current transient can be divided into two parts. The capacitive part j_0 is the current induced by the linear voltage ramp alone, without the laser excitation. The linear voltage rise results in a rectangular current response with a plateau value corresponding to the capacitive displacement current

$$j_0 = \frac{1}{A}\frac{\mathrm{d}Q}{\mathrm{d}t} = \frac{C}{A}\frac{\mathrm{d}U}{\mathrm{d}t} = \frac{\varepsilon\varepsilon_0 U'}{d} \tag{3.1}$$

where A is the area of the electrodes, Q the electric charge at the electrodes, C the capacitance of the OLED, U the applied voltage, ε the dielectric constant of the organic semiconductor, ε_0 the vacuum permittivity and d the thickness of the organic layer.

In addition to the displacement current induced by the linear voltage ramp, the laser pre-illumination creates another contribution to the current response. The photogenerated charge carriers that have not recombined during the delay time between the laser pulse and the beginning of the voltage ramp are extracted from the device during the triangular voltage pulse. This extraction creates a photocurrent with a maximum value Δj, which is reached after a time t_{max}

after the beginning of the voltage ramp. The extracted charge Q can be obtained by integrating the extraction current Δj over time[94]:

$$Q = A \int \Delta j \mathrm{d}t \tag{3.2}$$

The mathematical expression for both current components was derived by Juška et al. [88]. It is assumed that the densities of the photogenerated electrons and holes are equal, and that the charge carrier density $n_e = n_h = n$ is homogeneously distributed in the whole bulk. Furthermore, it can be assumed that the charge carrier transport in the organic layer is dominated by one charge carrier type. Because in PPVs $\mu_h >> \mu_e$ holds true, the holes can safely be treated as the mobile species. In reverse bias conditions, the positively charged cathode lies at $z = 0$ and the negatively charged anode at $z = d$; d is the thickness of the organic layer. As a result of the voltage ramp, at a time t the holes are extracted from the bulk up to an extraction depth $l(t)$. The situation is illustrated in Fig. 3.6(b). The front of the extracted holes moves through the semiconductor layer with a velocity $\frac{dl}{dt} = \mu E(l(t), t)$. Because of the low mobility of the electrons, they are considered immobile. The total charge density $\rho(z, t)$ is

$$\rho(z,t) = \begin{cases} -en & \text{for} \quad 0 \leq z \leq l(t) \\ 0 & \text{otherwise} \end{cases} \tag{3.3}$$

The electric field is coordinate dependent in the depletion (i.e. hole extracted) region $0 < z < l(t)$ and constant at $l(t) < z < d$. Now, combining continuity, current and Poisson equations [88] gives a mathematical expression for the current response

$$j(t) = \frac{\varepsilon\varepsilon_0 U'}{d} + en\left(1 - \frac{l(t)}{d}\right)\left(\frac{\mu U' t}{d} - \frac{en\mu}{2\varepsilon\varepsilon_0 d} l^2(t)\right) \tag{3.4}$$

Numerical calculations [89] lead to an expression for mobility

$$\mu = \frac{2d}{3U' t_{max}^2}\left(1 + 0.36\frac{\Delta j}{j_0}\right) \tag{3.5}$$

The possibilities offered by dark-CELIV and photo-CELIV are not limited to mobility investigations. For example, it is possible to study charge relaxation phenomena by varying the delay time t_{del} between the laser pulse and the beginning of the voltage ramp [92, 95–97]. The concentration and field dependence of the mobility can be determined by changing the incoming light intensity [91, 92, 98] and the maximum of the applied voltage pulse [91, 99], respectively. In case of a system

with equilibrium charge carriers (CELIV without laser illumination), the recovery of equilibrium can be investigated by varying the time between two consecutive voltage ramps [88]. In a recent publication, the trap density as a function of escape energy has been evaluated using an application of the photo-CELIV technique [100]. The dispersion of charge transport (manifested in how fast the transient rises before and decays after reaching the maximum value) can be reflected with the ratio of extraction current at full width half maximum $t_{1/2}$ and t_{max} [90].

The photo-CELIV setup is depicted in Fig. 3.7. The charge carriers were photoexcited with laser pulses from an optical parameter oscillator (OPO) pumped by a Nd:YAG laser with a repetition frequency of 10 kHz. The wavelength of the excitation pulses was 532 nm, which lies within the fundamental absorption of OC_3C_8-PPV. The samples were excited through the transparent anode. The delay time between the laser excitation and the voltage ramp was 5 μs. The triangular voltage ramps were created with an Agilent 3320A pulse generator and the extraction current transients were recorded with a Tektronix TDS 5052 digital oscilloscope using a Femto DHPCA-100 current-voltage amplifier. The current transients were averaged over 300 measurements in order to increase the signal-to-noise ratio.

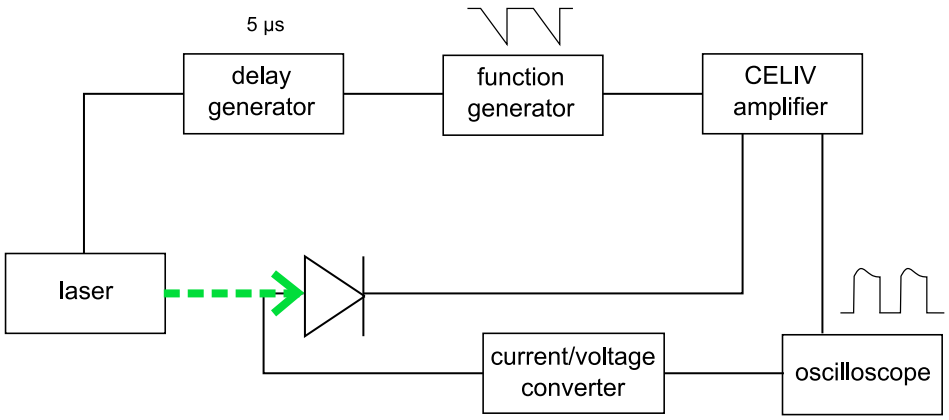

Figure 3.7: *Photo-CELIV setup.*

3.3.4 Photoinduced absorption

Photoinduced absorption (PIA) is a pump-probe method that is often used to investigate the dynamics of excited states in organic semiconductors. The triplet absorption measurements presented in this thesis were performed with a quasi-steady-state setup (see Fig. 3.8). The sample is excited by a laser or an LED, which is modulated by an optical chopper. This excitation is called the pump light. The transmission of the sample in ground and excited state is measured by the probe light, a monochromated light beam of a white light source. In other words, the probe light measures the changes in sample transmission induced by the pump excitation (which explains why the method is named photoinduced absorption). The measured signal is analyzed with a lock-in amplifier which

uses the modulation frequency of the chopper as a reference. The change in sample transmission is monitored as a function of wavelength. The ground state transmission is recorded prior to the PIA measurement; in addition to this, the measurements are corrected for photoluminescence. The measurements are performed at 80 K; at higher temperatures the lifetimes of the triplet states are too short for the method.

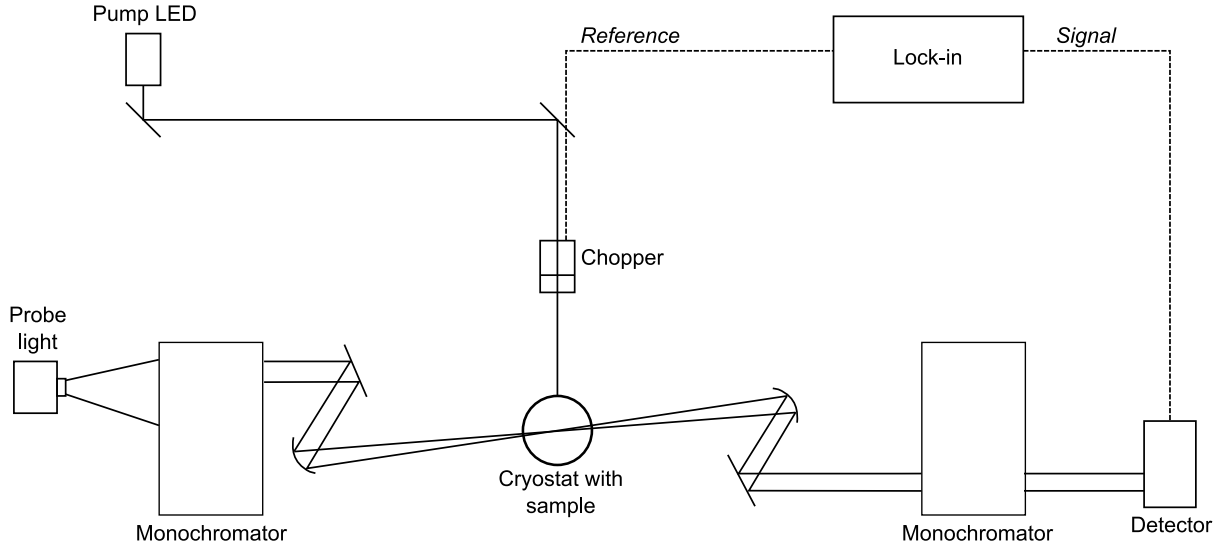

Figure 3.8: *Photoinduced absorption measurement setup.*

The measured signal is expressed as ΔT/T; that is, the change in transmission normalized to the ground state transmission. Additionally, the results are normalized to the optical density of the samples to ensure comparability between different materials. The ΔT/T signals can be either positive or negative; the $T_1 \rightarrow T_n$ absorption is observed as a negative signal. The pump light excites the first triplet state which then absorbs the probe light. This is observed as a negative change in transmission.

The PIA measurements were performed with the help of Fabian Etzold at the Max Planck Institute of Polymer Research in Mainz in the Research Group of Organic Optoelectronics supervised by Dr. Frédéric Laquai. As the pump light, a Newport LED (LED-527-HP) with an excitation wavelength of 527 nm and 100 $^{mW}/_{cm^2}$ was used. The pump frequency was 317 Hz. The probe light consisted of a 100 W tungsten-halogen lamp and a LOT-Oriel Omni-λ 300 monochromator. An additional monochromator was placed behind the sample to suppress false signals due to sample photoluminescence. The transmitted probe light was detected with three detectors depending on the wavelength: for 450-1100 nm, an amplified Si photodetector (Thorlabs PDA 100A) and for 800-1800 nm an amplified Ge photodetector (Thorlabs PDA 50B) were used, whereas for the range 1700-4500 nm a liquid nitrogen cooled InSb photodetector was chosen. The changes in transmission were recorded by a lock-in amplifier from EG&G Princeton Applied Research, model 5210. The samples were mounted in a nitrogen-cooled optical cryostat (Oxford Instruments Optistat CF) at 80 K in a helium atmosphere.

3.3.5 Secondary ion mass spectrometry

Seoondary ion mass spectrometry is applied for the investigation of the composition of surfaces and thin films. In SIMS, the sample is bombarded with primary ions, leading to the ejection of secondary ions from the material. These are sent to a mass spectrometer, where they are analyzed qualitatively based on their masses and detected quantitatively. SIMS offers a depth dependent analysis of a sample when the rate of arrival of given secondary ions (measured as intensity in counts per second) is plotted against sputtering time. The SIMS measurements were performed in collaboration with Dr. Stefan Flege from the Material Analytics group lead by Prof. Ensinger at TU Darmstadt.

3.3.6 Infrared thermography

The lifetime of an OLED is influenced by its operation temperature [101, 102]. The temperature distribution on the OLED surface can be determined with infrared thermography. Infrared thermograms were recorded with the ImageIR 8300 infrared camera from InfraTek GmbH and analyzed with the IRBIS 3 software. The available objective was able to focus on an area that was approximately 1/4 of the diode surface. For long-term measurements during electrical stressing, a thermogram was captured every 10 minutes.

4 Experimental techniques for the investigation of PPV-based devices

This chapter presents two techniques that were developed for the investigation of PPV-based diodes. First, the removal of the cathode with acetic acid is introduced, enabling the analysis of the polymer layer after the operation of the device. This is necessary for example in situations in which the morphology of the active layer is of interest. The second topic of this chapter is the accelerated aging of the diodes. In many cases, it is necessary to accelerate the fatigue of the devices by operating them at higher current densities. A scaling law for OC_3C_8-PPV-based diodes was determined, enabling the comparison of lifetime measurements performed at different current densities.

4.1 Removing the cathode

In some situations the direct investigation of the polymer layer in the diode structure is of interest. Investigations of the structure or morphology of the polymer after degradation are examples of such cases. In order to examine the polymer layer in the diode structure, it is necessary to remove the cathode after the device has been operated. With small molecules, this can conveniently be done with tape [103]. The adhesion between the organic material and the cathode is low enough so that the cathode can be stripped off. However, this approach proved not to be applicable for the PPVs. Due to the strong adhesion between the polymer and the cathode, the polymer film was always stripped away with the cathode. It was therefore necessary to develop another approach for the removal of the cathode.

Etching the metal stripe away instead of stripping it off proved to be a reasonable alternative. First experiments were done with hydrochloric acid (HCl) diluted with water with the ratio of 1:4. The diluted acid was dropped directly on the cathode stripe. The etching of the Ca layer could be easily observed by eye, and after the original layer was not visible, the acid was immediately washed away with deionized water and dried in nitrogen. After this, the sample was dried for 2 h in a vacuum oven at 100 ° C in order to remove residual water from the layer.

The etching of the cathode with HCl lead to faster degradation, however, as seen in Fig. 4.1. The temporal evolution of luminance is plotted for a continuously operated reference sample with an original cathode and for a sample, the cathode of which was removed and replaced by a new one after ca. 70 h of operation. It is clear that the degradation is accelerated after the removal of the original cathode.

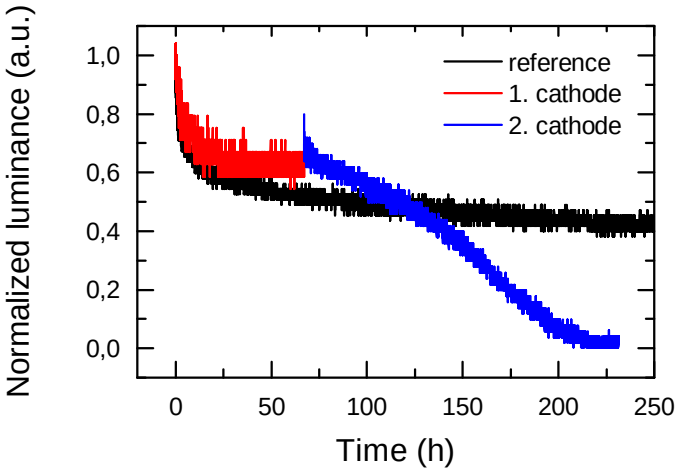

Figure 4.1: *Temporal evolution of luminance of devices with the structure ITO / PEDOT:PSS / OC_3C_8-PPV/ Ca. Black: the reference diode with an original cathode operated without interruptions. Red/blue: A diode that was operated for ca. 70 h with the first cathode (red), after which the cathode was removed with diluted HCl and replaced with a freshly deposited one (blue).*

One possible reason for the shortened lifetime is the presence of residual chlorine in the polymer layer, originating from the treatment with HCl. Secondary Ion Mass Spectrometry (SIMS) measurements were performed in order to clarify whether residual chlorine was present in the samples after the etching procedure. Three samples were measured: one neat OC_3C_8-PPV film on an ITO substrate without a top electrode, one OC_3C_8-PPV film that was treated with the diluted HCl, also without a top electrode, and one complete device with the structure ITO / OC_3C_8-PPV/ Ca, etched with diluted HCl. The results are shown in Fig. 4.2, where the intensities of relevant elements are plotted agains the sputtering time. It is possible to detect the different layers of the sample: throughout the polymer layer, the intensity of carbon stays constant. At the interface between polymer and the ITO substrate, the C intensity drops and the intensity of indium reaches its maximum plateau. The intensities of the other elements, Ca and Cl, are low throughout the scans in all samples. The reference sample with the untreated OC_3C_8-PPV layer does not contain these elements, nor does the etched reference OC_3C_8-PPV layer contain Ca. As the Ca intensity of the sample with an etched Ca cathode is not considerably higher than that of the other two samples, it is assumed that the cathode is etched away with the acid treatment. The intensity of the chlorine secondary ions does not differ considerably between the untreated and the treated OC_3C_8-PPV layers. A slightly higher Cl secondary ion intensity is seen in the etched OC_3C_8-PPV/ Ca sample, but the difference is not large enough to lead to a sure conclusion that Cl is present in the HCl-treated sample.

Although it could not be explicitely shown that the presence of chlorine in hydrochlorid acid is harmful, the removal of the cathode with HCl did damage the device, leading to faster degradation after the removal of the cathode. In an optimal case the removing of the cathode has no influence on the performance of the device; additionally, for investigations of the underlying polymer layer one must be certain that the etching process does not damage the layer of interest. Therefore an

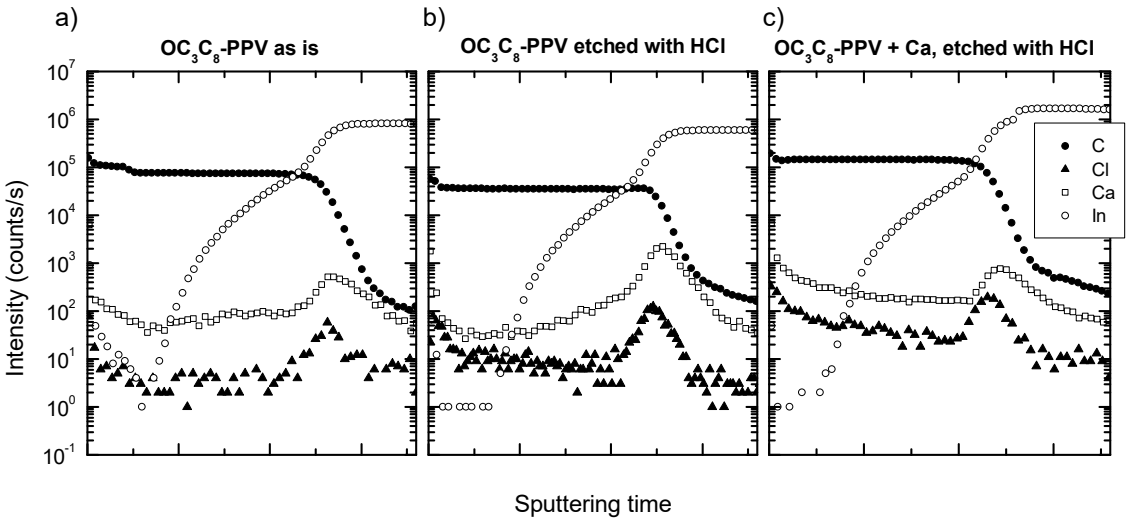

Figure 4.2: *Etching away the Ca cathode with diluted HCl: SIMS experiment. a) A reference sample with the structure ITO/OC_3C_8-PPV left as is. b) A sample with the structure ITO/OC_3C_8-PPV, etched with HCl. c) A sample with the structure ITO/OC_3C_8-PPV/Ca, the metal layer etched with HCl.*

alternative etching media was searched. Acetic acid proved to be a good alternative for hydrochlorid acid. Fig. 4.3 plots the temporal evolution of luminance of a reference diode with an original cathode as well as of a diode, the cathode of which was removed and replaced with a new one directly after preparation. No substantial differences between the two samples can be observed: the evolution of the luminance is very similar. The initial luminances were very similar as well. The operation of both samples was paused at 140 h for the recording of IVL characteristics; this explains the small-scale discontinuity in the luminance of both samples.

The optimized procedure of removing the cathode with acetic acid is summarized in Fig. 4.4. It should be noted that for such samples, the normally used Al shielding layer is left out and the thickness of the Ca is increased to 100 nm. The calcium cathode is etched away by dropping few drops of acetic acid directly on the cathode stripe. After a waiting time of ca. 2 min, the acid is quickly washed away with deionized water and dried with nitrogen. The samples are subsequently dried in a vacuum oven at 100 ° C for 2 h.

4.2 Electrical stressing in accelerated conditions

Typical t_{50} lifetimes for OC_3C_8-PPV are some hundreds of hours, which makes the electrical stressing very time-consuming. The possibility to shorten the electrical stressing is therefore desired in situations in which the available time is limited. This can be achieved by driving the devices at a higher current density, which leads to faster degradation. If a correlation between the lifetimes obtained at different current densities exists, the electrical stressing can be accelerated.

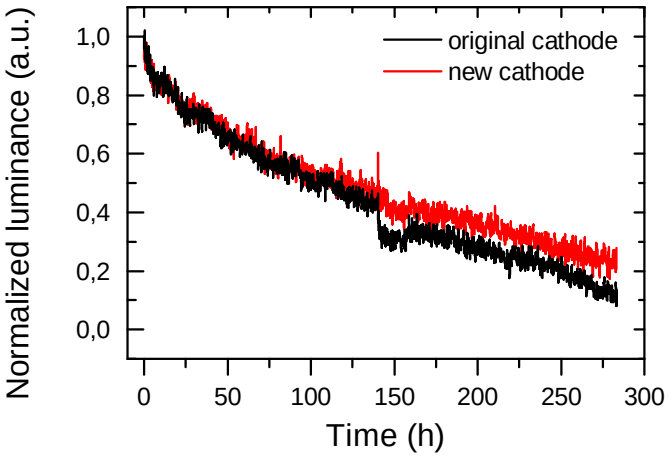

Figure 4.3: *The influence of the cathode removal with acetic acid. Black: the development of luminance of a reference sample with an original Ca cathode during operation. Red: a sample from the same preparation run; the original cathode was removed and replaced with a new one directly after the preparation of the samples. The operation of both devices was paused at 140 h for the recording of IVL characteristics. Both devices had the structure ITO / PEDOT:PSS / OC_3C_8-PPV/ Ca and were operated at a constant current density of 50 mA/cm^2.*

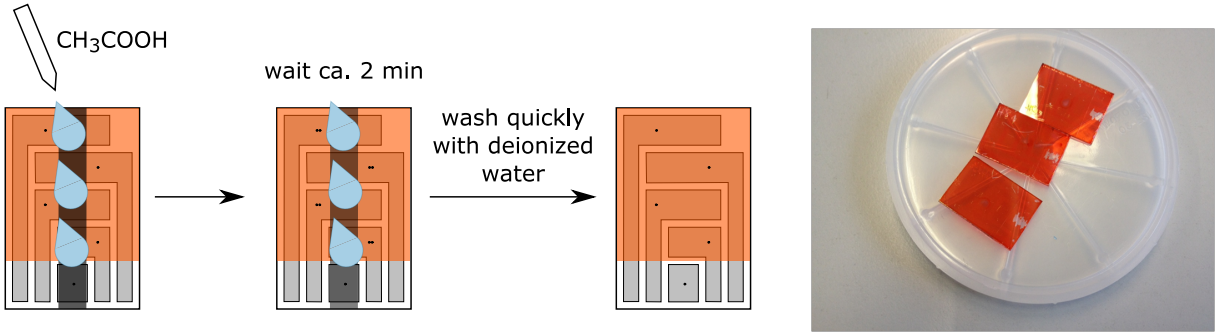

Figure 4.4: *Removing the cathode with acetic acid.*

The initial luminance is proportional to the applied current density. In experiments with different organic materials, the t_{50} lifetime has been experimentally observed to scale with the initial luminance [49, 104, 105]. This can be expressed as the so-called scaling law:

$$t_{50} \times L_0^n = const \tag{4.1}$$

where L_0 is the initial luminance and n a system specific acceleration factor.

It was investigated whether the scaling law that was first introduced by Van Slyke and co-workers [49] and later by Popovic et al. [104] can be applied for OC_3C_8-PPV-based diodes. A set of diodes with the structure ITO / PEDOT:PSS / OC_3C_8-PPV/ Ca / Al were prepared and stressed electrically at current densities of 50, 100, 200 and 400 mA/cm^2, leading to different values for initial luminance. The corresponding t_{50} lifetimes were then extracted.

The t_{50} lifetimes of the diodes are plotted against the initial luminance on a double-logarithmic scale in Fig. 4.5. Despite the scattering of the lifetime values, there is a clear correlation between the initial luminance and the t_{50}. [1] The parameters for the scaling law can be extracted by fitting the presented data with a linear fit, which is shown in the Figure as the dotted line. For the tested OC_3C_8-PPV-based devices, the fit yields an acceleration factor of approximately $n = -4.2$. It could be shown that the scaling law can be applied to OC_3C_8-PPV-based devices. It is therefore possible to perform the electrical stressing under accelerated conditions if needed.

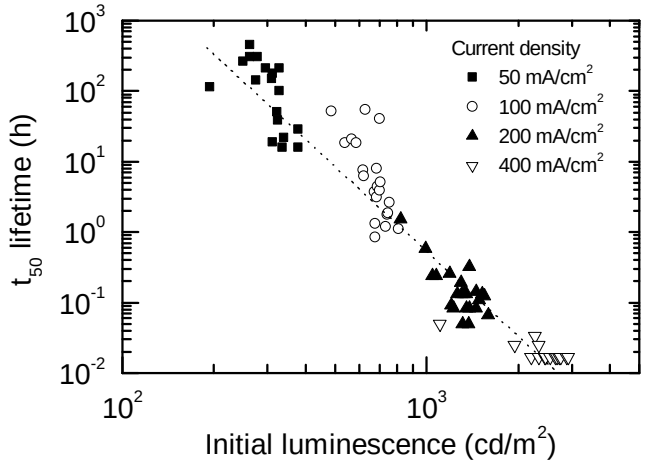

Figure 4.5: *t_{50} lifetime against initial luminance of diodes operated at current densities of 50, 100, 200 and 400 mA/cm^2. The data sets were fitted using Eq. 4.1 and the fit is shown as the dotted line. The diode structure was ITO / PEDOT:PSS / OC_3C_8-PPV/ Ca / Al.*

[1] The scattering of the lifetimes as well as the initial luminance values is a common phenomenon. The I-V-L characteristics as well as the electrical stressing results presented in this thesis are therefore averaged from several devices.

5 Dark-CELIV investigations on OC_3C_8-PPV

This chapter utilizes dark-CELIV for the investigation of equilibrium charge carriers in OC_3C_8-PPV. Due to the low intrinsic charge carrier density in PPVs, no extraction current is observed in dark-CELIV measurements of freshly prepared devices. However, it will be shown that during aging in the glovebox, an unexpected density of equilibrium charges is observed to develop. This storage-related charge carriers will be attributed to doping by residual oxygen in the glovebox, and the process will be monitored by dark-CELIV measurements. Additionally, the time scale of the establishment of the thermal equilibrium in doped OC_3C_8-PPV after charge carrier extraction by CELIV will be monitored experimentally.

5.1 Previous investigations with dark-CELIV

Due to their low density of intrinsic charge carriers, organic semiconductors have typically been investigated with photo-CELIV, in which charge carriers are created by exciting the material with a laser pulse. However, in some cases the density of equilibrium charge carriers is large enough so that the photoexcitation of the semiconductor is not necessary and dark-CELIV can be utilized. In organic semiconductors, such equilibrium charge carriers can originate from doping, impurities or space charge near the contacts, for example [106]. In recent publications, dark-CELIV has been applied for the investigation of the influence of postproduction treatment of P3HT on the density of intrinsic charge carriers and the charge transport [106], a charge carrier reservoir at the interface TiO_2/P3HT:PCBM [94] as well as the oxygen-induced doping concentration in P3HT:PCBM bulk heterojunction solar cells [107–110]. Additionally, one work connects equilibrium charges in P3HT:PCBM to injection from the contacts due to energy level alignment caused by Fermi level pinning [111], and a very recent publication utilizes dark-CELIV for the investigation of the time dependence of the build-up of a space charge at the interface ITO / P3HT [112].

5.2 Origin of equilibrium charge in OC_3C_8-PPV

To begin, Fig. 5.1 illustrates the energetic situations at different stages of a dark-CELIV measurement as performed throughout this chapter. The measured samples had the structure ITO / PEDOT:PSS / OC_3C_8-PPV/ Ca / Al. For clarity, band bending and the presence of charge carriers are omitted. On top left, the energetic levels of the used materials are illustrated prior to contact, in absence of thermal equilibrium. On top right, the situation is depicted after the equalization of the Fermi levels of the contacts, i.e. in thermal equilibrium, with zero volt applied bias. The work function

difference of the electrode materials induces a built-in voltage U_{BI} to the sample. The dark-CELIV ramp sequence is illustrated on bottom left. Before the linear voltage ramp, a constant offset voltage $U_{offset} = 2\,\mathrm{V}$ is applied in order to compensate the built-in voltage (bottom middle). The dark-CELIV voltage ramp is then applied in reverse bias (bottom right), meaning a negative applied voltage at the ITO / PEDOT:PSS contact. The reverse bias is important in order to prevent injection of charge carriers during the voltage ramp.

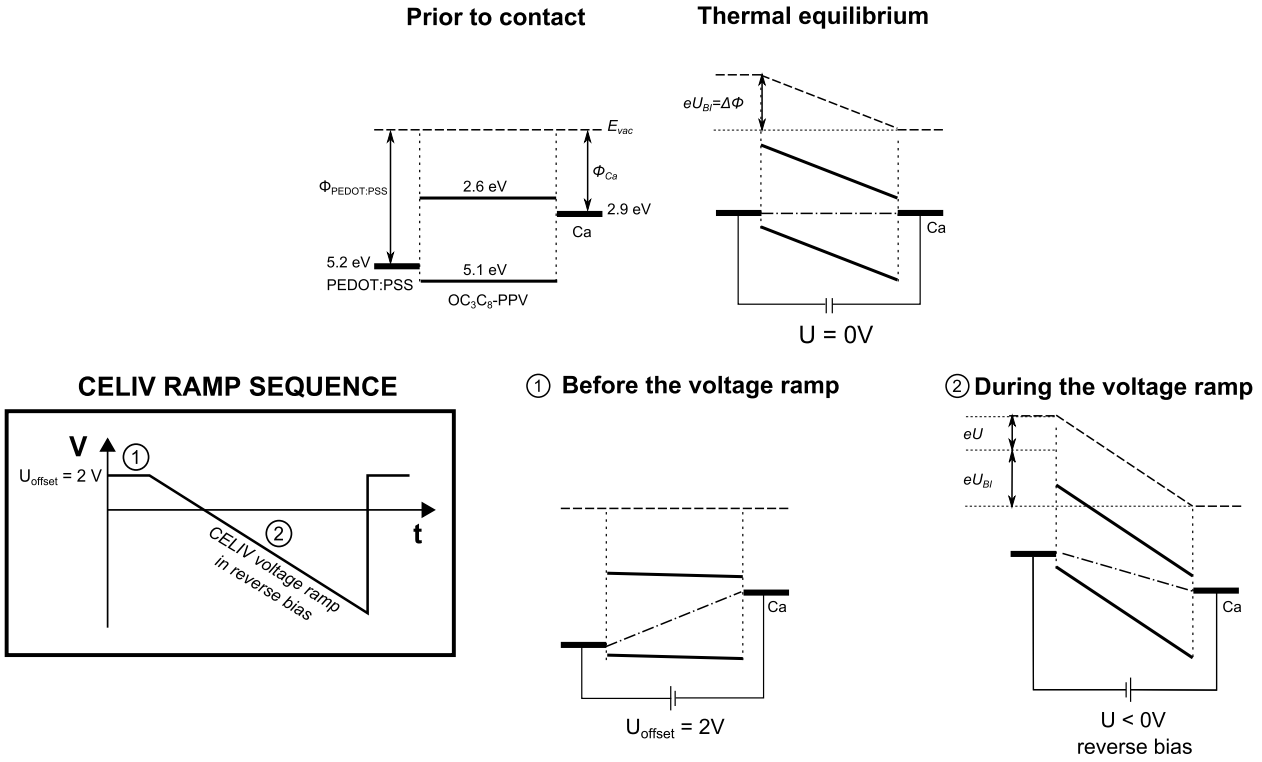

Figure 5.1: *A schematic illustration of the dark-CELIV measurement as performed throughout this chapter. Top left: The energetic levels of the materials being not in thermal equilibrium. Top right: The situation in thermal equilibrium with zero volt applied voltage. The equalization of the Fermi levels of the contact materials induces a built-in voltage U_{BI} that equals the work function difference of the electrodes. Bottom: The dark-CELIV measurement sequence. The dark-CELIV voltage ramp is illustrated on the left; before the ramp, an offset voltage $U_{offset} = 2\,V$ is applied (1). The offset voltage approximately compensates the built-in voltage of the device, leading to flat band conditions. The linear voltage ramp in reverse bias (2) means a negative applied voltage on the ITO / PEDOT:PSS contact; the reverse bias prevents the injection of charge carriers from the contacts.*

Without a significant intrinsic charge carrier concentration, the linear dark-CELIV voltage ramp results in a constant rectangular current response that corresponds the capacitive displacement current (see Section 3.3.3). Due to the low charge carrier density in undoped OC_3C_8-PPV, this is expected to be the case for the dark-CELIV current response of a standard diode with the structure ITO / PEDOT:PSS / OC_3C_8-PPV/ Ca / Al as was used in this work. Indeed, diodes that are measured in a fresh state shortly after preparation show only the rectangular displacement current, as shown in Fig. 5.2 a). In both graphs in Fig. 5.2, CELIV measurements are plotted for samples with

the standard structure ITO / PEDOT:PSS / OC_3C_8-PPV/ Ca / Al at $U_{offset} = 2\,V$. In photo-CELIV measurements the samples were excited optically at 506 nm, i.e. at the absorption maximum of OC_3C_8-PPV, 5 μs prior to the beginning of the triangular voltage ramp; the photo-CELIV responses of both samples exhibit a significant peak originating from the extraction of the photogenerated charge carriers. Additionally and contrary to the expectations, in some measurements as plotted exemplarily in Fig. 5.2 b), a distinct extraction current signal originating from the extraction of mobile charge carriers is present in the dark-CELIV response in addition to the displacement current.

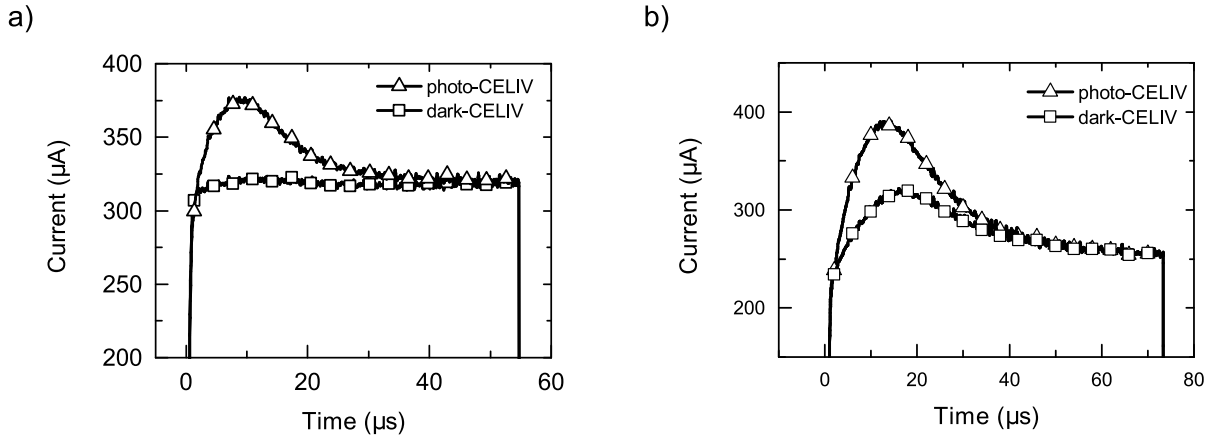

Figure 5.2: *Exemplary current transients of two CELIV measurements without (dark-CELIV, rectangles) as well as with optical excitation (photo-CELIV, triangles). An offset voltage $U_{offset} = 2\,V$ was applied in both measurements. In photo-CELIV, the sample was excited with a laser pulse at 506 nm 5 µs prior to the beginning of the triangular voltage ramp. a) A fresh sample measured directly after preparation; b) a sample that was measured after a longer (some weeks) storage in the glovebox.*

Detailed investigations showed that such an extraction current without the optical generation of charge carriers is primarily observable when the samples are measured after storing them in the glovebox for several days. It was possible to conduct successful CELIV measurements without the appearance of extraction current in the dark on freshly prepared as well as electrically stressed samples (the results will be shown in Chapter 6), provided that the measurements were started immediately after preparation without a storing time in the glovebox. The extraction current in dark-CELIV did not increase with electrical stress and is therefore not directly related to electrical fatigue. It is thus a storage effect that is related to aging during storage in the glove box.

The similarity of the form of the extraction current peaks in Fig. 5.2 is obvious. The extraction current in the photo-CELIV measurement is caused by holes, which are known to have a significantly higher mobility than electrons in PPV [113–115]. They are created by the optical excitation of the sample and stem from the bulk of the polymer layer. The similarity of the form of the peaks as well as the positions of the current maxima give hints on the type of charge carriers that cause the dark-CELIV signal. In CELIV, the mobility is calculated utilizing Eq. 3.5. The calculated mobilities for the photo- and dark-CELIV responses in Fig. 5.2 a) and b) are $5 \cdot 10^{-6}\ \frac{cm^2}{Vs}$ and $4 \cdot 10^{-6}\ \frac{cm^2}{Vs}$, respectively.

The mobility of electrons in PPV derivates is known to be considerably smaller than that of holes [115], and the obtained values are both typical hole mobilities in OC_3C_8-PPV. It is concluded that the dark-CELIV voltage ramp extracts holes from OC_3C_8-PPV.

Next, the location of these holes is of interest. In general, in present devices there are three possibities for the location of the equilibrium charge that is extracted with the dark-CELIV voltage ramp: the interface PEDOT:PSS / OC_3C_8-PPV, the interface OC_3C_8-PPV/ Ca and the bulk of the polymer. As depicted in Fig. 5.1, the dark-CELIV voltage ramp in reverse bias extracts holes at the PEDOT:PSS contact and electrons at the Ca contact. As discussed above, it is known that the extracted charge carriers are holes. A hole accumulation region at the interface PEDOT:PSS / OC_3C_8-PPV would be extracted immediately at the contact and would therefore not cause a CELIV extraction current response as observed in the present devices. Accordingly, if the extraction current stems from a space charge region at one of the contacts, it must be the interface PPV / Ca. However, a possible accumulation region at this contact should consist of electrons due to the low barrier between OC_3C_8-PPV LUMO and Ca. Firstly, the observed dark-CELIV extraction current is caused by holes, and secondly, in consequence of the voltage ramp in reverse bias, electrons would be extracted immediately at the contact and would not contribute to the CELIV current signal. A charge carrier reservoir at both contacts is therefore excluded, and the source of the extracted charge has to be the polymer bulk. This conclusion is supported by the similarity of the extraction current peaks of photo- and dark-CELIV (Fig. 5.2).

In photo-CELIV, it is important to apply an offset voltage to the device to compensate the built-in voltage. In this way, flat band conditions are created and the photogenerated charge carriers stay in the semiconductor bulk until they are extracted with the voltage ramp. The magnitude of the offset voltage affects the extraction current response in the present dark-CELIV measurements, too. Dark-CELIV curves of two diodes, both with the structure ITO / PEDOT:PSS / OC_3C_8-PPV/ Ca / Al, at different offset voltages are plotted in Fig. 5.3. During the measurements, the voltage ramp was kept constant, meaning that the peak-to-peak voltage of the ramp was always 8 V and the voltage rate was kept constant during each measurement series. Both samples show the highest extraction current at the offset voltage $U_{offset} = 2\,\mathrm{V}$; decreasing the offset voltage from this value decreases the current. The diode plotted on the left was measured until an offset of 1 V at a voltage rate of -182 kV/s; at this value, a small contribution of extraction current is still observable. The diode on the right-hand side was measured until $U_{offset} = 0.6\,\mathrm{V}$ at -61 kV/s, and offset voltage values of 0.6 and 0.8 V show only the rectangular displacement current. Thus, an offset voltage of at least 1 V is necessary for the appearing of an extraction current signal. The noise in the current transients on the right-hand side is a measurement-related artifact.

Based on the values of the capacitive discharge current (see Eq. 3.1), one notices a difference in the capacitances of the two devices shown in Fig. 5.3; capacitance values of 2.2 nF and 1.9 nF are obtained for the devices shown on the left and on the right, respectively. The difference is likely to be based on variations in the thickness of the OC_3C_8-PPV layer. The shown diodes were prepared on different days from different polymer batches, and despite the routine of layer thickness

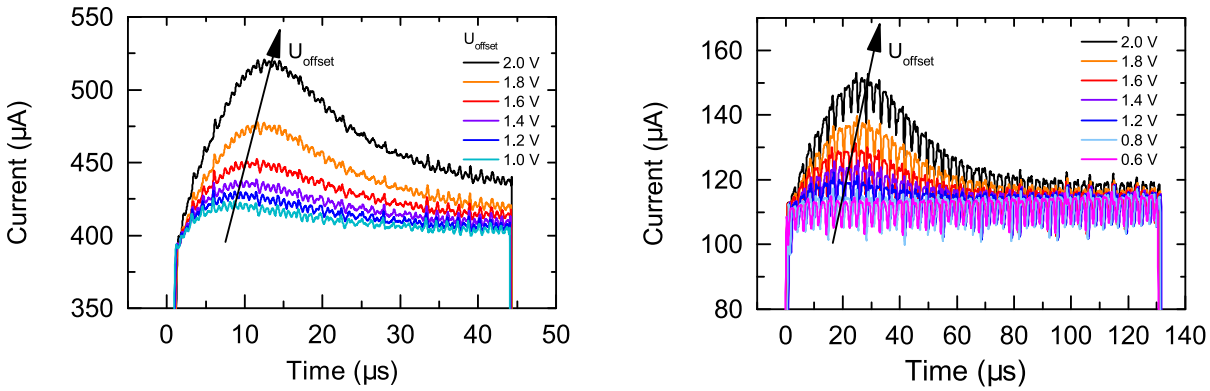

Figure 5.3: *Influence of offset voltage on the extraction current transient. Both samples had the structure ITO / PEDOT:PSS / OC_3C_8-PPV/ Ca / Al. The strong noise in the transients on the right is a measurement-related artifact. The rates on the voltage ramps were -182 kV/s on the left and -61 kV/s on the right.*

determination for each prepared solution, variations on the processing parameters cannot always be excluded.

The dependence of the extraction current on offset voltage in a dark-CELIV measurement is like in photo-CELIV. In the case of a bulk charge carrier density, the decreasing extraction current with decreasing U_{offset} is explained with an increasing internal field in the semiconductor as the offset voltage decreases. $U_{offset} = 2\,\mathrm{V}$ is close to the built-in voltage of the sample, leading to approximately flat-band conditions. Smaller U_{offset} values are connected with an increasing field that drives the existing charge carriers to the electrodes before the beginning of the voltage ramp, leading to lower extraction currents. If U_{offset} is increased further from 2 V, charge carrier injection from both electrodes begins as the applied voltage exceeds the built-in voltage of the device. To illustrate this, Fig. 5.4 plots dark-CELIV current transients at offsets between 2 - 3 V. The diode (structure ITO / PEDOT:PSS / OC_3C_8-PPV/ Ca / Al) was measured within few days after preparation so that it was still in a fresh state. This means that no aging-related extraction current as seen in Fig. 5.2 and 5.3 is observed. In other words, both Fig. 5.3 and 5.4 show current transients at $U_{offset} = 2\,\mathrm{V}$. In Fig. 5.3, the devices have been stored in the glovebox long enough to obtain a clearly observable extraction current that is due to aging. As a contrast to this, no aging-related extraction current can be observed in Fig. 5.4 because the device was measured in a fresh state.

In Fig. 5.4, the current response at 2 V consists of displacement current only. As U_{offset} is increased, the applied voltage exceeds the built-in voltage of the device and charge carriers are injected into the polymer layer from both electrodes until the CELIV voltage ramp begins and the applied voltage begins to decrease. The injection is seen as a constant negative current component before the voltage ramp, i.e. at times $t < 0$. The magnitude of the current increases with increasing U_{offset}, as the injection current increases. During this time, the bulk of the semiconductor is filled with charge carriers that are being injected from the contacts. The extraction of these charge carriers is seen as

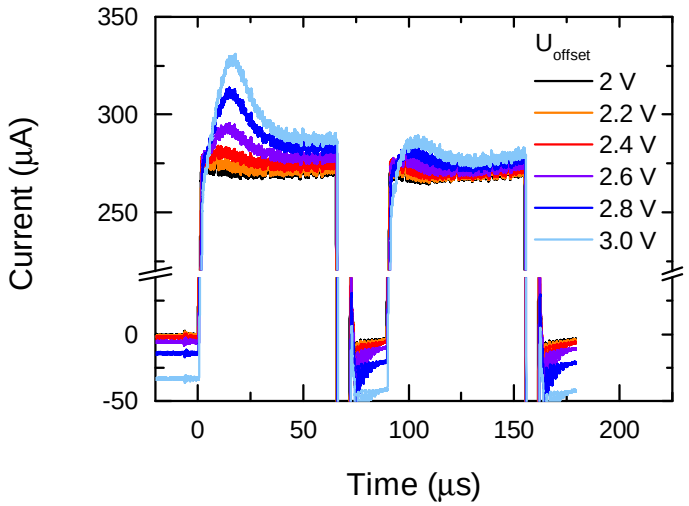

Figure 5.4: *Dark-CELIV current response at offset voltages between 2-3 V. The device was measured directly after preparation in a fresh state, i.e. before the rise of a storage-related extraction current signal; at $U_{offset} = 2$ V, only the rectangular capacitive displacement is observed. As U_{offset} increases above the built-in voltage U_{BI} of the device, charge carriers are injected from the contacts and a constant negative injection current is observed before the beginning of the voltage ramp. Additionally, an extraction current component is superpositioned on the capacitive displacement current during the ramp. The device structure was ITO / PEDOT:PSS / OC_3C_8-PPV/ Ca / Al and the applied voltage ramp $U' = -122$ kV/s.*

an extraction current component that appears on top of the displacement current during the voltage ramp.

The applied offset voltage influences not only the magnitude of the extraction current but also the position of the current maximum t_{max}. Both Fig. 5.3 and 5.4 show that in addition to the increasing extraction current, the current maximum shifts to higher times with increasing offset voltage. In literature it has previously been argued that a shift of t_{max} is due to an increase of the RC time constant due to an increase of the capacitance [116]. In the work in question, extraction current in the dark was attributed to an injection of charge carriers into the semiconductor from not ideally blocking contacts. The assumed injection was reasoned to lead to an increase in the capacitance and therefore to an increase of τ_{RC}, which limits the time resolution of the measurement. It is clear that such an assumed increase in the RC time constant is seen in the beginning of the ramp in the slowed charging of the capacitor. In present measurements, no such behavior is observed; the rise of the capacitive displacement current is not affected when the extraction current is increased and the t_{max} is shifted to higher times. In present work, the shift of the current maximum to higher times with increasing offset voltage can be explained with the voltage ramp. The peak-to-peak voltage as well as the frequency of the triangular voltage ramp are constant, so by varying U_{offset} the absolute position of the voltage ramp is shifted. This is illustrated in Fig. 5.5, where the position of the extraction current maximum t_{max} is plotted against offset voltage for the diode shown on the left in Fig. 5.3. The position of the extraction current maximum shifts linearly to higher times when the

offset voltage is increased. A higher offset voltage means that a longer time is needed to reach a voltage that is sufficient to extract the charge carriers from the layer.

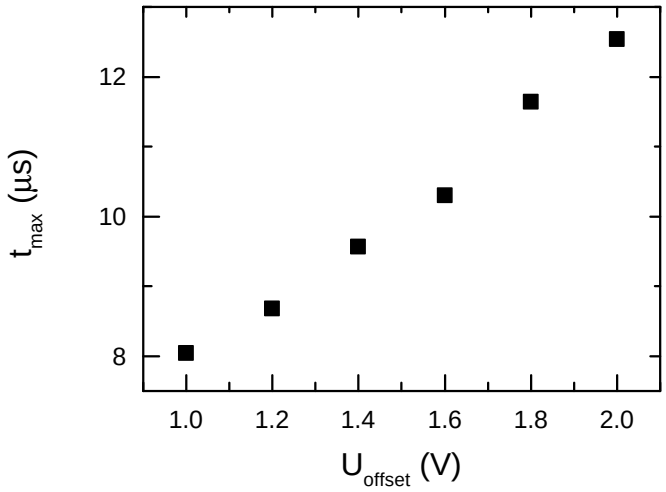

Figure 5.5: *The influence of offset voltage on the position of the extraction current maximum. The device structure was ITO / PEDOT:PSS / OC_3C_8-PPV/ Ca / Al and the applied voltage ramp U' = -182 kV/s. The data is for the device shown in Fig. 5.4 on the left.*

5.3 Oxygen doping of OC_3C_8-PPV

In the following, the mobile holes in OC_3C_8-PPV will be connected to residual oxygen. After demonstrating a steady increase of extraction current and thus the density of free charge carriers with time, the focus will set on the dynamics of the doping-induced holes. The concentration of the holes will be monitored with dark-CELIV.

5.3.1 Gradual increase of extraction current in present devices

As mentioned above, the amount of extraction current in dark-CELIV measurements depends on the time the devices were aged after preparation. Fig. 5.6 plots a dark-CELIV measurement of a device with the standard structure ITO / PEDOT:PSS / OC_3C_8-PPV/ Ca / Al that was measured on the day following sample preparation (day 1) as well as 2, 5 and 8 days after preparation. An offset voltage U_{offset} = 2 V was applied prior to the voltage ramp and the peak-to-peak voltage was 8 V. The extraction current increases steadily as the device is aged in the glovebox, as enlarged on top right. Despite the measurement-related noise, the increase of the extraction current is clearly observable. The enlargened negative current tail (on bottom right) will be discussed later on. Interestingly, the displacement current of the sample measured in the fresh state (black) seems to be slightly higher than the current measured on other days. This behavior cannot currently be explained.

A gradual increase in the extraction current as a function of time points to a slow doping process. For conjugated polymers, oxygen doping has been often reported for P3HT [107–110, 117–119].

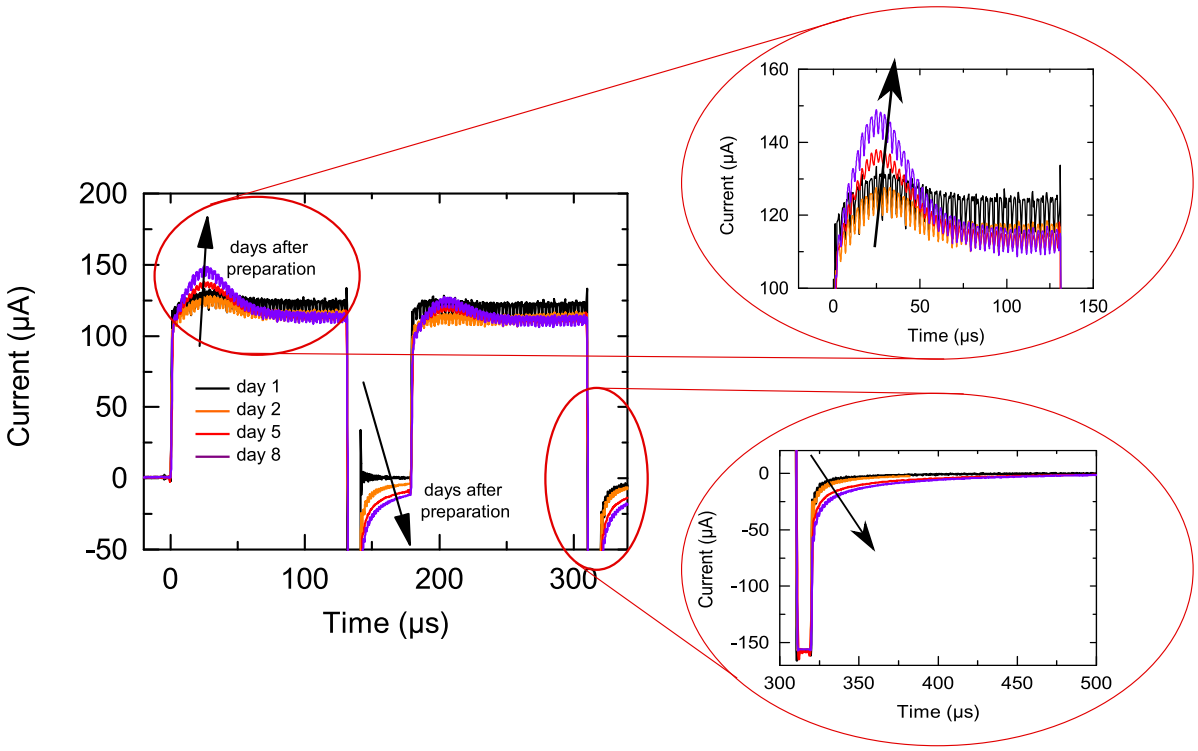

Figure 5.6: *The increase of equilibrium charge in OC_3C_8-PPV. The device had the structure ITO / PEDOT:PSS / OC_3C_8-PPV/ Ca / Al and was measured on the day after preparation (black) as well as 2 (orange), 5 (red) and 8 (purple) days after preparation. An offset voltage of 2 V was applied prior to the voltage ramp, the peak-to-peak voltage of which was 8 V. An increasing extraction current peak can be seen superimposed on the displacement current, as enlarged on top right. On bottom right, the stretched negative current after the voltage ramp is enlarged; the stretching is discussed below.*

The doping mechanism is described as follows [117]: Oxygen diffuses into the devices, creating a trap state for electrons. The trap can be filled optically by exposing the device to visible light, if the field in the semiconductor is high enough to dissociate the optically created exciton. The filling of traps with electrons leaves behind free holes on the HOMO, leading to p-doping of the polymer. In addition to P3HT, also PPV has often been reported to be sensible to oxygen [114, 120–124]. One would presume that reactions with oxygen are limited to the exposure to ambient air, but oxygen-related defects have been observed in inert atmosphere, too [114, 121, 123]. The albeit small but nevertheless present oxygen concentration in the glovebox is sufficient for the doping. The assumption of oxygen doping in the present work is supported by a significant extraction current in a fresh device with the standard structure that was measured directly after preparation after being exposed to air for 1-2 minutes before the CELIV measurement, plotted in Fig. 5.7 a). As comparison, Fig. 5.7 b) plots an exemplary dark-CELIV measurement of a freshly prepared diode that was measured directly after preparation without exposure to air. In all samples stored solely in

the glovebox without exposure to air, extraction currents as in Fig. 5.7 a) were observed only after a remarkably longer storage time of several days.

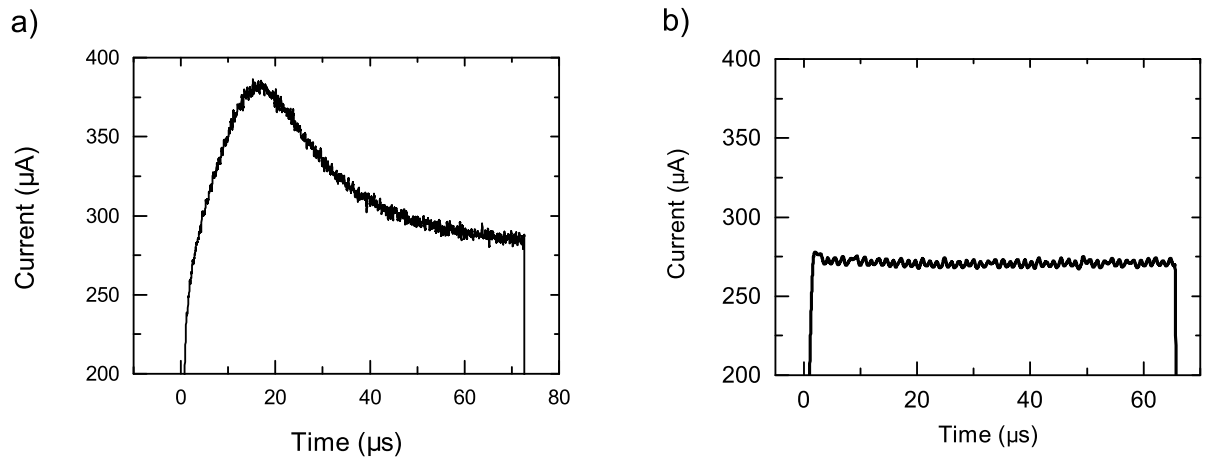

Figure 5.7: *a) Dark-CELIV current response for a freshly prepared diode with the structure ITO / PEDOT:PSS / OC_3C_8-PPV/ Ca / Al after it was exposed to air for 1-2 minutes. A distinctive extraction current signal is seen in addition to the capacitive displacement current. b) A freshly prepared diode with the same structure, measured without exposure to air. An offset voltage $U_{offset} = 2\,V$ was applied in both cases.*

In Fig. 5.6, a change in the negative discharge current after the dark-CELIV voltage ramps is observed as the extraction current increases with the proceeding doping of the polymer. This is highlighted in the enlargement on the bottom right in the figure. The sharp negative current after each CELIV ramp is the capacitive discharge current that is induced by the capacitive charges that are leaving the electrodes. Like the rise of the capacitive displacement current in the beginning of the voltage ramp, its rate is dependent on the RC time constant. Measured on the first day after preparation, the current is sharply defined without a tail. With increasing storage time, however, it develops a tail that stretches towards longer times as denoted with the arrow. The stretching increases with increasing extraction currents and thus with increasing doping. The extension of the current tail is attributed to the recovery of the doping-induced holes that were extracted from the device with the dark-CELIV voltage ramp. Their return in the polymer layer is a relatively slow process, which is reflected in the stretching of the negative current.

The attribution of the extended tail to the recovery of the doping-induced holes is supported by the behavior of a freshly prepared, undoped sample that was measured at higher offset voltages as observed in Fig. 5.4. The figure plots the extraction of charge carriers that were injected into the polymer before the dark-CELIV voltage ramp at offset voltages exceeding the built-in voltage of the sample. In this case, the negative current does not change its form as the extraction current increases; it stays sharply defined. The difference between these two measurements is based on the different origins of the exctracted charge carriers. In Fig. 5.4, charge carriers are constantly injected from both contacts before the voltage ramp that extracts them completely from the polymer. The

charge carriers are only driven into the polymer layer by injection from the contacts. In Fig. 5.6, the situation is different. The extracted charge carriers originate from doping, and are driven back into the polymer by the electric field that is initiated by the trapped electrons in the polymer as well as the gradient in the chemical potential. Their slow return is seen as the long tail of the negative current.

5.3.2 Dynamics of charges in oxygen-doped OC_3C_8-PPV

In the measurements presented in this work, the oxygen concentration in the glovebox was in the range of 1-3 ppm. The devices were stored in the glovebox in ambient light. The process of the oxygen doping of the polymer is expected to be like that reported for P3HT [117]. Directly after preparation, the sample is in an oxygen-free state. As the device is stored in the glovebox, the residual oxygen diffuses into the polymer and creates electron traps that are filled optically due to the exposure of the devices to ambient light and the following dissociation of the optically created excitons by the built-in voltage of the device. The first CELIV ramp then extracts the mobile, doping-induced holes from the polymer. After the extraction, they recover back to the semiconductor, initiated by the electric field that is created by the trapped electrons and the gradient in the chemical potential.

The recovery of the holes can be conveniently monitored with a two-pulse CELIV voltage sequence that is illustrated schematically in Fig. 5.8 a). Each dark-CELIV sequence consists of two voltage ramps. The first voltage ramp extracts the doping-induced holes from the semiconductor, and their recovery can be probed by varying the delay time t_{del} between the ramps. The time between two successive dark-CELIV sequences is 100 ms, which is long enough for the sample to reach its initial conditions. An offset voltage of 2 V is applied during the measurement, and the rate of the ramps as well as the peak-to-peak voltage are kept constant. An example of resulting current transients is plotted in Fig. 5.8 b). Shown are the current transients of two-pulse dark-CELIV sequences with different delays for an aged diode with the standard structure ITO/PEDOT:PSS/OC_3C_8-PPV/Ca/Al. The doping-induced holes are removed from the semiconductor bulk by the first voltage ramp. During the delay time between the ramps, the sample is held at the offset voltage of 2 V and the carriers are able to return to the sample. Short delay times of some tens of microseconds are not sufficiently long for the return of the charge carriers into the polymer, which is seen as very small extraction current signals in comparison to the original signal of the first ramp. As the delay time is increased, the intensity of the extraction current increases as more holes have returned into the polymer between the two voltage ramps. The strong stretching of the negative current tail that follows the voltage ramps is observed in Fig. 5.8, too, underlining its attribution to the recovery of the extracted holes. In this strongly doped sample, the tail of the negative current reaches as far as 400 μs.

The density of extracted holes is obtained by integrating the extraction current of each voltage ramp. Fig. 5.9 plots the densities of the extracted holes as a function of the delay time t_{del} between the

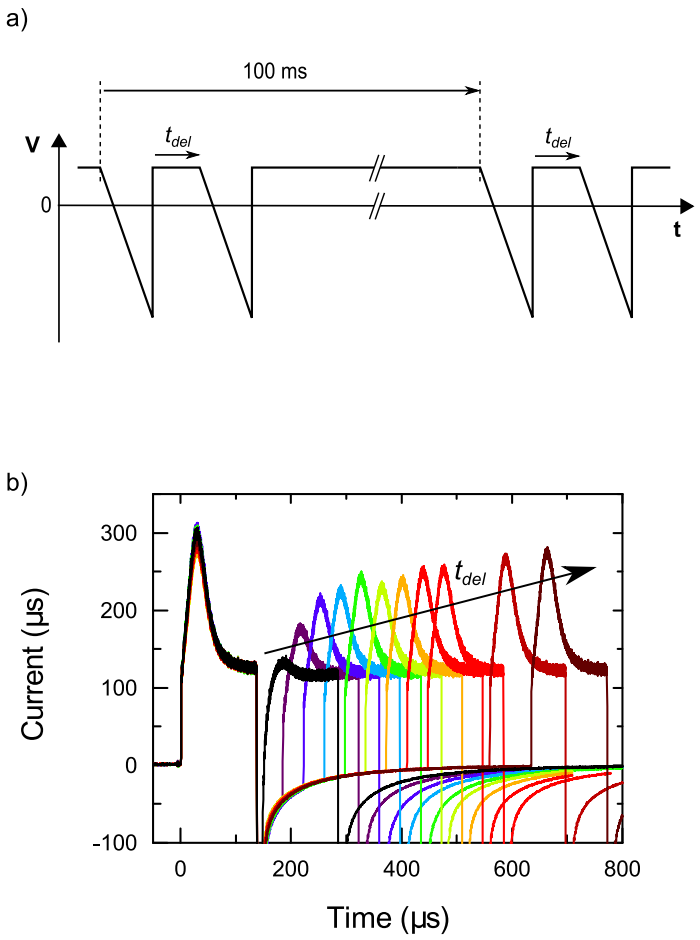

Figure 5.8: *a) Schematic illustration of the dark-CELIV method as used for the investigation of the dynamics of hole diffusion from PEDOT:PSS to OC_3C_8-PPV. b) The recovery of the equilibrium charge carriers as monitored by varying the delay time between the two dark-CELIV voltage ramps. The sample was a standard diode with the structure ITO / PEDOT:PSS / OC_3C_8-PPV/ Ca / Al that had been aged for 14 days by storing it in the glovebox. The rate of the voltage ramps was -60.1 kV/s and U_{offset} 2 V.*

two CELIV voltage ramps for two samples. The first diode was measured on the day directly after sample preparation (day 1) as well as on days 2, 5 and 8. The second diode is the one shown in Fig. 5.8 b); it was aged for 14 days before the dark-CELIV measurement. The crossed symbol at $t_{del} = 0$ s denotes the density of the holes that were extracted in the first voltage ramp, and the other ones correspond the charge that was extracted with the second ramp. The development of the doping is observed clearly as the increasing density of holes as the sample is aged after preparation. The density of the extracted mobile holes increases from $1{\cdot}10^{15}$ cm^{-3} to $7.2{\cdot}10^{15}$ cm^{-3} from day 1 to day 8; the other sample at day 14 reaches $3.4{\cdot}10^{16}$ cm^{-3}. The recovery of the extracted holes is seen on all days as the gradual increase of the charge carrier density as the delay time between the ramps is increased. The dotted lines are guides for the eye and mark the initial charge carrier densities that were extracted with the first peaks. A complete recovery of the extracted holes on days 1-8 takes

approximately 1.2 ms; the delay times for the sample measured 14 days after preparation were not long enough to recover the initial density of holes.

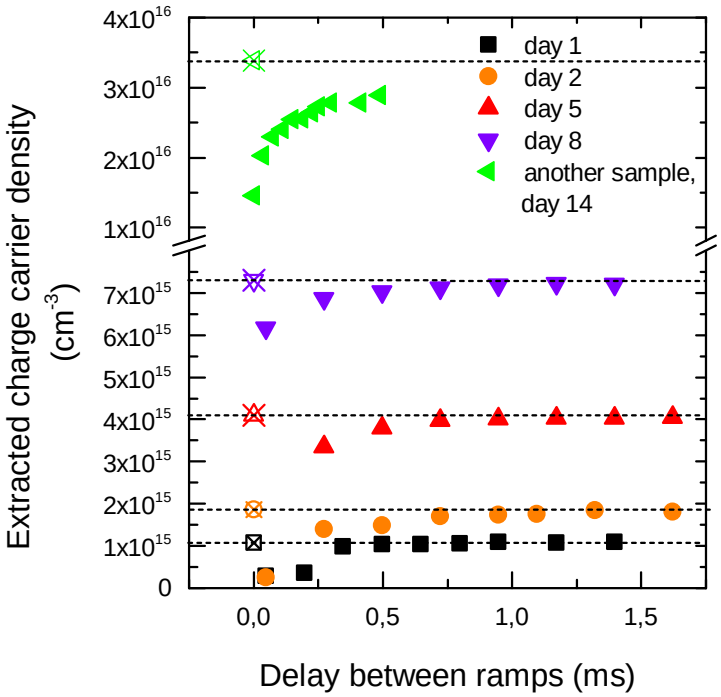

Figure 5.9: *The density of extracted holes measured on multiple days after sample preparation as a function of delay time between voltage ramps. Day 1 denotes the first day after preparation. The structure of the sample was ITO / PEDOT:PSS / OC_3C_8-PPV/ Ca / Al, the rate of the voltage ramps $U' = -60.9\,kV/s$ and $U_{offset} = 2\,V$.*

5.4 Summary

An increasing density of equilibrium charge carriers in OC_3C_8-PPV was observed as the diodes were aged by storing them in the glovebox. The carriers were identified as holes that stem from the PPV bulk and originate from p-doping by residual oxygen in the glovebox. The doping process evolved slowly during several days after sample preparation and was observed as a gradually increasing extraction current in dark-CELIV measurements. Moreover, the dynamics of the creation of steady-state conditions in a doped sample was investigated. The recovery of the extracted holes into the polymer after a dark-CELIV voltage ramp was monitored in real time by varying the delay time between the ramps. The recovery is a slow process, and it takes on the order of 1.2 ms to build up the initial density of holes after their extraction with the dark-CELIV voltage ramp.

The results presented in this chapter show that even when stored in inert atmosphere, unencapsulated PPV-based devices can suffer from oxygen exposure. The sensibility of PPV and other conjugated polymers has been addressed by the group of Blom [114] that reported on a universal oxygen-based trap level at -3.6 eV for many different conjucated polymers even in diodes that were fabricated and characterized in inert atmosphere. In general, it is possible that phenomena

that have been contributed to sole aging are in reality related to oxygen. Even a small residual concentration is enough to cause changes in the material. This possibility has to be taken into account when evaluating aging-related changes in the devices. The increasing concentration of mobile holes may have a negative influence on the efficiency of the diodes as well. Due to the imbalanced charge transport, where the mobility of holes is much higher than that of electrons, the recombination zone lies in close proximity to the cathode. Increasing the density of holes is likely to shift the recombination zone even closer to the cathode, increasing losses. In general, the finding of oxygen doping even in inert atmosphere is highly relevant for the investigations on the stability of PPV-based devices.

6 Influence of triplet excitons on device lifetime

The aim of this chapter is to investigate and clarify the role of triplet excitons in the degradation of fluorescent, PPV-based OLEDs. Despite the fact that the majority of the excitons in an OLED are triplets, the influence of these excitons on the operational stability of the devices has not been subject to widespread interest. Due to the spin-forbidden transition from the excited triplet state to the ground state, the energy of the triplet excitons cannot be released by the emission of a photon. Instead, it has to be dissipated non-radiatively, which might have consequences on the long-term stability of the diodes. In order to investigate whether the energy of the triplet excitons is harmful to the lifetime of OLEDs, the concentration of triplet excitons in the active polymer will be deliberately increased and the changes in the electronical and optical properties of the polymer films as well as in the performance and lifetime of the diodes will be subsequently monitored. It will be observed that an increased triplet exciton concentration strongly shortens the lifetime of the diodes. The phenomena that influence the accelerated degradation of the devices will then be investigated and discussed.

6.1 Background

The first generation of OLEDs, lead by the famous work by Tang and van Slyke [1], was based on fluorescent materials. Their emission originates solely from the singlet state, limiting the efficiency of the devices due to the low ratio of singlet to triplet excitons. Based on spin statistics, the fraction of singlet excitons formed is 1/4 [2, 31, 125]. However, many publications have reported larger singlet ratios for both small molecule [126] and polymer-based OLEDs [127–132]. Up to date, no consensus on the topic has been reached, although many possible mechanisms have been proposed.

Even with singlet exciton yields exceeding 25 %, the efficiency of fluorescent devices is limited due to the formation of non-emissive triplet excitons. In order to overcome this drawback, the second generation of OLEDs was introduced by the group of Stephen Forrest [133] in their work, in which they doped the fluorescent host material Alq_3 with the phosphorescent dye PtOEP. The phosphorescent, second-generation OLEDs utilize the weakening of the spin selection rules that is achieved by the incorporation of a heavy metal atom into the emitter material. The phosporescent emitters are organo-transition metal compounds. The presence of a heavy atom, typically platinum or iridium, increases spin-orbit coupling, favors intersystem crossing and allows thus transitions from the triplet to the singlet ground state. The allowed radiative transition from the triplet to

the singlet state enables the utilization of all excitons and increases the maximal internal quantum efficiency to 100 %. The progress in the field of phosphorescent emitters has been rapid; red and green phosphorescent emitters are nowadays widely used in commercial applications, and the more challenging blue emitters are also developing steadily [134].

Owing mainly to the rapid development of the phosphorescent emitters and the growing understanding of the excitonic interactions in organic materials, the triplet states in organic semiconductors have been investigated intensively in the last years [135–137]. Due to the forbidden transition to the ground state, triplet excitons in fluorescent materials reach high lifetimes on the order of several μs to ms [138, 139]. Additionally, they are formed in high concentrations because of the high triplet to singlet ratio. These factors lead to high triplet exciton densities in fluorescent materials. In recent publications, triplet excitons have been reported to participate in singlet exciton generation via triplet-triplet annihilation (TTA) [126, 140, 141] and thermally activated delayed fluorescence (TADF) [142, 143], thus contributing to the observed high singlet exciton yields exceeding the statistical limit of singlet formation. However, consequences of the high triplet densities on devices made of fluorescent materials have hardly been discussed. The influence of triplet excitons on the lifetime of the diodes has gained little attention up to date [140].

In one of the very few publications about the influence of triplet excitons on the lifetime, King et al. reported an increase in the lifetime of polyfluorene-based OLEDs when a triplet quenching additive was incorportated in the polymer matrix [140]. The triplet energy of the quenching additive lies below that of the polyfluorene, which enables the transfer of triplet excitons from polyfluorene to the quencher, thus removing them from the active polymer. The emissive singlet excitons of the polymer are not affected by the quencher, which has a higher singlet energy than the polyfluorene. The authors state that a significant part of the device emission is caused by singlets produced by triplet-triplet addition and that the triplet excitons are quenched rapidly during device operation, removing thus the TTA contribution to the emission. The lost contribution can be observed as a rapid initial decay of luminance during a lifetime test. By incorporating the triplet quenching additive to the host polymer, the fastly decaying TTA contribution is removed, which results in a higher t_{50} lifetime.

In the work of Stegmaier [144], it was found that optical stressing of unipolar devices with OC_3C_8-PPV does not lead to fatigue. During irradiation at the wavelength of peak absorption, singlet excitons are created in the polymer material. The rapidly decaying singlets alone are thus not causing degradation. However, it was found that combining the irradiation with an applied external voltage does lead to degradation of the devices. The field caused by the applied voltage dissociates the excitons, creating free charge carriers. The presence of holes was not observed to cause degradation, so possible reasons for the observed fatigue are firstly the sole presence of electrons and secondly the creation of triplet excitons. The free charge carriers can form new excitons, the majority of which are statistically triplets.

6.2 Singlet-to-triplet conversion in layers

In this work, the influence of triplet excitons on the stability of OC_3C_8-PPV-based diodes is investigated by deliberately increasing the concentration of triplet excitons in the polymer and monitoring the changes induced by the increased concentration. The higher triplet exciton concentration is achieved by increasing the ratio of triplets to singlets; in order to achieve this, a triplet sensitizer molecule has to be blended into the polymer matrix. This approach was first introduced by Laquai et al. [145] in their work with Superyellow-PPV, in which they, for the first time, showed intrinsic phosphorescence from a PPV derivate. The presence of the sensitizer in the matrix leads to a partial conversion of polymer singlet excitons to triplets and enables the investigation of the increased triplet-to-singlet ratio.

In an optimal case, the investigation would be completed by the use of a triplet quencher as in the work of King et al. [140] in order to monitor the consequences of both an increased and a decreased fraction of triplet excitons. However, it was not successful to find a suitable commercial quencher material that would meet the energetic requirements. For quenching the triplets on the host polymer, the triplet state of the quencher has to lie below that of the polymer. In addition, because the fluorescence of the host should stay unaffected, the quencher must have a higher singlet state. The combination of the low lying triplet state of OC_3C_8-PPV and the generally high energetical difference between the triplet and the singlet states of conjugated polymers [146] made the search for a suitable quencher very challenging.

The principle of singlet-to-triplet conversion can be seen in Fig. 6.1 and is explained in the following. The triplet sensitizer is a phosphorescent organometallic compound PtOEPK (platinum (II) octaethylporphyrine ketone), and its first excited singlet state lies energetically lower than that of the host polymer so that a singlet energy transfer from the polymer to the sensitizer can take place. For the transfer of singlet excitons, a Förster-type transfer [28] normally dominates [147]. The Förster transfer is a long-range process of dipole-dipole coupling of donor and acceptor molecules. The transitions between ground and excited states have to be allowed for both the donor and the acceptor; therefore, only singlet excitons can be transferred via the Förster mechanism.

As a requirement for an efficient transfer, the absorption spectrum of the sensitizer has to overlap with the emission of the polymer [28]. The absorption and photoluminescence spectra of OC_3C_8-PPV and PtOEPK are plotted in Fig. 6.2. OC_3C_8-PPV shows broad spectra for both absorption and emission that overlap at around 580 nm. The absorption maximum lies at 506 nm, whereas the emission peaks at 630 nm. The absorption spectrum of PtOEPK is typical for porphyrin derivates [76]. It consists of a strong transition to the second excited state at 403 nm, called the Soret band, and of the Q band at 599 nm, which is the transition to the first excited state. The PtOEPK emission at 758 nm is attributed to phosphorescence [75]. There is a good overlap between the polymer emission and the Q band absorption of the PtOEPK, fulfilling the requirement for singlet energy transfer.

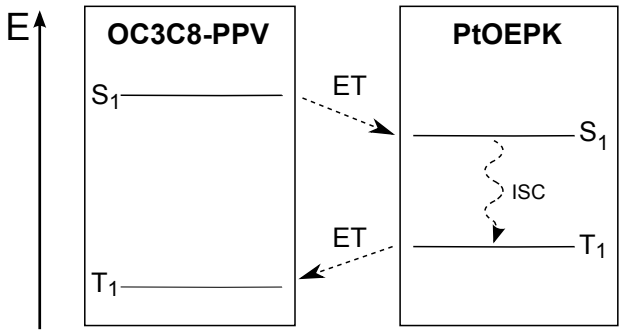

Figure 6.1: *Energy scheme showing the singlet-to-triplet conversion processes. First, a singlet exciton energy transfer (ET) from OC_3C_8-PPV to PtOEPK takes place, followed by an intersystem crossing (ISC) to the PtOEPK first excited triplet state. The triplet exciton is subsequently transferred to OC_3C_8-PPV, which has an energetically lower first excited triplet state.*

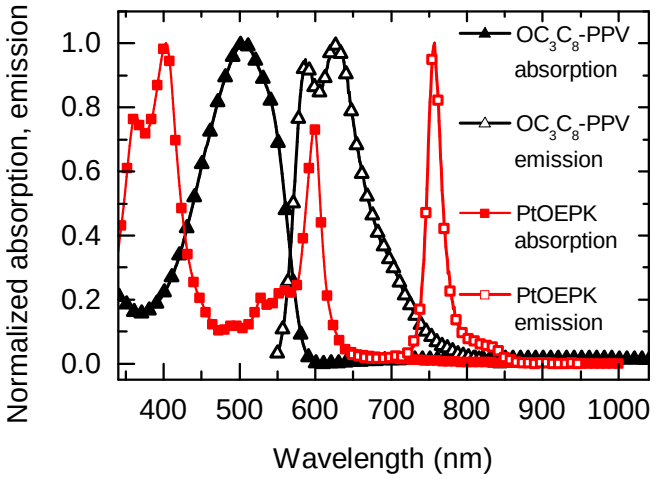

Figure 6.2: *Absorption and emission spectra of OC_3C_8-PPV and PtOEPK (both in solid state). OC_3C_8-PPV was excited at 506 nm and PtOEPK at 399 nm.*

Once the singlet excitons have been transferred to the sensitizer, they undergo a fast and efficient intersystem crossing (ISC) to the triplet state allowed by the presence of the platinum atom in PtOEPK. The heavy platinum increases spin-orbit coupling and weakens the spin selection rules, making transitions between singlet and triplet states allowed. These are generally efficient on organometallic phosphors and the probability for intersystem crossing in these materials is reported to be high (>99 %) [147]. The lowest triplet state of PtOEPK lies energetically higher than that of the polymer, which enables a triplet exciton transfer from the sensitizer back to the polymer. Triplet exciton transfers are generally of Dexter type [29]. A Dexter transfer, also called exchange transfer, is a short range process in which excitons diffuse from donor to acceptor via intermolecular exciton exchange. The Dexter processes only require that the total spin of the donor-acceptor pair is conserved, allowing thus both singlet-singlet and triplet-triplet transfers.

When the triplet excitons have been transferred from the sensitizer to the polymer, the complete singlet-to-triplet conversion as illustrated in Fig. 6.1 has taken place. Blending the polymer with small concentrations of the sensitizer increases the fraction of triplet excitons on the polymer. The extent of the conversion is dependent on the concentration of the sensitizer in the polymer host. Small sensitizer concentrations are desired in order to minimize the effects on charge transport on OC_3C_8-PPV; in this work, concentrations of 0.1 and 1 wt% PtOEPK were used.

The quality of the polymer films was investigated with optical microscopy and scanning electron microscopy (SEM), Fig. 6.3. Overall, both pristine and sensitized OC_3C_8-PPV films had an even appearance. The SEM pictures showed no structures on the films, and no PtOEPK clusters were identified. No Pt could be detected with energy-dispersive X-ray spectroscopy (EDX) on a sample with 1 wt% PtOEPK. The pristine OC_3C_8-PPV layer is shown in Fig. 6.3 a). The vertical stripes are due to the charging of the polymer during the measurement and are no structures on the layer itself. The images in the middle and on the right are OC_3C_8-PPV:PtOEPK (1 wt%). The spots in Fig. 6.3 b) are most likely dust particles on top of the polymer layer. In Fig. 6.3 c), a close-up of the layer is seen. In the bottom of the substrate, the polymer layer was scratched away from the ITO substrate; the substrate is seen as the lighter area in the image. The single particle on the polymer layer is probably a dust particle.

Fig. 6.4 a) plots the absorption spectra of pristine OC_3C_8-PPV, sensitized OC_3C_8-PPV layers with 0.1, 1 and 5 wt% PtOEPK and pristine PtOEPK. The spectrum of the sensitized sample with the lowest concentration of PtOEPK is identical with the spectrum of pristine OC_3C_8-PPV. With 1 wt% sensitizer concentration, the PtOEPK Soret peak starts to appear weakly at 400 nm. The sample with 5 wt% PtOEPK shows features of PtOEPK Soret and Q bands at 400 and 598 nm, respectively. These are shown magnified in Fig. 6.4 b) and c).

Changes in the population of the first excited singlet state of OC_3C_8-PPV and thus the exciton transfer between the polymer and the sensitizer can be investigated with steady-state photoluminescence. Photoluminescence spectra of pristine and sensitized OC_3C_8-PPV films with 0.1 and 1 wt% PtOEPK are plotted in Fig. 6.5 a). The spectra are all normalized to the optical density of the films to ensure that the photoluminescence intensities are compared correctly. All samples were excited at 506 nm, which is the peak wavelength of OC_3C_8-PPV absorption. Due to the negligible absorption of PtOEPK at this wavelength, only the polymer is excited. The photoluminescence intensity of OC_3C_8-PPV decreases when the polymer is blended with 0.1 wt% PtOEPK. When the concentration is increased to 1 wt%, a further strong decrease in luminescence intensity is observed. This points to a lowered population of the excited singlet state in the polymer induced by the presence of PtOEPK and the resulting transfer of singlet excitons from the polymer to PtOEPK.

The shape of the photoluminescence spectra does not change considerably upon blending of PtOEPK with the polymer, as can be seen in the normalized spectra in Fig. 6.5 b). This indicates that the presence of PtOEPK in OC_3C_8-PPV does not induce large-scale morphological changes in the polymer. Additionally, no features from the phosphorescence of PtOEPK at 758 nm can be observed in

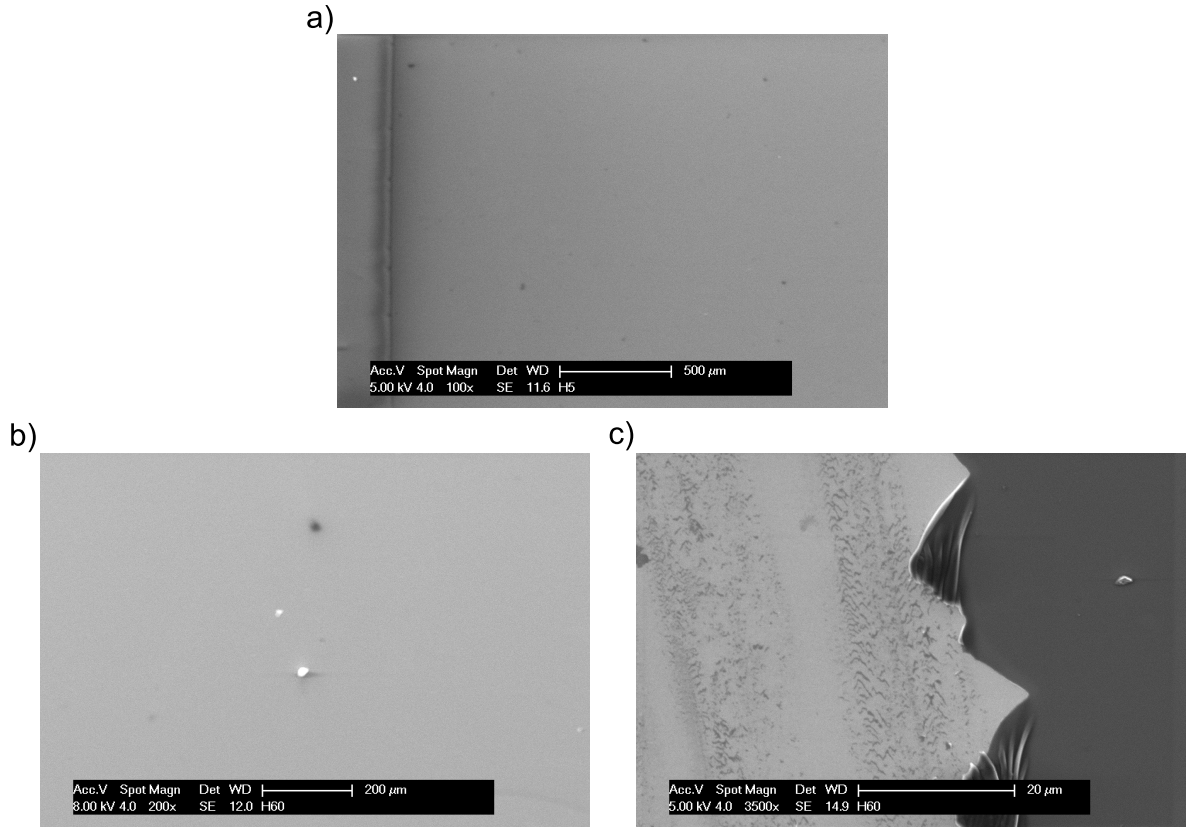

Figure 6.3: *SEM images of polymer films on ITO substrates. a) pristine OC_3C_8-PPV. The two vertical stripes on the left are caused by the charging of the polymer film during the measurement. b) and c): OC_3C_8-PPV:PtOEPK (1 wt%). The white spots in the middle picture are presumably dust particles on top of the layer. In c), the lighter area is the ITO substrate, on top of which the polymer layer was scratched away. The single particle on the polymer is likely to be a dust particle.*

.

any of the samples. Due to the efficient intersystem crossing on PtOEPK, in addition to the observation that the molecule emits solely through phosphorescence [75], it can be assumed that an intersystem crossing to the triplet state takes place as soon as the singlet excitons have been transferred to PtOEPK. Because of the complete lack of phosphorescence from the porphyrin sensitizer, it can further be concluded that a triplet exciton transfer from the sensitizer back to the polymer host is very likely to take place.

Because of the invisibility of the triplet states of conjugated polymers in direct spectroscopic measurements, their generation and decay has most often been investigated with indirect techniques like photoinduced absorption (PIA) [148–151]. In this work, the technique was used to examine the transfer of triplet excitons between OC_3C_8-PPV and PtOEPK and the resulting change in the triplet exciton population in OC_3C_8-PPV. The samples were excited at the pump light wavelength of 524 nm. Because of the low absorption of PtOEPK at this wavelength, only OC_3C_8-PPV is excited.

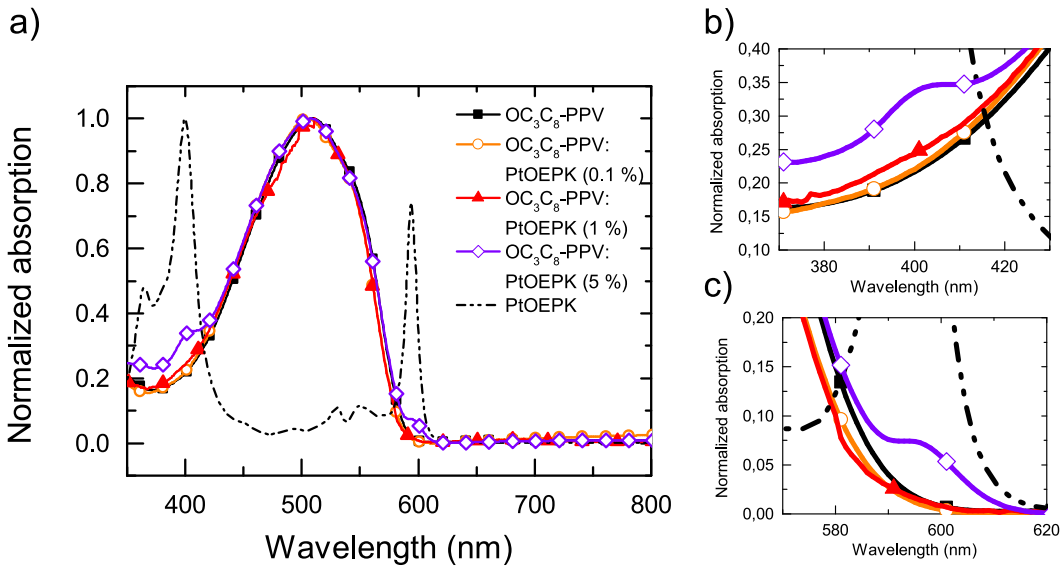

Figure 6.4: *a) Absorption spectra of pristine and sensitized OC_3C_8-PPV films as well as pristine PtOEPK. The thickness of the polymer films was 130 nm. b) Magnification of the PtOEPK Soret band area that is visible in the absorption of the sample with 5 wt% PtOEPK. c) Magnification of the PTOEPK Q band area, also visible in the absorption of the sample with 5 wt% PtOEPK.*

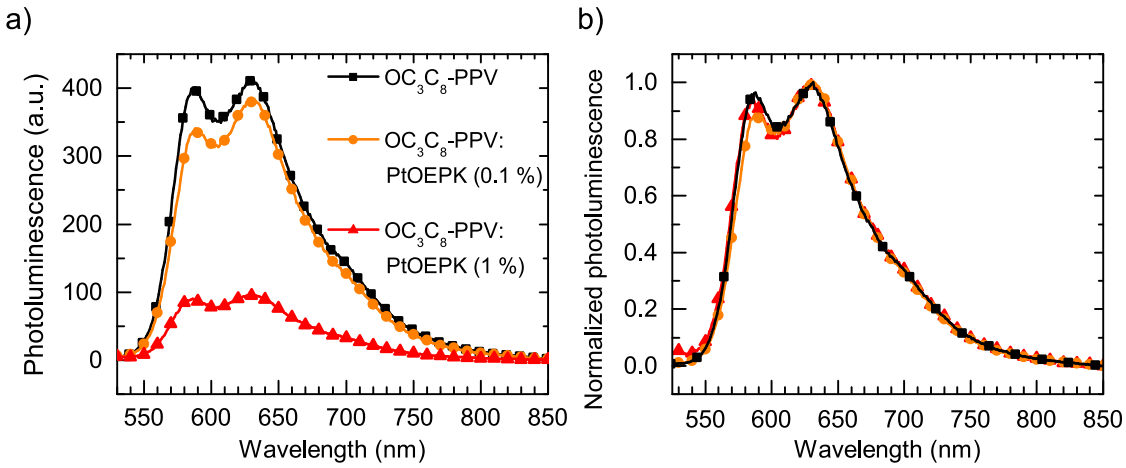

Figure 6.5: *a) Steady-state photoluminescence spectra of pristine and sensitized OC_3C_8-PPV layers. All films had a thickness of 130 nm. The excitation wavelength of 506 nm (the peak wavelength of OC_3C_8-PPV absorption) ensured the sole excitation of OC_3C_8-PPV, because PtOEPK does not absorb significantly at this wavelength. The spectra are normalized to the optical density of the samples. b) The spectra are normalized to the photoluminescence maximum.*

The PIA spectra of a pristine OC_3C_8-PPV layer as well as a sensitized layer with 1 wt% PtOEPK are plotted in Fig. 6.6. The spectra are normalized to the optical density of the samples.

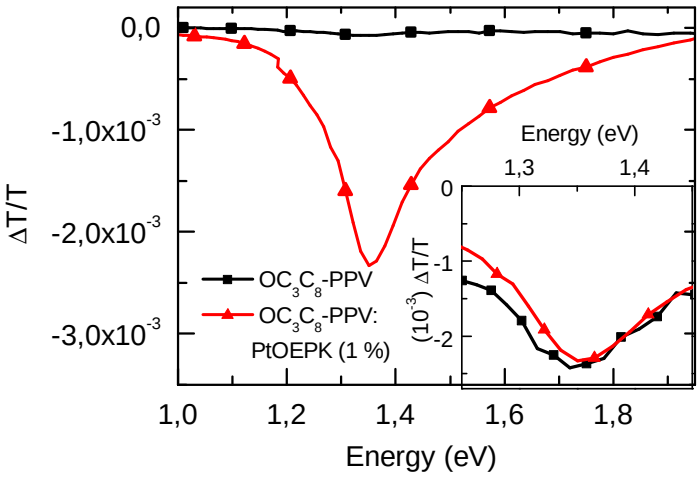

Figure 6.6: *Photoinduced absorption spectra of a pristine as well as 1 wt% sensitized OC_3C_8-PPV layers. The samples were excited with a pump wavelength of 524 nm that excites only OC_3C_8-PPV. Inset: the PIA spectrum of pristine OC_3C_8-PPV scaled with a factor of 32 together with the unscaled spectrum of the sample with 1 wt% PtOEPK for a better comparison of the shape and energetic position of the curves.*

In both spectra, an absorption band at 1.35 eV is observed. This absorption is generally attributed to the $T_1 \rightarrow T_n$ absorption of PPV derivates [152–154]. The excited triplet state absorption is very weak in the pristine OC_3C_8-PPV, which can be explained with the low intersystem crossing yield of PPV derivates [155, 156]. In the 1 % PtOEPK sensitized PPV sample, however, a considerable increase in PIA intensity is observed at 1.35 eV. The inset in Fig. 6.6 shows the spectrum of the pristine OC_3C_8-PPV film scaled with a factor of 32 together with the unscaled spectrum of the 1 wt% sensitized layer in order to enable the comparison of the shapes and positions of the absorption bands. No considerable changes in spectral shape are observed when OC_3C_8-PPV is blended with PtOEPK. The energetic position of the absorption band does not shift with the incorporation of PtOEPK in the polymer matrix, which indicates the same transition in both pristine and sensitized polymer layers. It is concluded that the presence of PtOEPK leads to a higher population of the lowest excited triplet state in the host OC_3C_8-PPV, as illustrated in the schematic Fig. 6.1.

Based on the results presented above, it can be concluded that the complete singlet-to-triplet conversion route does take place. The decrease in the population of the excited singlet state in OC_3C_8-PPV is observed in the photoluminescence spectra in Fig. 6.5, and the following increase in the triplet concentration can be seen in the photoinduced absorption measurements (Fig. 6.6). Additionally, no PtOEPK phosphorescence is detected in the OC_3C_8-PPV:PtOEPK samples, pointing to the absence of triplet excitons on the sensitizer molecule.

6.3 Increased triplet exciton concentration in OLED devices

After the introduction of the singlet-to-triplet conversion route and the observation that the OC_3C_8-PPV singlet excitons are successfully converted to triplets by blending PtOEPK with the polymer, the influence of the increased population of the excited triplet state on the operation of real OLED devices will be investigated. For this, diodes with pristine OC_3C_8-PPV as well as different concentrations of PtOEPK were prepared and examined in virgin state through I-V-L characteristics and electroluminescence as well as during prolonged operation in lifetime measurements. A substantial reduction in lifetime will be observed for devices with sensitized OC_3C_8-PPV layers. Additionally, the behavior of single-carrier devices during prolonged operation will be presented with the aim to monitor the differences between unipolar and bipolar charge transport in the presence of excitons. The influence of the sole presence of PtOEPK on the long-term degradation of the bipolar, sensitized diodes will be ruled out.

6.3.1 Bipolar devices

The performance of diodes with pristine as well as sensitized OC_3C_8-PPV layers with 0.1 and 1 wt% PtOEPK is presented in the I-V-L characteristics plotted in Fig. 6.7. The structure of the devices was ITO / PEDOT:PSS / PPV / Ca / Al. There are only minor differences in the current densities between samples with pristine and sensitized OC_3C_8-PPV layers. The current densities of sensitized samples are slightly lower at high operating voltages in comparison with the pristine diodes. The difference is, however, not large. In addition, the current densities of samples with PtOEPK are virtually equal regardless of its concentration. This implies that incorporating PtOEPK into the host polymer disturbs neither the injection of charge carriers nor their transport. This applies especially to holes because OC_3C_8-PPV is a strongly hole-dominated material and holes are the main contributor to the current. The current onset of all diodes lies approximately at 2 V, which is an indication for unchanged injection properties between pristine and sensitized devices.

In contrast to the current density, a more significant change is observed in the luminance of the diodes. The luminance decreases with increasing PtOEPK concentration, which is in accordance with the decreasing photoluminescence intensity of the sensitized samples. The difference between pristine devices and those with 1 wt% PtOEPK is about 1 order of magnitude during essentially the whole operation range from approximately 2 V to 12 V. The lower emission intensity of the devices with PtOEPK can be attributed to the decreased population of PPV the first excited singlet state, induced by the transfer to the singlet state of PtOEPK.

Having noted that the conversion of singlet excitons to triplets does take place both in films and real OLED devices, the influence of such additional triplet excitons on the lifetime of the diodes is of high interest. In order to find out whether the degradation of the OC_3C_8-PPV-based diodes is affected by the introduction of the singlet-to-triplet conversion, the development of luminance as well as of

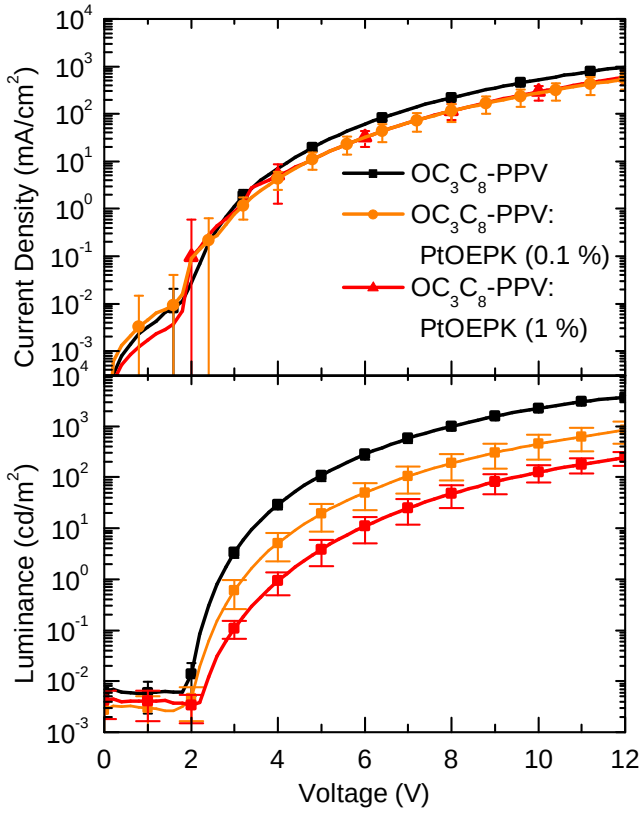

Figure 6.7: *Current density and luminance of diodes with pristine and sensitized OC_3C_8-PPV layers. The characteristics are averaged from 16-20 single devices for each concentration.*

operating voltage was monitored during prolonged operation. The left side of Fig. 6.8 plots the voltage and the luminance against operational time for diodes fabricated of pristine OC_3C_8-PPV as well devices that were blended with 0.1 and 1 wt% PtOEPK. As the lifetime of the pristine samples is much longer than that of the sensitized ones, the curves for the pristine OC_3C_8-PPV are displayed in full length on the right-hand side of the graph. The samples were all operated at a constant current of 50 $\mathrm{mA/cm^2}$. The fatigue of the diodes is seen in the decrease of the luminance with increasing operation time as well as in the rise of the operating voltage. The starting value of the operating voltage of the pristine samples is 4.7 V; the sensitized samples with 0.1 and 1 wt% PtOEPK start at higher values at 6.34 and 6.71 V, respectively, indicating an increase in device impedance. The increase in the starting values of the operating voltage is in accordance with the current-voltage characteristics that showed decreased current densities for both sensitized samples.

The luminance values are normalized in order to allow a better comparison of the curves; the absolute values are shown in the inset. The absolute initial luminance (L_0) decreases with increasing PtOEPK concentration, as already observed in the luminance-voltage characteristics as depicted in Fig. 6.7 as well as in the photoluminescence spectra (Fig. 6.5). This decrease of the initial

luminance illustrates again the lower population of the first excited singlet state of OC_3C_8-PPV when the polymer is blended with PtOEPK.

The 50 % luminance is marked in the graph with the green dotted line to emphasize the t_{50} lifetime of each material. The pristine samples reach the t_{50} after approximately 160 h. Blending the polymer with 0.1 wt% PtOEPK reduces the lifetime to 15 h, which corresponds to a decrease of 91 %. If the concentration of PtOEPK is increased to 1 wt%, the lifetime drops to 2 h. This equals a decrease of 99 % from the lifetime of the devices with pristine OC_3C_8-PPV layers.

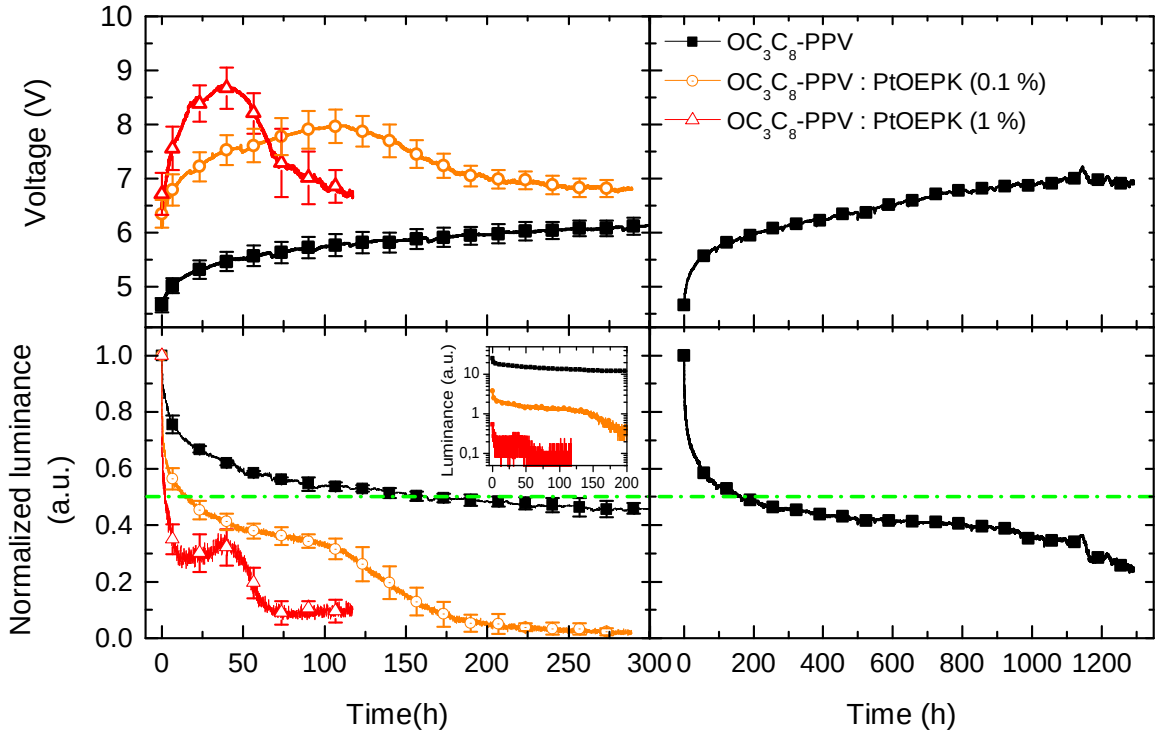

Figure 6.8: *Left: Voltage and luminance versus time plots of diodes with pristine and sensitized OC_3C_8-PPV layers illustrating the deteoriation of the t_{50} lifetime with increasing PtOEPK content. The inset shows the measured absolute values of luminance. Right: Voltage and luminance versus operating time for pristine OC_3C_8-PPV plotted in full length.*

All diodes show a rapid initial decrease of luminance that levels out to a more moderate, plateau-like region with a lower, gradual degradation rate as often observed for small-molecule and polymer-based OLEDs [36, 38, 105, 140]. Interestingly, in the present measurements the degradation accelerates again after the plateau and the plateau region of the samples with 1 wt% PtOEPK even involves a slight increase of luminance intensity. This late acceleration of luminance decrease is present in the samples with pristine OC_3C_8-PPV as well, where the kink in luminance at approximately 900 h is well visible. The non-monotonic evolution of luminance has been observed earlier for PPV derivates [156–158] but to the best of the author's knowledge no explanation on the reason has been found yet. In literature there are not many reports on the reacceleration of the degradation

after the plateau. However, it should be noted that in the results presented above, the accerelated decay of luminance following the plateau begins well after the t_{50} for all samples. Since it is common practice to operate especially long-lived diodes only to t_{50} or an earlier stage and extrapolate the measured values in order to obtain a value for the lifetime, behavior like observed here is likely to stay undocumented. It cannot therefore be said that it does not occur for other materials as well.

It is noteworthy that the second acceleration in luminance degradation is accompanied by a change in voltage evolution. In the beginning of the measurement, the operating voltage of all samples increases rather monotonically. The rise is approximately mirrored to the decrease of luminance, being rapid in the beginning and decelerating as the operation proceeds. As the luminance starts to decrease more rapidly, the rise of the voltage stops and it then begins to decline. This behavior is clearly visible for both concentrations of PtOEPK as well as for the pristine polymer. The time scale of the fatigue of the pristine OC_3C_8-PPV is so long that the complete degradation of the devices was not recorded before the operation of the samples was stopped after 1300 h.

A possible explanation for the observed phenomenon is the formation of preferred current paths in the devices. These could be formed by hot spots, for example. The conductivity in the hot spots is higher than in the rest of the film, leading to locally increased temperature. The increased conductivity causes a higher current density, accompanied by a decreased operating voltage. The lower voltage would cause the observed reduced luminance. The evolution of device temperature during operation is discussed in Section 6.3.3.

In order to investigate possible morphological changes in the polymer film during fatigue as well as the stability of the singlet-to-triplet conversion route, the electroluminescence of a diode with pristine OC_3C_8-PPV as well as of a sensitized sample with 1 wt% PtOEPK was monitored during operation. Fig. 6.9 plots the electroluminescence spectra that were recorded stepwise during operation at a constant current density of 50 $\mathrm{mA/cm^2}$. The diode with pristine OC_3C_8-PPV was driven for 280 and the one with a sensitized layer for 73 hours total; by the end of the operation, the luminance of both samples had fallen to well below 50 % of the initial value. The spectra are normalized to the maximum of the electroluminescence, which allows for the comparison of their shape.

The electroluminescence spectra consist of three overlapping peaks. As mentioned in Section 3.1, the peaks originate from morphological differences in the OC_3C_8-PPV film [10, 72–74, 159]. According to present knowledge, the high-energy peak corresponds to the 0-0 transition that stems from a single-chain chromophore, whereas the peaks at higher wavelengths are caused by aggregated parts of the polymer [72–74]. In pristine OC_3C_8-PPV in Fig. 6.9 a), no systematic changes are observed. There are small fluctuations in the intensity of the low-energy shoulder but they do not develop consequently in one direction as the sample degrades.

In the sample with 1 wt% PtOEPK (Fig. 6.9 b), the relative intensities of the peaks are observed to change chronologically with operation time; the sample was operated for 73 h total. The peak at 689 nm grows rather significantly, whereas the high-energy shoulder loses intensity. The largest

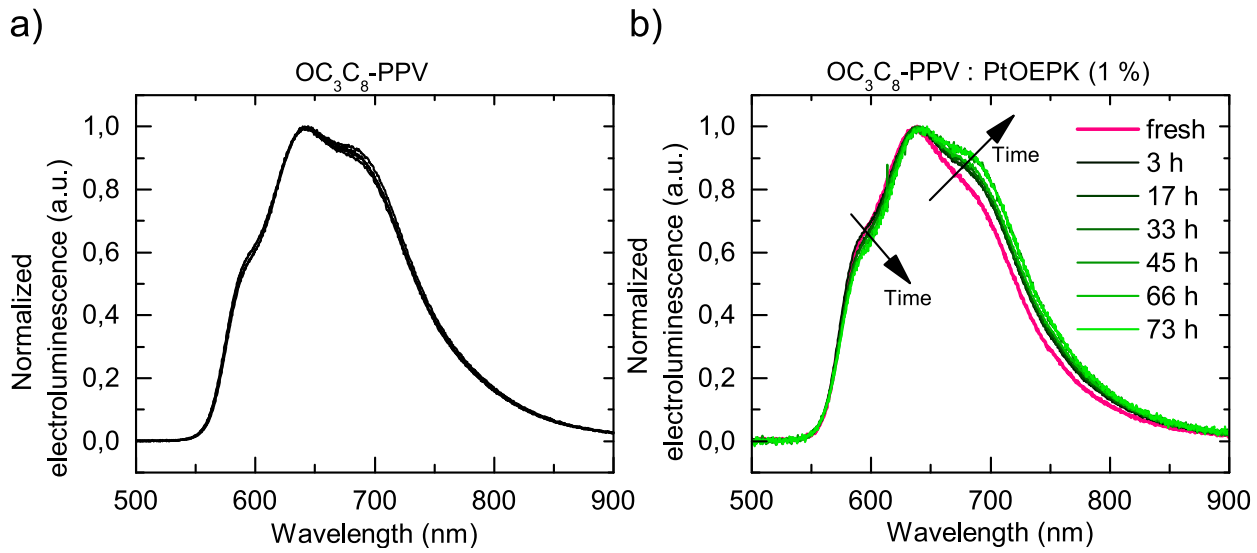

Figure 6.9: *Electroluminescence spectra of a diode with pristine OC_3C_8-PPV (a)) and 1 wt% PtOEPK (b)) recorded stepwise between operation steps at a constant current density of 50 mA/cm^2.*

change takes place immediately within the first three hours of operation, which is in accordance with the fast degradation of the 1 wt% PtOEPK-sensitized devices in the lifetime measurement in Fig. 6.8. Knowing that the peaks originate from morphological differences, the observed change in the relative intensities can be attributed to changes in the polymer layer. During operation, the temperature in the polymer film increases, which leads to small-scale motion of the polymer chains and changes the preferred origin for emission. The increase of the intensity of the low-energy shoulder indicates that the electronic transition from the agglomerated part becomes more favored. It will be shown in Section 6.3.3 that the operation temperature of PtOEPK-sensitized diodes is higher than that of devices with pristine OC_3C_8-PPV. In addition to the changes in the relative intensities of the peaks of OC_3C_8-PPV electroluminescence, one should note that no features of PtOEPK emission at 758 nm start to appear with operation time as the diode fatigues. This indicates that the exciton conversion route between the host OC_3C_8-PPV and guest PtOEPK is not affected by the prolonged operation or the degradation of the device.

6.3.2 Unipolar devices

After observing that sensitizing OC_3C_8-PPV with the singlet-to-triplet converter PtOEPK and the thus increased ratio of triplet excitons to singlets leads to a drastic decrease in the t_{50} lifetime of the diodes, the impact of PtOEPK on purely hole- and electron-related processes and the transport of charges without the presence of excitons is investigated. For this aim, single-carrier devices with pristine and sensitized polymer layers were prepared. Comparison of the temporal evolution of the operating voltage between bi- and unipolar devices allows one to separately evaluate the impact of hole- and electron transport on the degradation. In addition, the influence of the presence of PtOEPK on the stability of charge transport can be examined. Because there are no excitons

present in unipolar devices, their influence on device behavior can be excluded. If differences in the temporal evolution of the voltage were observed between pristine and sensitized devices, it could be concluded that the incorporation of PtOEPK as such in OC_3C_8-PPV has an influence in the long-term behavior of the devices.

Like the bipolar diodes, also the single-carrier devices were prepared with three different polymer layers: the pristine OC_3C_8-PPV and the sensitized polymer with 0.1 and 1 wt% PtOEPK. The results are averaged from 16-20 samples. The structure of the hole-only devices was ITO / PEDOT:PSS / OC_3C_8-PPV/ Au. They are identical to the bipolar diodes with the only exception that Au was used as the top electrode. The replacement of Ca that was used in the bipolar samples with Au leads to purely unipolar charge carrier injection due to the high energy barrier for electrons on both contacts. The unipolar charge transport is manifested by the abscence of light emission from the hole-only devices.

Fig. 6.10 displays the current-voltage characteristics of the hole-only devices. Similarly to the bipolar devices, no significant differences in the current densities between sensitized and pristine OC_3C_8-PPV can be observed. However, it is noteworthy that the samples with 1 wt% PtOEPK have slightly higher current densities at voltages higher than 3 V. At negative voltages the differences between the samples are within the error bars. In general, the current-voltage characteristics are not symmetric. The current is significantly higher at positive voltages, i.e. during the injection of holes from PEDOT:PSS. The injection from Au seems to be less efficient, which might be due to a work function difference between PEDOT:PSS and Au as well as to the formation of an interface dipole between the gold and polymer layers. A dipole of 1.09 eV has been reported at the Au / MEH-PPV interface [160], increasing the injection barrier for holes rather significantly. Concerning this result it should be noted, however, that the value for the interface dipole was derived during the deposition of MEH-PPV on Au, which is the opposite to the present situation with Au as the top contact. The deposition sequence is of great importance for the energy level alignment at the interfaces. Additionally, the result was obtained on contamination-free interfaces prepared in-situ in UHV conditions. Contaminations in the form of gas adsorbates at the interfaces between metal electrodes and organic materials are known to decrease the interface dipoles [84].

Due to the absence of excitons and therefore also light emission in single-carrier devices, it is not possible to define a t_{50} lifetime like it is done for bipolar light-emitting diodes. The only possibility for comparisons between different devices is therefore offered by the development of the operating voltage during prolonged driving of the devices. The temporal evolution of operating voltage is plotted in Fig. 6.11. Similarly to the bipolar diodes, the hole-only devices were operated at a constant current density of 50 $^{mA}/_{cm^2}$. The devices were operated for 160 h, which corresponds the t_{50} lifetime of the bipolar diodes with a pristine OC_3C_8-PPV layer. All hole-only devices show an initial rapid decrease in operating voltage, which is followed by a slower, slight increase with operation time. The initial drop of ca. 0.5-0.8 V is possibly caused by the relaxation of the samples in the beginning of the operation. As seen in the figure, the evolution of the operating voltage of the devices with both sensitizer concentrations (0.1 and 1 wt% PtOEPK) is essentially identical, the only

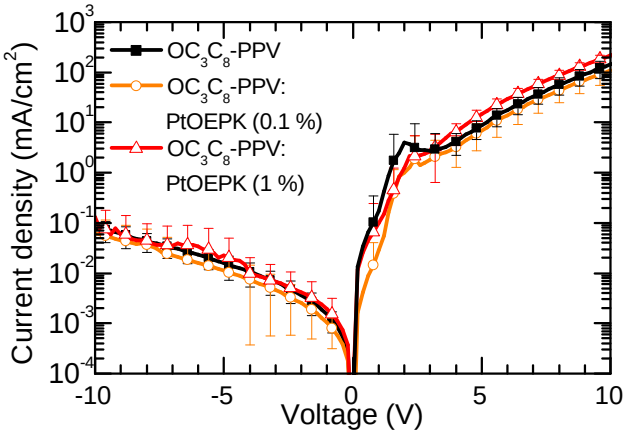

Figure 6.10: *Current-voltage characteristics of hole-only devices with pristine and sensitized OC_3C_8-PPV layers.*

difference being observed in the starting values of the voltage. The voltage rises approximately 0.5 V during the recording time of 160 h. The devices with pristine OC_3C_8-PPV layers exhibit a slightly higher voltage increase of ca. 0.7 V, but the overall behavior of the sample is very similar to that of the samples with sensitized layers. As the deviation between all samples of each batch is large (note the error bars), the difference between pristine and sensitized samples cannot be considered significant. The presence of PtOEPK does not induce substantial changes in the temporal evolution of the hole transport as seen in the lifetime measurements of bipolar samples.

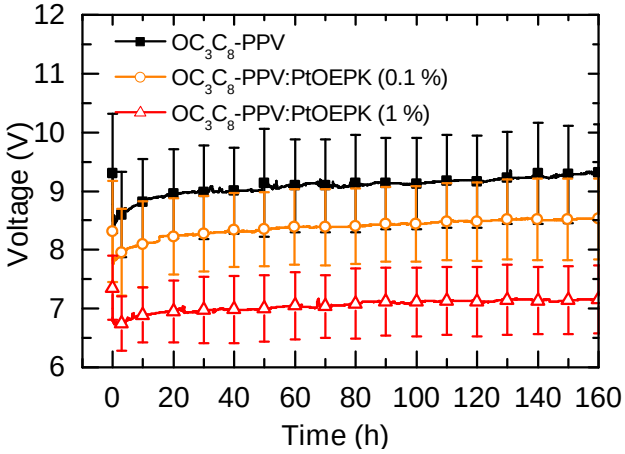

Figure 6.11: *Temporal evolution of the operating voltage of hole-only devices with pristine (black rectangles) and sensitized OC_3C_8-PPV layers with 0.1 (orange circles) and 1 wt% PtOEPK (red triangles). The devices were operated with a current density of 50 mA/cm^2.*

However, the absolute operating voltage is influenced by PtOEPK. The voltage of the devices decreases with increasing PtOEPK concentration, varying from ca. 8.5 V (devices with pristine OC_3C_8-PPV films) to around 7 V for devices with 1 % PtOEPK. This behavior was not observed for the

bipolar diodes; there, the current densities of sensitized devices were slightly lower than what was observed for diodes with pristine OC_3C_8-PPV films (see Fig. 6.7), which resulted in higher voltages for sensitized samples (Fig. 6.8). The presence of PtOEPK seems to be beneficial for the transport of holes or their injection. Doping as a cause for the effect can most likely be excluded, as the LUMO of PtOEPK lies well above the OC_3C_8-PPV HOMO. In p-doping, the dopant accepts an electron from the matrix, meaning that its LUMO should lie at the same energy or below the HOMO of the host material. The HOMO and LUMO levels of PtOEPK are not known in literature, but the energy levels of the very similar PtOEP can be used as a reference. Depending on the source, the HOMO and LUMO levels of PtOEP are reported to lie at 5.3 and 2.8 - 3.2 eV, respectively [77, 161]. The energy gap of PtOEP is 0.2 - 0.3 eV larger than that of PtOEPK, meaning that the HOMO, the LUMO or both of PtOEPK are slightly shifted with respect to PtOEP. As the OC_3C_8-PPV HOMO lies at 5.2 eV, the possibility of p-doping can be excluded. A speculative contribution for the enhanced transport of holes could be a PtOEPK-influenced change in the orientation of the polymer chains that would improve the overlap of the HOMO orbitals of OC_3C_8-PPV. Considering the injection of holes, the contact between PEDOT:PSS and OC_3C_8-PPV is taken as ohmic due to the aligned work function of PEDOT:PSS and the PPV HOMO (both 5.2 eV). An ohmic contact has also been reported for the interface PEDOT:PSS / MEH-PPV [162, 163]. The injection is not likely to be enhanced by the presence of PtOEPK. The final reason for the decreased operating voltage in sensitized devices cannot be explained with present knowledge.

In addition to the investigation of the transport of holes, which are the main charge carriers in these devices [164, 165], electron-only devices were prepared as well. Their structure was Al/LiF/OC_3C_8-PPV/Ca/Al; the difference to the bipolar diodes is the LiF/Al bottom contact. LiF/Al was chosen as the bottom electrode instead of Ca because of its higher stability: electron-only devices with a Ca bottom electrode are generally difficult to prepare reliably. The Ca film is easily damaged when a polymer layer is spin coated on it, which would make the evaluation of long-term measurements difficult as differences might be caused by Ca layers oxidized to different extents. The work function of LiF/Al has been reported to be 2.89 eV when a 1 nm thick LiF layer was used [87]. This value is very similar to that of Ca (2.9 eV). The high barrier for holes on both contacts ensures the unipolar injection of electrons.

The charge transport in PPV derivates is generally hole-dominated and the electron mobility is limited by the presence of deep traps [164]. This results in low current densities for electron-only devices. Additionally, neither the current-voltage characteristics nor the temporal evolution of the operating voltage are as smooth as for the bipolar and hole-only devices. The current-voltage characteristics of electron-only devices with pristine and sensitized OC_3C_8-PPV films are plotted in Fig. 6.12. The current densities are up to two orders of magnitude lower than those of hole-only or bipolar devices. Despite the stable LiF/Al bottom electrode, the variation between devices is rather significant especially at negative voltages (injection from LiF/Al). The rectification in the electron-only devices is smaller than in the bipolar ones, which is due to the more symmetric contacts. In the electron-only devices, the current densities are higher at positive voltages, indicating a more efficient

electron injection from the Ca top contact. This can be explained with the less than optimal electron injection injection capacity of a LiF/Al bottom electrode when LiF is deposited on Al [166]. The current density of the samples with 0.1 wt% PtOEPK is generally higher than those of the two other devices. At high positive voltages the devices with 1 wt% PtOEPK reach the lowest current densities. However, it must be kept in mind that the characteristics are averaged from multiple devices that all showed considerable scattering (with the exception of the samples with 1 wt% PtOEPK at high voltages).

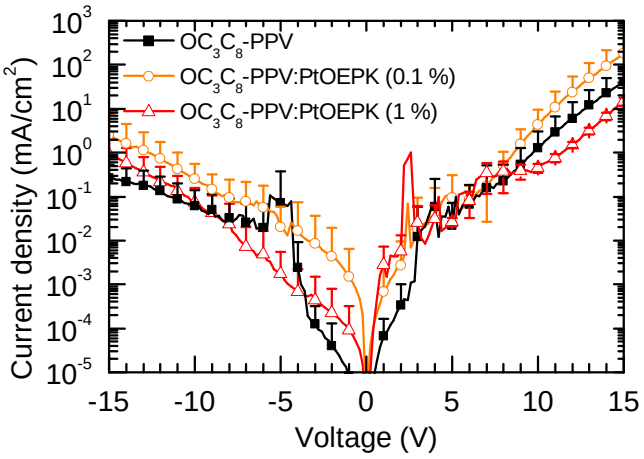

Figure 6.12: *Current-voltage characteristics of electron-only devices with pristine and sensitized OC_3C_8-PPV layers.*

The investigation of electron-only diodes is generally a difficult topic because of their instability. Already the current-voltage characteristics showed a rather large scattering between the samples, and examining the evolution of operating voltage during prolonged operation (Fig. 6.13) turned out to be even more challenging. The voltage does not develop smoothly and scattering between devices is substantial. In contrast to the bipolar and hole-only devices that reach generally higher currents, the electron-only devices were operated at a constant current density of 10 $^{mA}/_{cm^2}$ in order to avoid high operating voltages.

The operating voltage of bipolar diodes increases with increasing PtOEPK concentration, as observed both in I-V characteristics and during the lifetime measurements. In contrast to this, the behavior of electron-only devices seems to differ between fresh devices and those operated for a longer time. In I-V characteristics that were measured directly after the preparation of the samples, the devices with 0.1 % PtOEPK show the highest current density at operating voltages higher than 8 V, whereas the current density of the devices with 1 wt% is lower than that of the other devices. During long-time operation, however, the voltage increases with increasing PtOEPK concentration. In general, the substantial scattering between the samples should be taken into account. The connection between PtOEPK concentration and the operating voltage is opposite to the hole-only devices, in which the presence of PtOEPK decreased the voltage. Due to the position of its LUMO, PtOEPK is likely to act as an electron trap for OC_3C_8-PPV, which explains the observed increase in voltage. As discussed

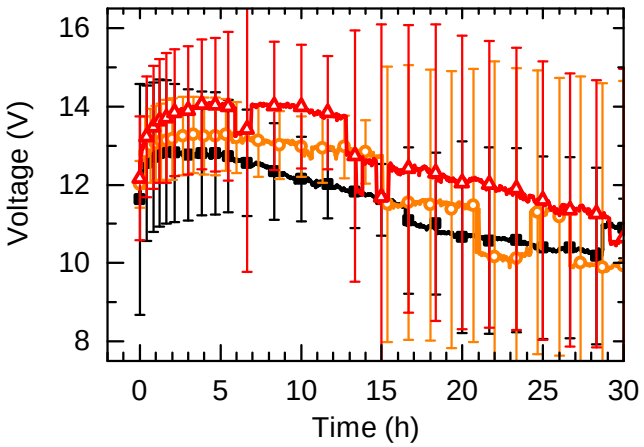

Figure 6.13: *Temporal evolution of the voltage of electron-only devices with with pristine (black rectangles) and sensitized OC_3C_8-PPV layers with 0.1 (orange circles) and 1 wt% PtOEPK (red triangles) during operation at a constant current density of 10 $^{mA}/_{cm^2}$.*

earlier, the LUMO of PtOEP lies at 2.8 - 3.2 eV (OC_3C_8-PPV LUMO lies at 2.6 eV), and due to the smaller energy gap of PtOEPK, it is well possible that its LUMO lies at even lower energies. Based on the I-V characteristics and the continuous operation, however, a small concentration of PtOEPK does not seem to disturb the electron transport in OC_3C_8-PPV a great deal.

Regardless of the concentration of PtOEPK, all electron-only devices behave similarly during prolonged operation. During the first stages, the applied voltage increases slightly (the change is on the order of 1.5-2 V). Interestingly, the voltage rise in the present devices lasts only for the first 2-3 hours of operation; after that, the voltage begins to decrease. In general, an altering operation voltage can be caused by a change in transport or injection properties. An obvious culprit for changes in charge transport are traps. Electron transport in PPV is known to be trap-limited [164, 167]. One publication reports a voltage rise in electron-only devices with time and relates this to the formation of electron traps during electron transport [37]. However, the decrease in voltage observed in present devices contradicts the proposed trap formation at least during the complete duration of the device operation.

Another possibility is a change in injection properties, leading to better injection of electrons after the kink. Because the prolonged operation is performed with the electron injection from the Ca top electrode, the possible change must be located at this contact. The top electrode has indeed often been reported to be unstable, but the changes in its function have generally not been related to gradual changes like observed in present measurements but rather to the phenomenon of the so-called sudden death. This abrupt drop of voltage and luminance [38, 168–170] is often caused by local overheating. In the cases in which sudden death is finally caused by the formation of a localized short cut, self-healing of the device has been observed and attributed to the isolation of the short cut by self-induced melting of the electrode [168]. In addition to the formation of local short cuts, a reversible work function change of a contact layer has been proposed as a cause for sudden death

[170]. Sudden death was observed in many of the present electron-only devices regardless of the presence of PtOEPK, often followed by self-healing. This indicates stability problems at the interface between the polymer and the calcium electrode and is manifested as sudden steplike changes in the operating voltage in Fig. 6.13, in which the voltage is presented as an average of multiple devices. Interestingly, in the present work sudden death is observed almost solely in electron-only devices although the bipolar devices have an identical Ca top electrode. The bipolar and hole-only devices do not show sudden death behavior; instead, the voltage develops smoothly without drastic changes. The devices in which the transported charge carriers are only electrons are less stable than the ones with hole or bipolar transport. This indicates that the sudden death is not only related to the stability of the top Ca electrode alone but is influenced by the active material and the type of the device. In the present case, the presence of holes seems to compensate the factors that participate in the sudden death. The presence of PtOEPK had no influence on the sudden death behavior.

The general difficulty of the investigation of PPV-based electron-only devices can be seen in the large scattering between samples; however, the rising and then declining trend of the operating voltage is observed in all samples. The similar behavior for samples with both pristine and sensitized OC_3C_8-PPV layers suggests that the presence of PtOEPK is not greatly influencing the temporal evolution of electron transport. Since the same conclusion was made with hole-only devices as well, it can be assumed that the significant degradation of the bipolar diodes with sensitized polymer layers is not caused by the presence of PtOEPK as such. Therefore the substantial decrease in lifetime is concluded to be due to the additional triplet excitons on the polymer rather than the presence of the sensitizer.

It is noteworthy that the temporal development of the voltage in bipolar devices is not a superposition of the behavior of the hole- and electron-only devices. When the development of the operating voltage of the bi- and unipolar devices is compared, certain similarities between electron-only and bipolar samples can be observed, whereas the behavior of the hole-only devices differs from the frist-mentioned two. Both the bipolar as well as the electron-only devices show nonmonotonic behavior with an initial increase in the operating voltage followed by a kink and a decrease. However, both the magnitude as well as the time scale of the phenomena are different. The voltage increase of all electron-only devices is limited to ca. 1 V, whereas the bipolar diodes manifest a larger, PtOEPK concentration-dependent change of 1,5 - 3 eV. The voltage of the electron-only samples increases for the first 2-3 hours regardless of the presence or concentration of PtOEPK and is followed by a long, monotonic decrease. The kink appears much later in the bipolar diodes and its position depends on PtOEPK concentration, ranging from ca. 40 hours for devices with 1 wt% PtOEPK to approximately 1200 h for pristine OC_3C_8-PPV. In general, the time scale and amplitude of the voltage change of only the pristine OC_3C_8-PPV samples depend on PtOEPK concentration. The unipolar samples are affected only through a shift of the operating voltage. It cannot straightforwardly be said that one of the charge carrier types would be mainly responsible for fatigue, because the degradation-induced changes in voltage of bipolar devices are not reproduced with unipolar charge transport.

In the work of Stegmaier, the fatigue of PPV-based diodes was attributed to the presence of electrons [64, 144]. No fatigue was observed during either electrical or optical stressing of unipolar, hole-only devices. The transport of holes and the presence of singlet excitons could thus be excluded as the cause for fatigue. In contrast, combining the optical irradiation of the hole-only devices with an applied external voltage did lead to degradation of the devices. The field that is created by the applied voltage dissociates the excitons and creates free charge carriers. These can either remain in the material as free carriers or recombine, creating new excitons, the majority of which is statistically triplets. As holes and singlet excitons (both now also present in the material) were ruled out as the causes for fatigue, possible culprits are thus either the electrons or the triplet excitons. If electrons were the main reason for degradation, one could assume that a rising operating voltage would be observed during the operation of electron-only devices as is the case for bipolar diodes. However, the rise of the operating voltage is not reproduced during the operation of the electron-only devices. The behavior of the electron-only devices during operation can be taken as a hint for the harmfulness of the triplet excitons.

6.3.3 Consequences of a higher concentration of triplet excitons

In the following, possible consequences of the increased population of the excited triplet state are discussed, aiming to form a picture of the factors that could participate in the processes leading to the degradation of the devices.

Infrared Thermography

The non-radiative recombination of excited states leads to the production of phonons, producing heat. One hypothesis regarding the degradation of the diodes is that the heat generated in the active layer during the non-radiative decay of the triplet excitons is responsible for the fatigue. Firstly, it could lead to a general increase in the temperature of the active layer. Increased temperature has been reported to accelerate the degradation of organic materials [48, 171–173]. A lifetime reduction of a factor of 20 has been reported for diodes with an MEH-PPV active layer when the operating temperature has been increased from 30 to 60 °C [172]. Additionally, especially the thermal stability of the hole transport material TPD has been in the focus of attention due to its low glass transition temperature of 60 °C [48–50], and device failure has been associated with the thermal degradation of the low-T_g layer during operation. The glass transition temperature of MEH-PPV, a polymer very similar to OC_3C_8-PPV, lies at 65 °C [174–176] and is thus in the same range than that of TPD. It could be possible that the temperature within the active layer rises high enough to cause degradation. Another possible consequence of an increased temperature within the active layer is a morphological change. During the spin-coating process, the solvent evaporates rapidly. The resulting polymer films possess a kinetically determined morphology rather than an equilibrium morphological state. This means that the films are prone to further relaxation and

reorganization. These processes are accelerated at elevated temperatures [177]. It could be that already a rather small increase in the temperature of the active layer changes the morphology, influencing the lifetime of the devices.

Secondly, the energy that is dissipated during the non-radiative recombination of the triplet excitons could cause local phenomena like a nonuniform temperature distribution within the device, potentially leading to local degradation. Thermography offers a possibility to investigate both of these processes in real time during the operation of the diodes. In order to detect possible differences between pristine and sensitized devices, diodes with pristine OC_3C_8-PPV layers and those with an increased triplet exciton concentration were investigated.[1]

The experiments took place in air, and the devices were encapsulated directly after preparation. The diodes were operated at a constant current density of 50 mA/cm^2 and the operating voltage was monitored manually during the measurement. Determined by the available objective, the thermograms cover approximately 1/4 of the complete active area of the diodes. All devices were operated at room temperature. The rise of temperature during the first 120 s of operation is plotted with respect to the temperature in the off state in Fig. 6.14 for diodes with pristine and 1 wt% PtOEPK-sensitized OC_3C_8-PPV layers. The temperature is shown as a difference to the temperature in off state (room temperature). After turn on, the temperature of the diodes quickly rises to a saturation value within less than the first 60 s. At later stages, the temperature stays approximately constant as long as there are no substantial changes like the formation of local temperature differences within the film. The temperature rise of the diode with pristine OC_3C_8-PPV amounts to ca. 4.7 K, whereas the diode with PtOEPK reaches a higher temperature increase of 7.5 K. Regarding to the temperatures it must be kept in mind that the measured temperature outside the encapsulated device does not fully equal the temperature within the active polymer layer. However, because all devices were prepared and encapsulated equally, a comparison is possible.

The difference in average temperature between diodes with pristine and sensitized PPV layers during operation is ca. 3 K. Alone this difference is not likely to cause the accelerated degradation that is observed in devices with a higher concentration of triplet excitons, although it is possible that it plays a minor role in the fatigue. However, in addition to comparing the temperatures of diodes with different polymer compositions, thermography enables the general investigation of the temperature-related phenomena like the development of hot spots that take place during the fatigue of OC_3C_8-PPV-based diodes.

In general, a pristine OC_3C_8-PPV layer can be described as rather stable when it comes to temperature distribution within the diode area. The temperature of a diode with pristine OC_3C_8-PPV could be recorded during a time period of ca. 1000 h during operation and is plotted in Fig. 6.15. Because the thermography setup prohibited the positioning of a photodiode above the diode, the luminance could only be monitored by eye and the determination of the t_{50} lifetime was not possible. However,

[1] The measurements were performed by Dr. Andrea Gassmann; the data analysis was done within this work.

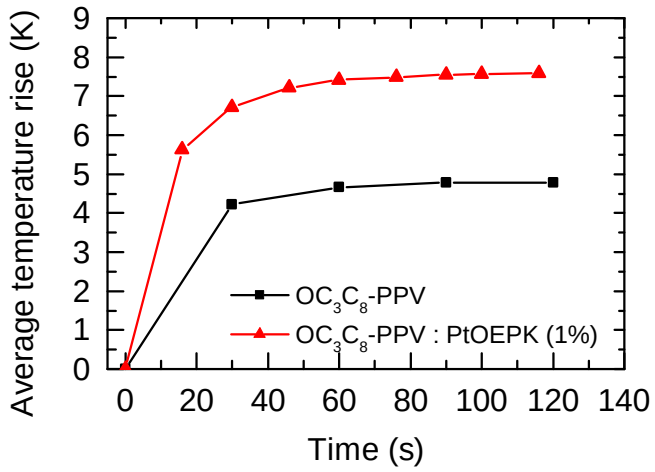

Figure 6.14: *Average temperature rise of diodes with pristine and 1 wt% PtOEPK-sensitized OC_3C_8-PPV layers during the first 120 s of operation at room temperature, ca. 23 °C. The temperature rise refers to the starting value at room temperature. The devices were operated at a constant current density of 50 mA/cm^2.*

as the average t_{50} lifetime of the diodes with OC_3C_8-PPV in this work is 150 h, the total operation for over 1000 h exceeds the lifetime several times.

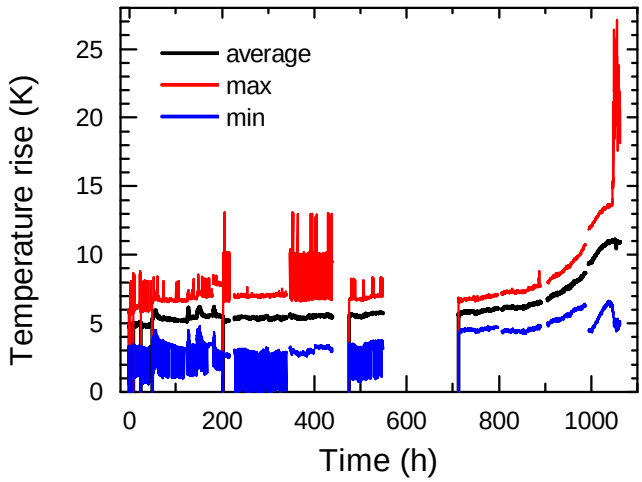

Figure 6.15: *Temporal development of temperature of a diode with pristine OC_3C_8-PPV. The diode was operated at a constant current density of 50 mA/cm^2. A temperature rise of 0 K refers to room temperature, ca. 23 °C.*

The difference to the temperature in the off state (which equals room temperature, ca. 23 ° C) stays constant at 5 K during the initial rise, whereas the following, slow rise is accompanied by an approximately constant temperature difference of 5.5 K. During the last stages of operation, the temperature rises sharply until the diode finally fails. In the course of operation, black spots were formed steadily on the complete diode area. They were, however, not observed as hotter or colder spots in the thermogram, which is noteworthy since black spots are typically assigned to a local

delamination of the cathode, which should be observed as a nonuniform temperature distribution on the diode. Immediately before the final failure, the diode was observed to emit rather dimly but homogeneously over the whole area, including the former black spots. There was one bright area on the diode surface that was also warmer than the remaining area as seen in the increase of the maximum temperature of the diode. The failure of the diode turned out to be reversible, and homogeneous emission could be reestablished for a short time period by operating the diode at higher current densities. Before the final, complete degradation, multiple hot spots emerged and the overall temperature of the diode rose to 50 ° C.

Hot spots were observed in the majority of diodes with sensitized OC_3C_8-PPV layers. Their development could be witnessed during the operation of a diode with 1 wt% PtOEPK as shown in Fig. 6.16. Fig. 6.16 a) shows the temperature distribution before any hot spots are formed. In Fig. 6.16 b), after ca. 75 h of operation, one can observe three warmer areas in the middle of the picture. The temperature in these areas rises during operation, and finally one of them forms a short cut and burns through as seen in Fig. 6.16 c). In the end, the temperature in the hot spot that caused the final degradation was 52.1 ° C whereas the temperature on the remaining diode area decreased back to room temperature (same as the temperature in off state before the operation of the diode). The cooler area in all thermograms is not real; it is caused by the presence of the objective and was present in all thermograms of this device regardless of whether the diode was operated or not.

Fig. 6.17 a) shows an exemplary thermogram of a device with 1 wt% PtOEPK in which multiple hot spots were detected. Fig. 6.17 b) and c) plot the average, maximum and minimum temperatures during the operation of the sample and the operating voltage as a function of time, respectively. The diode was operated for over 30 h until its final degradation that is seen as a sudden drop of temperature back to that of the off state.

The average temperature difference with respect to the off state decreased from 7 to 5 K during operation. The maximum temperature in the hot spots was considerably higher and the difference to room temperature reached up to 45 K as shown in Fig. 6.17 b). It is seen that the hot spots emerged almost immediately after turn-on: the maximum temperature was considerably high during the complete operation. The operating voltage that is plotted in Fig. 6.17 c) decreased gradually from 9.2 to 8.2 V until the abrupt, complete failure of the device. Because the voltage was recorded manually (no automatic recording was built in the measurement setup), no continuous monitoring was possible and measuring points around the final failure were not obtained.

The gradual decrease of the voltage during the presence of hot spots is similar to that observed in the lifetime measurements of the diodes. The decreasing voltage can be explained with the acting of hot spots as preferred current paths. The resistance in the area of the hot spot is lower than in the remaining parts of the film, which increases the current flow locally. To clarify the situation, Fig. 6.18 shows a very schematic illustration of a semiconductor layer without (Fig. 6.18 a)) and with hot spots (Fig. 6.18 b)). In the layer without hot spots, a current I flows through the device. The resistance of the intact semiconductor layer is illustrated with R and the voltage with U.

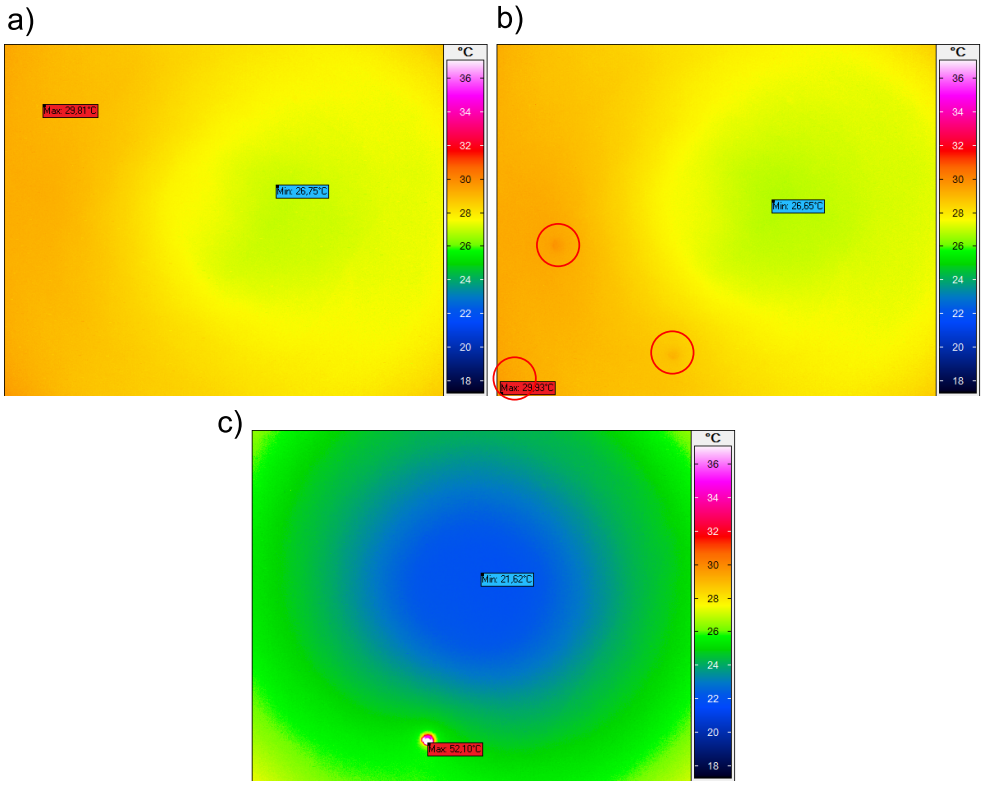

Figure 6.16: *The development of a hot spot in a diode with 1 wt% PtOEPK. a) The temperature distribution prior to the formation of hot spots; b) Three warmer areas have appeared (denoted with red circles); c) One of the warm areas has burned through and formed a hot spot. The diode structure was ITO / PEDOT:PSS / OC_3C_8-PPV:PtOEPK (1 wt%) / Ca / Al.*

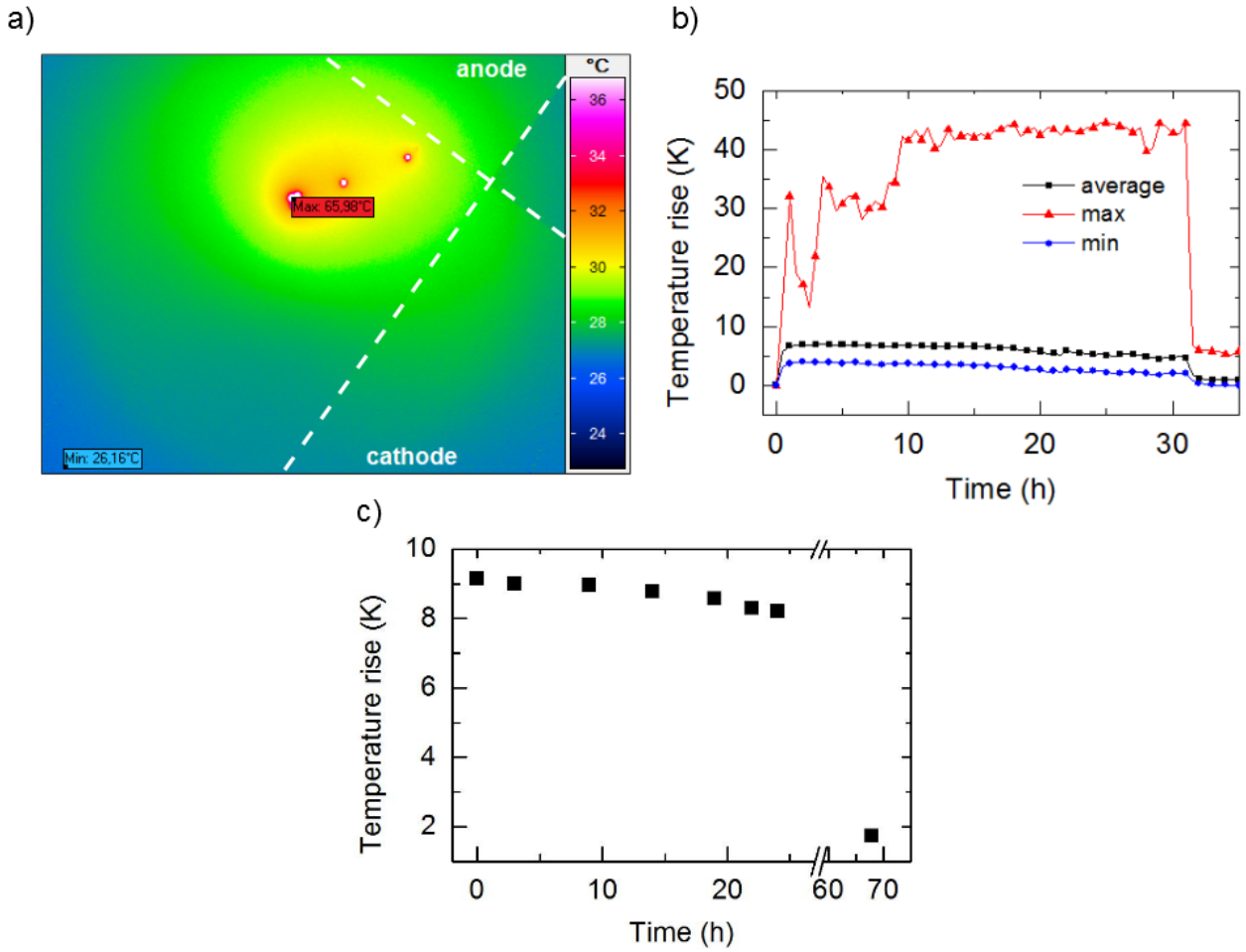

Figure 6.17: *a) Hot spots in a diode with 1 wt% PtOEPK. The hot spots are in the corner of the active area; the contact stripes of the cathode and the anode are seen in the thermogram. b) The maximum, average and minimum temperatures of the diode plotted over operation time. c) The operating voltage of the diode plotted over operation time. The device was operated at a constant current density of 50* mA/cm^2 *and a thermogram was taken every 30 s.*

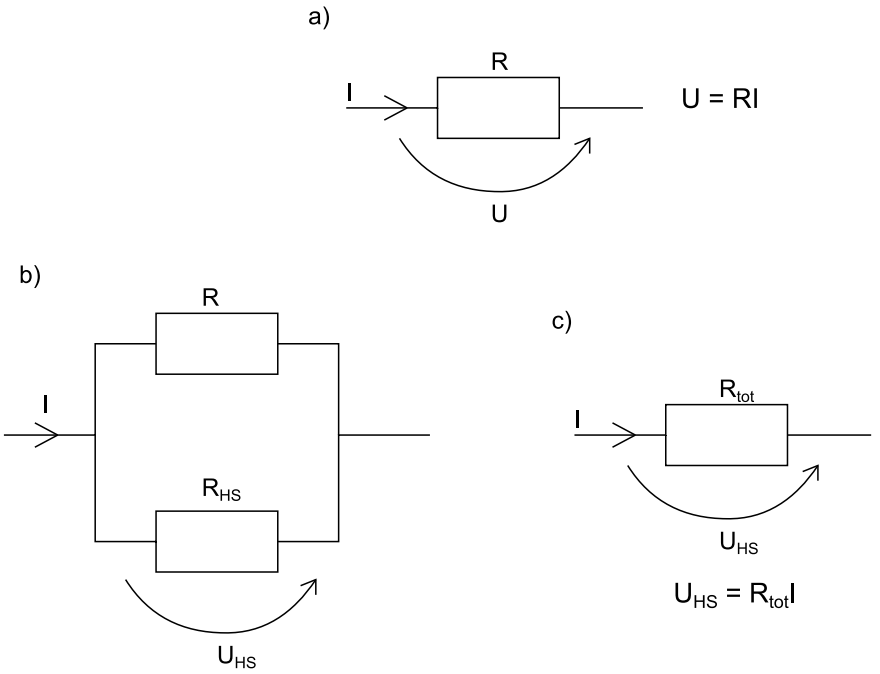

Figure 6.18: *Schematic illustrations of resistance, current and voltage in devices with and without hot spots. a) An intact device without hot spots. b) A device with one hot spot. c) An equivalent circuit to b).*

$$U = RI \tag{6.1}$$

Fig. 6.18 b) shows the situation with one hot spot with a resistance R_{HS}. The voltage is now U_{HS}. The total current I is a sum of the current through the hot spot I_{HS} and the rest of the layer I_{rest}:

$$I = I_{HS} + I_{rest} \tag{6.2}$$

The currents can be expressed as follows:

$$I_{HS} = \frac{U_{HS}}{R_{HS}} \tag{6.3}$$

$$I_{rest} = \frac{U_{HS}}{R} \tag{6.4}$$

Because $R_{HS} < R$, the current through the hot spot I_{HS} is higher than the current through the intact rest of the semiconductor layer I_{rest}. The higher temperature in the hot spot as observed in the thermograms is a result of Joule heating.

An equivalent circuit to Fig. 6.18 b) (the situation with one hot spot in the semiconductor layer) is illustrated in Fig. 6.18 c). R_{tot} describes the total resistance in the semiconductor so that

$$U_{HS} = R_{tot} I \tag{6.5}$$

where

$$R_{tot} = \frac{R R_{HS}}{R + R_{HS}} \tag{6.6}$$

The resistance of the hot spot $R_{HS} < R$, and therefore $R_{tot} < R$. The presence of hot spots decreases the total resistance of the semiconductor. Considering Eq. 6.1 and 6.5, it follows that $U_{HS} < U$. Decreasing resistance in the hot spots leads to decreasing driving voltage across the sample, as is observed in Fig. 6.17. Both measured voltage and average temperature decrease monotonically during the presence of the hot spots. The decreasing temperature is caused by the decreasing current in the intact parts of the semiconductor layer.

In order to investigate the cathode, a sample with 1 wt% PtOEPK was investigated by scanning electron microscopy (SEM) after it was operated until complete failure on hot spots. For the SEM investigations, the encapsulation was removed by breaking the glass at the edges of the substrate. Delaminated areas on the cathode surface could be identified, as shown in Fig. 6.19. The delamination of the metal is in accordance with previous findings in the group, where the diodes with hot spots were investigated with an optical microscope. The hot spots could be identified through both the top and the bottom side of the diode and it was concluded that the metal layer was removed at these areas. It can be concluded that the high temperature in the hot spot area (that is caused by Joule heating) and the locally high current density finally lead to a local destruction of the cathode and therefore the complete degradation of the device.

The development of hot spots is a significant difference between pristine and sensitized OC_3C_8-PPV films. In general, the hot spots in PtOEPK-containing devices appear much earlier than observed with pristine OC_3C_8-PPV. The operation of devices with pristine OC_3C_8-PPV layers is possible for hundreds of hours without the development of hot spots, whereas in devices with 1 wt% PtOEPK they were detected within some tens of hours. The appearing of hot spots does not necessarily lead to an instant failure of the device; instead, they can exist for tens of hours without breaking the device. The low resistance of the hot spot leads to a monotonically decreasing operating voltage.

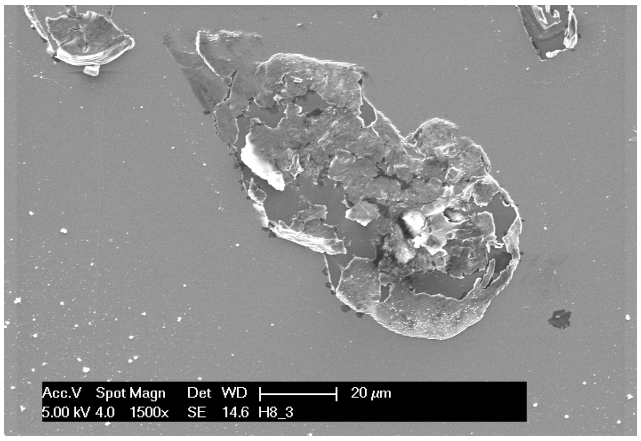

Figure 6.19: *A SEM image showing delaminated areas on the cathode of a sample with the structure ITO / PEDOT:PSS / OC_3C_8-PPV:PtOEPK (1 %) / Ca / Al.*

The findings of the thermography measurements help understand the behaviour of the bipolar devices in the lifetime measurements in Section 6.3.1. In the beginning of the operation, the diodes behaved as expected; the luminance decreased and the operating voltage increased. However, after a characteristic time that decreased with increasing PtOEPK concentration, the decrease of luminance accelerated and the operating voltage began to decrease. The decreasing operating voltage and the luminance are due to the formation of preferred current paths in form of hot spots. Their reduced resistance lowers the voltage and the current in the intact parts of the film. The lower current is seen as a lower luminance.

Influence of sensitizer concentration on charge carrier mobility

The degradation of OLEDs is often manifested as a decreased charge carrier mobility [53, 144, 178]. The development of the mobility of the diodes with different triplet sensitizer concentrations during fatigue is therefore an evident topic of interest. The mobilities were deterimined with CELIV.

For mobility determination, diodes with pristine and sensitized OC_3C_8-PPV layers were prepared and stressed stepwise at same conditions as in the lifetime measurements. In order to monitor the development of the charge carrier mobility, CELIV transients were measured directly after device preparation (denoted with t_{100}) and between stressing steps at t_{90}, t_{80} etc., i.e. at 10 percent point intervals. t_x denotes the time it has taken for the luminance to decrease to x % of the initial value. Fig. 6.20 plots extraction currents of a diode with pristine OC_3C_8-PPV. The laser wavelength was 530 nm and the delay time 5 μs. The intensity of the extraction current decreases with increasing fatigue and the maximum shifts to higher times. Additionally, broadening of the peak is observed, which is a sign of an increasing dispersion of the charge transport [64, 179]. The increasing dispersivity of the transport during fatigue has previously been observed in TOF measurements with different PPV derivatives including OC_3C_8-PPV [64].

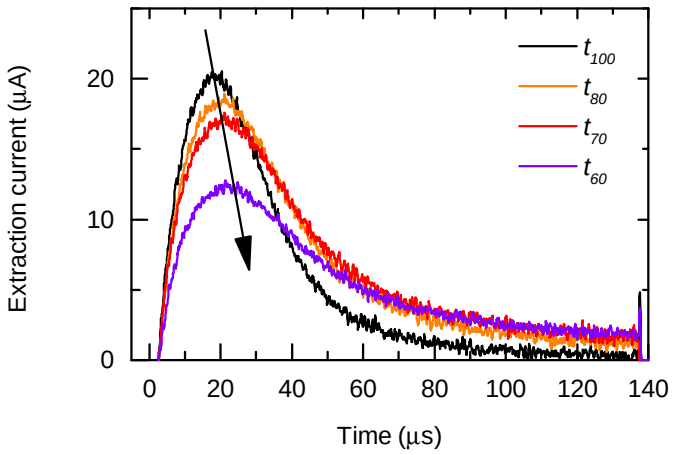

Figure 6.20: *Extraction currents of a sample with pristine OC_3C_8-PPV recorded between stressing steps at a constant current density of 50 mA/cm^2, calculated as the difference between the current after illumination by a laser pulse and the displacement current. The CELIV measurements were carried out after each decrease of luminance of 10 percent points, and the arrow indicates the increasing fatigue of the sample.*

Extraction currents of 0.1 and 1 wt% sensitized samples are shown in Fig. 6.21 and Fig. 6.22, respectively. Again, the intensity of the extraction current decreases with fatigue; an exception is the sample with 0.1 wt% PtOEPK at t_{70}. Here, the extraction current is at the level of the current at t_{100}. The origin of the increase is unclear, but fluctuation in the intensity of the laser excitation can be excluded due to the fixed position of the sample holder during all CELIV measurements. The extraction peak broadens in both samples, but the change is more drastic in the sample with 1 wt% PtOEPK. No shift of the extraction current maximum is observed for the sample with 1 wt% PtOEPK.

The CELIV mobilities for all samples and stressing steps were calculated with Eq. 3.5 (Subsection 3.3.3). The obtained values for samples with pristine OC_3C_8-PPV as well as 0.1 and 1 wt% PtOEPK are summarized in Fig. 6.23. For pristine OC_3C_8-PPV in the unstressed state, a value of $6.0 \cdot 10^{-6}$ $\frac{cm^2}{Vs}$ was obtained. The value is of the same order of magnitude as reported previously [144]. The sensitized samples with 0.1 and 1 wt% PtOEPK yield lower mobilities of $3.2 \cdot 10^{-6}$ $\frac{cm^2}{Vs}$ and $3.5 \cdot 10^{-6}$ $\frac{cm^2}{Vs}$, respectively. The generally lower mobilities of the sensitized samples are in accordance to the I-V characteristics, in which the current densities of the samples with PtOEPK were slightly lower than that of pristine OC_3C_8-PPV (see Fig. 6.7). The slightly higher mobility of the sample with 1 wt% PtOEPK in comparison to the sample with the smaller PtOEPK concentration is unexpected; however, the difference is so small that the mobilities can be considered equal.

As expected [144], the mobility of the sample with pristine OC_3C_8-PPV decreases during fatigue. A decrease from $6.0 \cdot 10^{-6}$ $\frac{cm^2}{Vs}$ to $3.2 \cdot 10^{-6}$ $\frac{cm^2}{Vs}$ is observed as the sample degrades to t_{50}. The samples with sensitized polymer layers behave differently. For 0.1 % PtOEPK, the mobility stays approximately constant between 3.2 and $3.7 \cdot 10^{-6}$ $\frac{cm^2}{Vs}$ until t_{60}; only the value at t_{50} is significantly

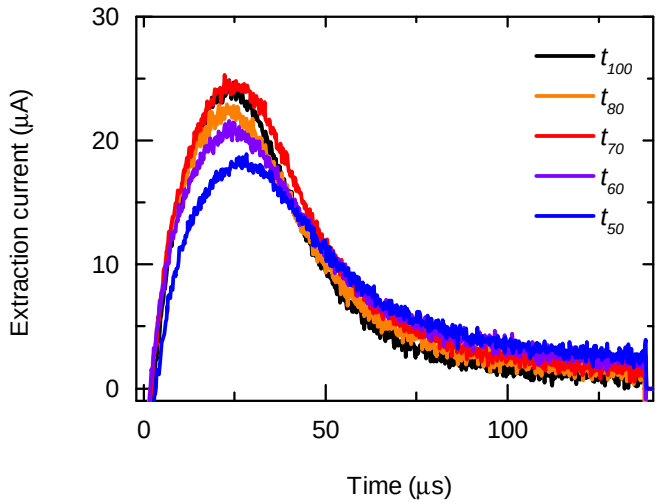

Figure 6.21: *Extraction currents of a sample with OC_3C_8-PPV sensitized with 0.1 wt% PtOEPK recorded between stressing steps at a constant current density of 50 mA/cm^2, calculated as the difference between the current after illumination by a laser pulse and the displacement current.*

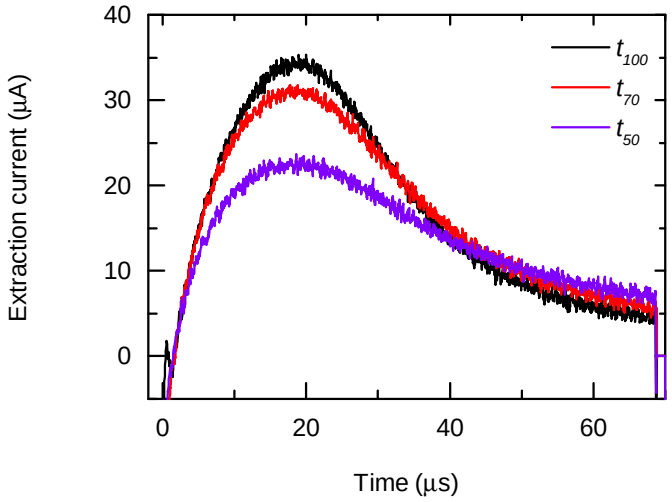

Figure 6.22: *Extraction currents of a sample with OC_3C_8-PPV sensitized with 1 wt% PtOEPK recorded between stressing steps at a constant current density of 50 mA/cm^2, calculated as the difference between the current after illumination by a laser pulse and the displacement current.*

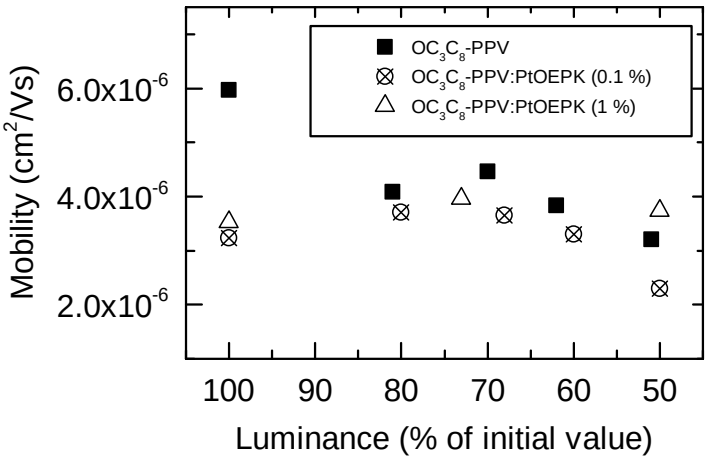

Figure 6.23: *Evolution of charge carrier mobility for samples with pristine and sensitized OC_3C_8-PPV layers during fatigue caused by electrical stress. The samples were operated at a constant current density of 50 $^{mA}/_{cm^2}$. The operation was shortly paused for each CELIV measurement.*

lower at $2.3 \cdot 10^{-6}\ \frac{cm^2}{Vs}$. The sample with 1 wt% PtOEPK shows similar behavior: a slightly increased mobility was measured after operation to t_{70}, and the value for t_{50} is again closer to the one for the fresh state. Again, the variation of the measured mobility is not large and the measured values are within $0.5 \cdot 10^{-6}\ \frac{cm^2}{Vs}$. Such a difference can be considered insignificant and the mobilities can be said to remain approximately constant.

On the whole, the mobility of pristine OC_3C_8-PPV shows a more clearly decreasing trend than the two sensitized samples. The sample with 0.1 % PtOEPK shows a small decrease as well, whereas the mobility of the sample with a larger PtOEPK concentration stays approximately constant. The differences in the development of hole mobility during electrical stress imply that the processes that lead to fatigue are not necessarily equal in pristine and sensitized samples. As shown in the previous subsubsection, an increased formation of hot spots was observed in the devices with PtOEPK. The decrease in the operating voltage in the late stages of driving in the lifetime measurements was explained with the development of hot spots that act as preferred current paths. The increasing mobility in the preferred paths could compensate the fatigue-induced decrease in bulk mobility as observed in the pristine sample.

Considering the accelerated fatigue in the presence of additional triplet excitons, one plausible hypothesis would be that the increased amount of triplets on the polymer would lead to more pronounced trap generation through the energy released by nonradiative recombination. Such a process was proposed by Silvestre et al. in their work with OC_1C_{10}-PPV [55], where they correlated both the luminance decay and the voltage drift with trap formation within the band gap of the polymer. However, the nature of traps was not specified. Because CELIV only provides information about majority charge carriers, it is only possible to draw conclusions about hole transport based on the CELIV measurements presented above. Should hole traps be formed during the operation of

the devices, the mobility of the samples with sensitized OC_3C_8-PPV layers and thus with a higher concentration of nonradiatively recombinating triplet excitons should decrease with fatigue as more and more traps are created by the nonradiative recombinations. Such a behavior is not observed for either of the samples with PtOEPK. The mobility values of the sensitized samples in undriven state are lower than that of pristine OC_3C_8-PPV, but they do not change drastically with fatigue. Therefore an increasing formation of hole traps during the degradation of the PtOEPK-containing devices is unlikely. Based on CELIV measurements, it is impossible to draw conclusions about the development of electron mobility.

6.4 Summary

In this chapter, the harmful effect of triplet excitons on the lifetime of OC_3C_8-PPV-based OLEDs was demonstrated. The polymer was blended with a triplet sensitizer PtOEPK, leading to an increase in the triplet exciton population and a substantial decrease of the t_{50} lifetime of the devices. Regardless of the concentration of the sensitizer, all devices show similar behavior in both luminance and operating voltage during prolonged operation, but the excess triplet excitons are found to affect the time scale of the degradation of the devices. The operating voltage and the luminance of the devices were found to develop nonmonotonically during operation: the voltage increased in the first stages of operation, mirroring the decrease in luminance, but at a certain time it started to decrease. This kink in voltage was accompanied by a steeper decrease in luminance. The kink was attibuted to the formation of preferred current paths with a lower resistance than the intact part of the layer that were observed as hot spots in themograms. The presence of the hot spots lead to an increased current flow through the spots and decreased the driving voltage of the devices as well as the luminance, until the diodes finally degraded completely as the hot spots burned through, damaging the cathode. After the final failure of the devices, the hot spots could be detected as destroyed areas on the cathode.

The formation of hot spots was enhanced in devices with an increased triplet exciton concentration, which explains their shorter lifetimes. Additionally, the operating temperatures of the triplet-enriched devices were ca. 3 K higher than the temperature of pristine devices; this could result in small-scale changes in the morphology of the polymer. Due to the generally high concentration of triplet excitons in single layer fluorescent OLEDs, the presented results underline the important role of the seemingly inactive triplet excitons in fluorescent diodes and are of significant importance for the efforts to improve the stability of the devices.

7 Summary and outlook

The aim of this work was to investigate phenomena that influence the stability of OC_3C_8-PPV-based OLEDs. The results were divided into three major topics. The first part, presented in Chapter 4, focused on methods that were developed for general investigations on PPV-based diodes. In order to monitor possible changes in the polymer layer that occur during fatigue, it is necessary to remove the cathode to access the polymer directly. A removal procedure with acetic acid was introduced. Etching the calcium cathode and replacing it with a new one did not affect the behaviour of the devices in lifetime measurements. Another topic of Chapter 4 was the accelerated electrical stressing of OC_3C_8-PPV-based diodes. Performing lifetime measurements at higher current densities is desirable for long-lived devices, because it leads to faster degradation and shortens the duration of the measurements. A scaling law that links the initial luminance and the t_{50} lifetime was derived from lifetime measurements at different current densities, enabling the stressing of the diodes at accelerated condiditions.

The next chapter focused on the interaction of OC_3C_8-PPV with oxygen. Many conjugated polymers are sensitive towards oxygen, which is why the devices are typically encapsulated or handled solely in inert atmosphere. In Chapter 5, it was shown that even a residual oxygen concentration in the glovebox, typically on the order of 1-3 ppm, is enough to cause changes in OC_3C_8-PPV. Oxygen was found to diffuse into the polymer during storage in the glovebox, which lead to the creation of electron traps and the subsequent p-doping of the active material. The doping could be observed as an increasing density of equilibrium charges in dark-CELIV measurements with increasing storage time, and a density of doped charge of $7{\cdot}10^{15}\,\mathrm{cm}^{-3}$ was calculated for the day 8 after sample preparation. Chapter 5 also utilized a two-ramp dark-CELIV sequence for the real-time monitoring of the establishment of steady-state conditions of the doped material. The first dark-CELIV voltage ramp removed the mobile holes from the polymer layer, and by varying the delay time between the ramps their return into the polymer could be monitored. The recovery is a slow process, and it takes on the order of 1.2 ms to build up the initial density of holes after their extraction with the dark-CELIV voltage ramp.

The findings of Chapter 5 are important for scientific and commercial applications of PPV-based devices. It is possible that phenomena that have previously been contributed to sole aging while storing in inert atmosphere are in reality related to oxygen. It was shown that even a small residual concentration is enough to unintentionally dope the polymer material. The possibility of oxygen doping has to be taken into account when evaluating changes in devices that have been aged in the glovebox.

In order to deepen the understanding of the oxygen doping of OC_3C_8-PPV, other cathode materials have to be applied. With the present Ca top electrode, a systematic exposure of the samples to oxygen was not possible due to the strong oxidation of Ca. More inert top electrodes would enable the controlled monitoring of the temporal evolution of oxygen doping outside the glovebox. A strict requirement for the top electrode is a low work function. The in CELIV measurements typically as top electrode used Al is not suitable for OC_3C_8-PPV due to the injection of holes from Al to OC_3C_8-PPV HOMO. A possible alternative would be LiF / Al.

In Chapter 6, the influence of triplet excitons on the lifetime of OC_3C_8-PPV-based diodes was investigated. The majority of the excitons in fluorescent OLEDs are non-radiatively decaying, long-lived triplets. Despite the high density of triplet excitons in fluorescent diodes, their role in the degradation has so far gained only little attention. In this work, the concentration of triplet excitons in OC_3C_8-PPV was increased by incorporating a triplet sensitizer molecule PtOEPK into the polymer. The sensitizer converted part of the OC_3C_8-PPV singlet excitons to triplets, increasing the triplet-to-singlet ratio. The influence of the increased ratio of triplet to singlet excitons on the stability of the devices was then investigated. The increased concentration of triplet excitons could be observed in photoinduced absorption measurements as increased triplet-triplet absorption in the sensitized polymer.

The increased concentration of triplet excitons lead to a substantial decrease of the t_{50} lifetime of the diodes. All devices (with and without PtOEPK) showed similar, non-monotonic behavior of luminance and operating voltage during electrical stressing, but the excess triplet excitons were found to affect the time scale of the degradation. The lifetime decreased from 150 h for pristine OC_3C_8-PPV to 15 h for devices with 1 % PtOEPK. As the presence of PTOEPK did not greatly influence the evolution of electron and hole transport in unipolar devices, it was concluded that the significant degradation that was observed in PtOEPK-sensitized bipolar devices was not caused by the presence of PtOEPK as such. The substantial decrease in lifetime was concluded to be due to the additional triplet excitons on OC_3C_8-PPV.

It was found in thermography measurements that the devices with an increased concentration of triplet excitons are more prone to hot spot formation than their pristine counterparts. The hot spots act as preferred current paths, decreasing the current flow through the intact part of the device and therefore the luminance. Additionally, the overall temperature of diodes with sensitized polymer layers was ca. 3 K higher than that of pristine diodes, which might lead to small-scale morphological changes. The results that were presented in this work are important for fluorescent OLEDs, the triplet excitons of which have been largely ignored so far.

As outlook, the use of a triplet quencher would complement the results that were introduced in this work. A triplet quencher material would remove the triplet excitons from the active polymer without affecting the emissive singlet state; as a requirement, the triplet state of the quencher has to lie below that of the host material, and the exchange energy needs to be higher. This approach was desired in the present work, too, but to the best of present knowledge it is not possible to find

such a material for OC_3C_8-PPV due to the low lying triplet state and the large exchange energy. To further unveil the mechanisms behind the triplet-related degradation, the investigations could be extended to other fluorescent materials. Previous work with a polyfluorene derivate [140] suggests that the influences of triplet excitons on the stability of the diodes are not identical in PPV- and polyfluorene-based devices.

List of Figures

2.1 Examples of organic semiconductors . . . 9
2.2 Formation of a double bond as well as anti-bonding σ and π molecular orbitals . . . 10
2.3 Gaussian density of states . . . 12
2.4 Perrin-Jablonski diagram for an organic semiconductor . . . 13
2.5 Singlet and triplet states . . . 13
2.6 Working principle of an OLED . . . 15
2.7 Contact formation between a metal and a semiconductor . . . 16
2.8 Schottky effect . . . 17
2.9 Models for charge carrier injection over an injection barrier . . . 18
2.10 Förster and Dexter transfer mechanisms . . . 21
2.11 Operation schemes of an OLED . . . 23
2.12 Exemplary lifetime measurement of an OLED . . . 24

3.1 Molecular structures of unsubstituted PPV and OC_3C_8-PPV . . . 28
3.2 Absorption and electroluminescence spectra of OC_3C_8-PPV . . . 28
3.3 Molecular structure of PtOEPK . . . 29
3.4 Absorption and emission spectra of PtOEPK . . . 29
3.5 Sample layout . . . 31
3.6 Schematic illustration of a photo-CELIV measurement . . . 34
3.7 Photo-CELIV setup . . . 36
3.8 Photoinduced absorption measurement setup . . . 37

4.1 IVL characteristics of a fatigued diode before and after cathode removal and a subsequent deposition of a new cathode . . . 40
4.2 SIMS measurement after etching away the cathode with HCl . . . 41
4.3 Lifetime of a diode after the etching of the original cathode with acetic acid and the subsequent deposition of a new cathode as well as that of a reference diode with an original cathode . . . 42
4.4 Removing the cathode . . . 42
4.5 Scaling law . . . 43

5.1 Schematic illustration of the dark-CELIV measurement conditions . . . 46
5.2 Example transients from a CELIV measurement . . . 47
5.3 Influence of offset voltage on the extraction current transient in dark-CELIV . . . 49
5.4 Influence of offset voltages higher than U_{BI} on the CELIV current response . . . 50

5.5 Influence of offset voltages on the position of the current maximum 51
5.6 The increase of equilibrium charge in OC_3C_8-PPV 52
5.7 Extraction current signal after exposure to air 53
5.8 The recovery of the equilibrium charge carriers monitored with a varying delay time between the two dark-CELIV voltage ramps 55
5.9 Density of extracted holes as a function of delay time between voltage ramps 56

6.1 Energy scheme of the singlet-to-triplet conversion process 62
6.2 Absorption and photoluminescence spectra of OC_3C_8-PPV and PtOEPK 62
6.3 SEM images of pristine and sensitized PPV films on ITO 64
6.4 Absorption spectra of sensitized OC_3C_8-PPV films 65
6.5 Steady-state photoluminescence spectra of pristine and sensitized OC3C8-PPV layers 65
6.6 Photoinduced absorption spectra of pristine and sensitized OC3C8-PPV layers 66
6.7 Current density and luminance of diodes with pristine and sensitized OC_3C_8-PPV layers 68
6.8 Lifetime of diodes with pristine and sensitized OC_3C_8-PPV layers 69
6.9 Electroluminescence spectra of diodes with pristine OC_3C_8-PPV and 1 wt% PtOEPK recorded stepwise between operation steps 71
6.10 Current-voltage characteristics of hole-only devices with pristine and sensitized OC_3C_8-PPV layers 73
6.11 Temporal evolution of the operating voltage of hole-only devices with pristine and sensitized OC_3C_8-PPV layers 73
6.12 Current-voltage characteristics of electron-only devices with pristine and sensitized OC_3C_8-PPV layers 75
6.13 Temporal evolution of operating voltage of electron-only devices with pristine and sensitized OC_3C_8-PPV layers 76
6.14 Temperature of pristine and sensitized diodes during the first stages of operation . . . 80
6.15 Temporal development of temperature of a diode with pristine OC_3C_8-PPV 80
6.16 The development of a hot spot in a diode with 1 wt% PtOEPK 82
6.17 Hot spots in a diode with 1 wt% PtOEPK and the temporal evolution of temperature . 83
6.18 Schematic illustrations of resistance, current and voltage in devices with and without hot spots 84
6.19 A SEM image of a delaminated area on the cathode 86
6.20 Extraction currents of a sample with pristine OC_3C_8-PPV recorded between stressing steps 87
6.21 Extraction currents of a sample with OC_3C_8-PPV sensitized with 0.1 wt% PtOEPK recorded between stressing steps 88
6.22 Extraction currents of a sample with OC_3C_8-PPV sensitized with 1 wt% PtOEPK recorded between stressing steps 88
6.23 Evolution of charge carrier mobility during stress for samples with pristine and sensitized OC_3C_8-PPV layers 89

Bibliography

[1] C. W. Tang and S. A. Van Slyke. Organic electroluminescent diodes. *Applied Physics Letters*, 51(12):913, 1987.

[2] R. H. Friend, R. W. Gymer, A. B. Holmes, J. H. Burroughes, R. N. Marks, C. Taliani, D. D. C. Bradley, D. A. Dos Santos, J.-L. Brédas, M. Lögdlund, and W. R. Salaneck. Electroluminescence in conjugated polymers. *Nature*, 397:121–128, jun 1999.

[3] J. H. Burroughes, D. D. C. Bradley, A. R. Brown, R. N. Marks, K. Mackay, R. H. Friend, P. L. Burns, and A. B. Holmes. Light-emitting diodes based on conjugated polymers. *Nature*, 347:539–541, 1990.

[4] D. Braun and A. J. Heeger. Visible light emission from semiconducting polymer diodes. *Applied Physics Letters*, 58(18):1982, 1991.

[5] OLED-info. Company information: Pioneer.

[6] OTI Lumionics Inc. OLED History.

[7] OLED-info. OLED introduction and basic OLED information.

[8] OLED-info. Blue PHOLED breakthrough: researchers manage to extend the lifetime tenfold, 2014.

[9] Wolfgang Brütting, editor. *Physics of Organic Semiconductors*. Wiley-VCH, Weinheim, 2005.

[10] A. Köhler, S. T. Hoffmann, and H. Bässler. An Order-Disorder Transition in the Conjugated Polymer MEH-PPV. *Journal of American Chemical Society*, 134:11594–11601, 2012.

[11] S. Lehtimäki. *Ion gels as gate dielectrics in organic thin-film transistors*. Master of science thesis, Tampere University of Technology, 2011.

[12] M. Schwoerer and H. C. Wolf. *Organic Molecular Solids*. Wiley-VCH, Weinheim, 2005.

[13] H. Bässler. Charge Transport in Disordered Organic Photoconductors. *Physica Status Solidi (b)*, 175:15–56, 1993.

[14] B. Valeur. *Molecular Fluorescence: Principles and Applications*. Wiley-VCH, Weinheim, 2001.

[15] H. Yersin. *Highly Efficient OLEDs with Phosphorescent Emitters*. Wiley-VCH, Weinheim, 2008.

[16] L. S. Hung, C. W. Tang, and M. G. Mason. Enhanced electron injection in organic electroluminescence devices using an Al/LiF electrode. *Applied Physics Letters*, 70(2):152, 1997.

[17] G. E. Jabbour, Y. Kawabe, S. E. Shaheen, J. F. Wang, M. M. Morrell, B. Kippelen, and N. Peyghambarian. Highly efficient and bright organic electroluminescent devices with an aluminum cathode. *Appl Phys Lett*, 71(13):1762–1764, 1997.

[18] S. L. M. Van Mensfoort and R. Coehoorn. Determination of injection barriers in organic semiconductor devices from capacitance measurements. *Physical Review Letters*, 100:086802, 2008.

[19] A. Kahn, N. Koch, and W. Gao. Electronic structure and electrical properties of interfaces between metals and pi-conjugated molecular films. *Journal of Polymer Science, Part B: Polymer Physics*, 41:2529–2548, 2003.

[20] S. M. Sze. *Physics of Semiconductor Devices*. John Wiley & Sons, 2. edition, 1981.

[21] R. H. Fowler and L. Nordheim. Electron Emission in Intense Electric Fields. *Proceedings of the Royal Society of London A*, 119:173, 1928.

[22] A. Miller and E. Abrahams. Impurity conduction at low concentrations. *Physical Review*, 120(3):745–755, 1960.

[23] S. V. Novikov, D. H. Dunlap, V. M. Kenkre, P. E. Parris, and A. V. Vannikov. Essential role of correlations in governing charge transport in disordered organic materials. *Physical Review Letters*, 81(4):4472–4475, 1998.

[24] C. Li, L. Duan, H. Li, and Y. Qiu. Universal Trap Effect in Carrier Transport of Disordered Organic Semiconductors : Transition from Shallow Trapping to Deep Trapping Universal Trap Effect in Carrier Transport of Disordered Organic Semiconductors : Transition from Shallow Trapping to Deep. *The Journal of Physical Chemistry C*, 118:10651–10660, 2014.

[25] R. Schmechel and H. Von Seggern. Electronic Traps in Organic Transport Layers. In W. Brütting, editor, *Physics of Organic Semiconductors*, pages 273–303. Wiley-VCH, 2005.

[26] J. Steiger, R. Schmechel, and H. Von Seggern. Energetic trap distributions in organic semiconductors. *Synthetic Metals*, 129(1):1–7, 2002.

[27] S. M. Menke and R. J. Holmes. Exciton diffusion in organic photovoltaic cells. *Energy & Environmental Science*, 7(2):499, 2014.

[28] T. Förster. Transfer mechanisms of electronic excitation energy. *Discussions of the Faraday Society*, 27(10):7–17, 1959.

[29] D. L. Dexter. A Theory of Sensitized Luminescence in Solids. *The Journal of Chemical Physics*, 21(5):836, 1953.

[30] G. D. Scholes. Long-range resonance energy transfer in molecular systems. *Annual Review of Physical Chemistry*, 54(18):57–87, 2003.

[31] A. R. Brown, K. Pichler, N. C. Greenham, D. D. C. Bradley, and R. H. Friend. Optical spectroscopy of triplet excitons and charged excitations in poly(p-phenylenevinylene) light-emitting diodes. *Chemical Physics Letters*, 210(1-3):61–66, 1993.

[32] A. L. Burin and M. A. Ratner. Exciton Migration and Cathode Quenching in Organic Light Emitting Diodes. *The Journal of Physical Chemistry A*, 104(20):4704–4710, 2000.

[33] M. Stevens, C. Silva, D. Russell, and R. Friend. Exciton dissociation mechanisms in the polymeric semiconductors poly(9,9-dioctylfluorene) and poly(9,9-dioctylfluorene-co-benzothiadiazole). *Physical Review B*, 63(16):165213, 2001.

[34] R.G. Kepler, V.S. Valencia, S.J. Jacobs, and J.J. McNamara. Exciton-exciton annihilation in poly (p-phenylenevinylene) films. *Synthetic Metals*, 78(3):227–230, apr 1996.

[35] A. Ruseckas, M. Theander, L. Valkunas, M. R. Andersson, O. Inganäs, and V. Sundström. Energy transfer in a conjugated polymer with reduced inter-chain coupling. *Journal of Luminescence*, 76-77:474–477, feb 1998.

[36] D. Y. Kondakov, J. R. Sandifer, C. W. Tang, and R. H. Young. Nonradiative recombination centers and electrical aging of organic light-emitting diodes: Direct connection between accumulation of trapped charge and luminance loss. *Journal of Applied Physics*, 93(2):1108, 2003.

[37] F. So and D. Y. Kondakov. Degradation mechanisms in small-molecule and polymer organic light-emitting diodes. *Advanced Materials*, 22(34):3762–3777, sep 2010.

[38] J. McElvain, H. Antoniadis, M. R. Hueschen, J. N. Miller, D. M. Roitman, J. R. Sheats, and R. L. Moon. Formation and growth of black spots in organic light-emitting diodes. *Journal of Applied Physics*, 80:6002, 1996.

[39] Y.-F. Liew, H. Aziz, N.-X. Hu, G. Xu, and Z. Popovic. Investigation of the sites of dark spots in organic light-emitting devices. *Applied Physics Letters*, 77(2000):2650–2652, 2000.

[40] Shuang Fang Lim, Lin Ke, Wei Wang, and Soo Jin Chua. Correlation between dark spot growth and pinhole size in organic light-emitting diodes. *Applied Physics Letters*, 78(2001):2116–2118, 2001.

[41] S. Lim, W. Wang, and S. Chua. Degradation of organic light-emitting devices due to formation and growth of dark spots. *Materials Science and Engineering B*, 85(2-3):154–159, 2001.

[42] H. Aziz, Z. Popovic, C. P. Tripp, N.-X. Hu, A.-M. Hor, and G. Xu. Degradation processes at the cathode/organic interface in organic light emitting devices with Mg:Ag cathodes. *Applied Physics Letters*, 72(21):2642, 1998.

[43] Y. Kim, D. Choi, H. Lim, and C. S. Ha. Accelerated pre-oxidation method for healing progressive electrical short in organic light-emitting devices. *Applied Physics Letters*, 82(2003):2200–2202, 2003.

[44] P. E. Burrows, V. Bulovic, S. R. Forrest, L. S. Sapochak, D. M. McCarty, and M. E. Thompson. Reliability and degradation of organic light emitting devices. *Applied Physics Letters*, 65(1994):2922–2924, 1994.

[45] H. Aziz and Z. D. Popovic. Degradation Phenomena in Small-Molecule Organic Light-Emitting Devices. *Chemistry of Materials*, 16:4522–4532, 2004.

[46] S. Schmidbauer, A. Hohenleutner, and B. König. Chemical degradation in organic light-emitting devices: mechanisms and implications for the design of new materials. *Advanced Materials*, 25(15):2114–29, 2013.

[47] A. Gassmann, S. V. Yampolskii, A. Klein, K. Albe, N. Vilbrandt, O. Pekkola, Y. A. Genenko, M. Rehahn, and H. von Seggern. Study of electrical fatigue by defect engineering in organic light-emitting diodes. *Materials Science and Engineering B*, 192:26–51, 2015.

[48] P. Fenter, F. Schreiber, V. Bulovic, and S. R. Forrest. Thermally induced failure mechanisms of organic light emitting device structures probed by X-ray specular reflectivity. *Chemical Physics Letters*, 4(October):521–526, 1997.

[49] S. A.. Van Slyke, C. H. Chen, and C. W. Tang. Organic electroluminescent devices with improved stability. *Applied Physics Letters*, 69(15):2160, 1996.

[50] S. Tokito, H. Tanaka, A. Okada, and Y. Taga. High-temperature operation of an electroluminescent device fabricated using a novel triphenylamine derivative. *Applied Physics Letters*, 69(7):878, 1996.

[51] H. Aziz, Z. Popovic, S. Xie, A. M. Hor, N. X. Hu, C. Tripp, and G. Xu. Humidity-induced crystallization of tris (8-hydroxyquinoline) aluminum layers in organic light-emitting devices. *Applied Physics Letters*, 72(1998):756–758, 1998.

[52] Y. Sakamoto, T. Suzuki, A. Miura, H. Fujikawa, S. Tokito, and Y. Taga. Synthesis, characterization, and electron-transport property of perfluorinated phenylene dendrimers [16]. *Journal of the American Chemical Society*, 122(11):1832–1833, 2000.

[53] A. Turak. Interfacial degradation in organic optoelectronics. *RSC Advances*, 3(18):6188, 2013.

[54] M. Kuik, L. J. A. Koster, A. G. Dijkstra, G. A. H. Wetzelaer, and P. W. M. Blom. Non-radiative recombination losses in polymer light-emitting diodes. *Organic Electronics*, 13(6):969–974, 2012.

[55] G. C. M. Silvestre, M. T. Johnson, A. Giraldo, and J. M. Shannon. Light degradation and voltage drift in polymer light-emitting diodes. *Applied Physics Letters*, 78(11):1619, 2001.

[56] J. H. Lee, Ji. Huang, C. C. Liao, P. J. Hu, and Y. Chang. Operation lifetimes of organic light-emitting devices with different layer structures. *Chemical Physics Letters*, 402:335–339, 2005.

[57] Y. B. Lim, D. H. Yoon, H. H. Kim, D. J. Kim, J. A. Choi, J. M. Kim, D. S. Hwang, Y. J. Lee, and S. H. Jeong. Physical mechanism responsible for degradation of organic light-emitting diodes. *Microelectronic Engineering*, 129:21–23, 2014.

[58] Z. D. Popovic, H. Aziz, N. X. Hu, A. Ioannidis, and P. N. M. Dos Anjos. Simultaneous electroluminescence and photoluminescence aging studies of tris(8-hydroxyquinoline) aluminum-based organic light-emitting devices. *Journal of Applied Physics*, 89(2001):4673–4675, 2001.

[59] H. Aziz. Degradation Mechanism of Small Molecule-Based Organic Light-Emitting Devices. *Science*, 283(5409):1900–1902, 1999.

[60] Z. D. Popovic, H. Aziz, A. Ioannidis, N. X. Hu, and P. N. M. Dos Anjos. Time-resolved fluorescence studies of degradation in tris(8-hydroxyquinoline) aluminum (AlQ3)-based organic light emitting devices (OLEDs). *Synthetic Metals*, 123:179–181, 2001.

[61] H. Becker, H. Spreitzer, and W. Kreuder. Soluble PPVs with enhanced performance - a mechanistic approach. *Advanced Materials*, 12(1):42–48, 2000.

[62] H. Becker, H. Spreitzer, K. Ibrom, and W. Kreuder. New Insights into the Microstructure of GILCH- Polymerized PPVs. *Macromolecules*, 32:4925–4932, 1999.

[63] A. Fleissner, K. Stegmaier, C. Melzer, H. Von Seggern, T. Schwalm, and M. Rehahn. Residual halide groups in gilch-polymerized poly(p-phenylene-vinylene) and their impact on performance and lifetime of organic light-Emitting Diodes. *Chemistry of Materials*, 21(9):4288–4298, 2009.

[64] K. Stegmaier. *Elektrische Ermüdung polymerbasierter organischer Leuchtdioden*. Dissertation, Technische Universität Darmstadt, 2011.

[65] F. J. J. Janssen, L. J. van Ijzendoorn, A. W. Denier van der Gon, M. J. A. de Voigt, and H. H. Brongersma. Interface formation between metal and poly-dialkoxy-p-phenylene vinylene. *Physical Review B*, 70(October):1–11, 2004.

[66] S. T. Lee, Z. Q. Gao, and L. S. Hung. Metal diffusion from electrodes in organic light-emitting diodes. *Applied Physics Letters*, 75(1999):1404–1406, 1999.

[67] M. P. de Jong, D. P. L. Simons, M. A. Reijme, L. J. van Ijzendoorn, A. W. Denier van der Gon, M. J. A. de Voigt, H. H. Brongersma, and R. W. Gymer. Indium diffusion in model polymer light-emitting diodes. *Synthetic Metals*, 110:1–6, 2000.

[68] A. Elschner, F. Bruder, H.-W. Heuer, F. Jonas, A. Karbach, S. Kirchmeyer, S. Thurm, and R. Wehrmann. PEDT / PSS for efficient hole-injection in hybrid organic light-emitting diodes. *Synthetic Metals*, 111-112:139–143, 2000.

[69] J. S. Kim, P. K H Ho, C. E. Murphy, N. Baynes, and R. H. Friend. Nature of non-emissive black spots in polymer light-emitting diodes by in-situ micro-raman spectroscopy. *Advanced Materials*, 14(3):206–209, 2002.

[70] M. M. Murray and A. B. Holmes. Poly(arylene vinylene)s - Synthesis and Applications. In G. Hadziioannou and P. F. van Hutten, editors, *Semiconducting Polymers*. Wiley-VCH, Weinheim, 2000.

[71] H. G Gilch and W. L Wheelwright. Polymerization of α-halogenated p-xylenes with base. *Journal of Polymer Science Part A - Polymer Chemistry*, 4(6):1337–1349, 1966.

[72] N. Vilbrandt. *Poly(p-phenylen vinylen)e nach Gilch - Konstitutions- und Morphologieeinflüsse auf die Emissionsfarbe und das Ermüdungsverhalten in organischen LEDs*. Dissertation, Technische Universität Darmstadt, 2013.

[73] H. L. Chou, K. F. U. Lin, and Y. L. Fan. Enhancing quantum efficiency of MEH-PPV through the reduction of chain aggregations by thermal treatments. *Journal of Polymer Science, Part B: Polymer Physics*, 43(13):1705–1711, 2005.

[74] Z. E. Lampert, C. L. Reynolds, J. M. Papanikolas, and M. O. Aboelfotoh. Controlling morphology and chain aggregation in semiconducting conjugated polymers: The role of solvent on optical gain in MEH-PPV. *Journal of Physical Chemistry B*, 116(42):12835–12841, 2012.

[75] D. B. Papkovsky, G. V. Ponomarev, W. Trettnak, and P. O'Leary. Phosphorescent Complexes of Porphyrin Ketones: Optical Properties and Application to Oxygen Sensing. *Analytical Chemistry*, 67(22):4112–4117, 1995.

[76] M. Gouterman. Optical Spectra and Electronic Structure of Porphyrins and Related Rings. In David Dolphin, editor, *The Porphyrins, Volume III: Physical Chemistry, Part A*, chapter 1, page 12. Academic Press, New York, 1978.

[77] A. J. Mäkinen, I. G. Hill, and Z. H. Kafafi. Vacuum level alignment in organic guest-host systems. *Journal of Applied Physics*, 92(3):1598–1603, 2002.

[78] D. Hertel and K. Meerholz. Triplet-polaron quenching in conjugated polymers. *The Journal of Physical Chemistry B*, 111(42):12075–80, 2007.

[79] V. Cleave, G. Yahioglu, P. Le Barny, D.-H. Hwang, A. B. Holmes, and R. H. Friend. Transfer Processes in Semiconducting Polymer-Porphyrin Blends. *Advanced Materials*, 4095(1):44–47, 2001.

[80] K. Sugiyama, H. Ishii, Y. Ouchi, and K. Seki. Dependence of indium-tin-oxide work function on surface cleaning method as studied by ultraviolet and x-ray photoemission spectroscopies. *Journal of Applied Physics*, 87(1):295, 2000.

[81] T. M. Brown, J. S. Kim, R. H. Friend, F. Cacialli, R. Daik, and W. J. W. Feast. Built-in field electroabsorption spectroscopy of polymer light-emitting diodes incorporating a doped poly(3,4-ethylene dioxythiophene) hole injection layer. *Applied Physics Letters*, 1679(1999):1997–2000, 1999.

[82] Heraeus. Clevios P VP AI 4083 data sheet, 2014.

[83] R. L. Wells and T. Fort. Adsorption of water on clean gold by measurement of work function changes. *Surface Science*, 32:554–560, 1972.

[84] A. Wan, J. Hwang, F. Amy, and A. Kahn. Impact of electrode contamination on the a-NPD/Au hole injection barrier. *Organic Electronics*, 6(1):47–54, 2005.

[85] P. A. Anderson. Work function of gold. *Physical Review*, 115(3):553–554, 1959.

[86] J. Hwang, A. Wan, and A. Kahn. Energetics of metal-organic interfaces: New experiments and assessment of the field. *Materials Science and Engineering R*, 64:1–31, 2009.

[87] T. M. Brown, R. H. Friend, I. S. Millard, D. J. Lacey, T. Butler, J. H. Burroughes, and F. Cacialli. Electronic line-up in light-emitting diodes with alkali-halide/metal cathodes. *Journal of Applied Physics*, 93(10):6159, 2003.

[88] G. Juška, K. Arlauskas, M. Viliunas, and J. Kočka. Extraction current transients: new method of study of charge transport in microcrystalline silicon. *Physical Review Letters*, 84(21):4946–9, 2000.

[89] G. Juška, K. Arlauskas, M. Viliunas, K. Genevičius, R. Österbacka, and H. Stubb. Charge transport in -conjugated polymers from extraction current transients. *Physical Review B*, 62(24):235–238, 2000.

[90] G. Juška, N. Nekrašas, K. Genevičius, J. Stuchlik, and J. Kočka. Relaxation of photoexited charge carrier concentration and mobility in μc-Si:H. *Thin Solid Films*, 451-452:290–293, 2004.

[91] A. J. Mozer, N. Serdar Sariciftci, L. Lutsen, D. Vanderzande, R. Österbacka, M. Westerling, and G. Juška. Charge transport and recombination in bulk heterojunction solar cells studied by the photoinduced charge extraction in linearly increasing voltage technique. *Applied Physics Letters*, 86(11):112104, 2005.

[92] A. J. Mozer, G. Dennler, N. S. Sariciftci, M. Westerling, A. Pivrikas, R. Österbacka, and G. Juška. Time-dependent mobility and recombination of the photoinduced charge carriers in conjugated polymer/fullerene bulk heterojunction solar cells. *Physical Review B*, 72(3):1–10, 2005.

[93] S. Bange. *Transient Optical and Electrical Effects in Polymeric Semiconductors*. Dissertation, University of Potsdam, 2009.

[94] S. Sandén, O. Sandberg, Q. Xu, J.-H. Smått, G. Juška, M. Lindén, and R. Österbacka. Effect of a large hole reservoir on the charge transport in TiO2/organic hybrid devices. *Physical chemistry chemical physics : PCCP*, 14(41):14186–9, 2012.

[95] A. Pivrikas, N. S. Sariciftci, G. Juška, and R. Österbacka. A Review of Charge Transport and Recombination in Polymer/Fullerene Organic Solar Cells. *Progress in Photovoltaics: Research and Applications*, 15:677–696, 2007.

[96] R. Österbacka, A. Pivrikas, G. Juška, K. Genevičius, K. Arlauskas, and H. Stubb. Mobility and density relaxation of photogenerated charge carriers in organic materials. *Current Applied Physics*, 4(5):534–538, 2004.

[97] B. Homa, M. Andersson, and O. Inganäs. Photogenerated charge carrier transport and recombination in polyfluorene/fullerene bilayer and blend photovoltaic devices. *Organic Electronics*, 10(3):501–505, 2009.

[98] G. Juška, N. Nekrašas, V. Valentinavičius, P. Meredith, and A. Pivrikas. Extraction of photogenerated charge carriers by linearly increasing voltage in the case of Langevin recombination. *Physical Review B*, 84:1–5, 2011.

[99] A. Pivrikas, M. Ullah, H. Sitter, and N. S. Sariciftci. Electric field dependent activation energy of electron transport in fullerene diodes and field effect transistors: Gill's law. *Applied Physics Letters*, 98:10–12, 2011.

[100] H. Tajima, T. Suzuki, and M. Kimata. Direct determination of trap density function based on the photoinduced charge carrier extraction technique. *Organic Electronics*, 13(11):2272–2280, 2012.

[101] Xi. Qi and S. R. Forrest. Thermal analysis of high intensity organic light-emitting diodes based on a transmission matrix approach. *Journal of Applied Physics*, 110(12), 2011.

[102] K.J. Bergemann, R. Krasny, and S. R. Forrest. Thermal properties of organic light-emitting diodes. *Organic Electronics*, 13(9):1565–1568, 2012.

[103] I. R. de Moraes, S. Scholz, B. Lüssem, and K. Leo. Analysis of chemical degradation mechanism within sky blue phosphorescent organic light emitting diodes by laser-desorption/ionization time-of-flight mass spectrometry. *Organic Electronics*, 12(2):341–347, 2011.

[104] Z. D. Popovic, S. Xie, N. Hu, A. Hor, D. Fork, G. Anderson, and C. Tripp. Life extension of organic LED's by doping of a hole transport layer. *Thin Solid Films*, 363(1):6–8, 2000.

[105] C. Feery, B. Racine, D. Vaufrey, H. Doyeux, and S. Cinaa. Physical mechanism responsible for the stretched exponential decay behavior of aging organic light-emitting diodes. *Applied Physics Letters*, 87(21):213502, 2005.

[106] A. Pivrikas, P. Stadler, H. Neugebauer, and N. S. Sariciftci. Substituting the postproduction treatment for bulk-heterojunction solar cells using chemical additives. *Organic Electronics*, 9(5):775–782, 2008.

[107] O. Sandberg, M. Nyman, and R. Österbacka. Direct determination of doping concentration and built-in voltage from extraction current transients. *Organic Electronics*, 15(11):3413–3420, 2014.

[108] A. Armin, G. Juska, B. W. Philippa, P. L. Burn, P. Meredith, R. D. White, and A. Pivrikas. Doping-induced screening of the built-in-field in organic solar cells: Effect on charge transport and recombination. *Advanced Energy Materials*, 3(3):321–327, 2013.

[109] J. Schafferhans, A. Baumann, A. Wagenpfahl, C. Deibel, and V. Dyakonov. Oxygen doping of P3HT:PCBM blends: Influence on trap states, charge carrier mobility and solar cell performance. *Organic Electronics*, 11(10):1693–1700, 2010.

[110] A. Seemann, T. Sauermann, C. Lungenschmied, O. Armbruster, S. Bauer, H. J. Egelhaaf, and J. Hauch. Reversible and irreversible degradation of organic solar cell performance by oxygen. *Solar Energy*, 85(6):1238–1249, 2011.

[111] M. Nyman, F. Pettersson, and R. Österbacka. Origin of equilibrium charges in poly(3-hexylthiophene):[6,6]-phenyl-C61-butyric acid methyl ester solar cell devices. *Chemical Physics*, 404:60–63, 2012.

[112] D. J. Coutinho, G. C. Faria, R. M. Faria, and H. Von Seggern. Dynamics of energy level alignment at ITO/rr-P3HT interface studied by CELIV, 2015.

[113] H. T. Nicolai, M. M. Mandoc, and P. W. M. Blom. Electron traps in semiconducting polymers: Exponential versus Gaussian trap distribution. *Physical Review B*, 83(19):1–5, 2011.

[114] H. T. Nicolai, M. Kuik, G. A. H. Wetzelaer, B. de Boer, C. Campbell, C. Risko, J. L. Brédas, and P. W. M. Blom. Unification of trap-limited electron transport in semiconducting polymers. *Nature Materials*, 11(10):882–887, 2012.

[115] H. C. F. Martens, J. N. Huiberts, and P. W. M. Blom. Simultaneous measurement of electron and hole mobilities in polymer light-emitting diodes. *Applied Physics Letters*, 77(12):1852, 2000.

[116] A. Baumann. *Charge Transport and Recombination Dynamics in Organic Bulk Heterojunction Solar Cells*. Dissertation, Julius-Maximillians-Universität Würzburg, 2011.

[117] L. A. Kehrer, S. Winter, R. Fischer, C. Melzer, and H. Von Seggern. Temporal and thermal properties of optically induced instabilities in P3HT field-effect transistors. *Synthetic Metals*, 161(23-24):2558–2561, 2012.

[118] M. S. A. Abdou, F. P. Orfino, Y. Son, and S. Holdcroft. Interaction of oxygen with conjugated polymers: Charge transfer complex formation with poly(3-alkylthiophenes). *Journal of the American Chemical Society*, 119(7):4518–4524, 1997.

[119] E. J. Meijer, C. Detcheverry, P. J. Baesjou, E. van Veenendaal, D. M. de Leeuw, and T. M. Klapwijk. Dopant density determination in disordered organic field-effect transistors. *Journal of Applied Physics*, 93(8):4831, 2003.

[120] D. G. J. Sutherland, J. a. Carlisle, P. Elliker, G. Fox, T. W. Hagler, I. Jimenez, H. W. Lee, K. Pakbaz, L. J. Terminello, S. C. Williams, F. J. Himpsel, D. K. Shuh, W. M. Tong, J. J. Jia, T. a. Callcott, and D. L. Ederer. Photo-oxidation of electroluminescent polymers studied by core-level photoabsorption spectroscopy. *Applied Physics Letters*, 68(15):2046, 1996.

[121] V. Kažukauskas, H. Tzeng, and S. A. Chen. Trap levels and effect of oxygen in poly[2-methoxy-5-(2- ethyl-hexyloxy)-1,4-phenylene vinylene] diodes. *Applied Physics Letters*, 80(11):2017–2019, 2002.

[122] L. Ma, X. Wang, B. Wang, J. Chen, J. Wang, K. Huang, B. Zhang, Y. Cao, Z. Han, S. Qian, and S. Yao. Photooxidative degradation mechanism of model compounds of poly (p-phenylenevinylenes) [PPVs]. *Chemical Physics*, 285:85–94, 2002.

[123] H.Y. Low. Photo and photo-oxidative degradations of poly(phenylene vinylene) derivatives. *Thin Solid Films*, 413(1-2):160–166, 2002.

[124] F. Papadimitrakopoulos, M. Yan, L. J. Rothberg, H. E. Katz, E. A. Chandross, and M. E. Galvin. Thermal and Photochemical Origin of Carbonyl Group Defects in Poly-(P -Phenylenevinylene). *Molecular Crystals and Liquid Crystals Science and Technology. Section A. Molecular Crystals and Liquid Crystals*, 256(1):663–669, 1994.

[125] Lewis J. Rothberg and Andrew J. Lovinger. Status of and prospects for organic electroluminescence. *Journal of Materials Research*, 11(12):3174–3187, jan 2011.

[126] D. Y. Kondakov, T. D. Pawlik, T. K. Hatwar, and J. P. Spindler. Triplet annihilation exceeding spin statistical limit in highly efficient fluorescent organic light-emitting diodes. *Journal of Applied Physics*, 106(12):124510, 2009.

[127] Y. Cao, I. D. Parker, G. Yu, and C. Zhang. Improved quantum efficiency for electroluminescence in semiconducting polymers. *Nature*, 397:414–417, 1999.

[128] P. K. H. Ho, J.-S. S. Kim, J. H. Burroughes, H. Becker, S. F. Y. Li, T. M. Brown, F. Cacialli, and R. H. Friend. Molecular-scale interface engineering for polymer light-emitting diodes. *Nature*, 404:481–4, 2000.

[129] J. S. Wilson, A. S. Dhoot, A. J. A. B. Seeley, M. S. Khan, A. Köhler, and Richard H. Friend. Spin-dependent exciton formation in p-conjugated compounds. *Nature*, 413(October):828–831, 2001.

[130] M. Wohlgenannt, K. Tandon, S. Mazumdar, S. Ramasesha, and Z. V. Vardeny. Formation cross-sections of singlet and triplet excitons in pi-conjugated polymers. *Nature*, 409(6819):494–497, 2001.

[131] A. S. Dhoot, D. S. Ginger, D. Beljonne, Z. Shuai, and N.C. C. Greenham. Triplet formation and decay in conjugated polymer devices. *Chemical Physics Letters*, 360(3-4):195–201, 2002.

[132] A. Köhler, J. S. Wilson, and R. H. Friend. Fluorescence and Phosphorescence in Organic Materials. *Advanced Engineering Materials*, 4(7):453–459, 2002.

[133] M. A. Baldo, D. F. O'Brien, Y. You, A. Shoustikov, S. Sibley, M. E. Thompson, and S. R. Forrest. Highly efficient phosphorescent emission from organic electroluminescent devices. *Nature*, 395:151–154, 1998.

[134] Y. Zhang, J. Lee, and S. R. Forrest. Tenfold increase in the lifetime of blue phosphorescent organic light-emitting diodes. *Nature Communications*, 5:5008, 2014.

[135] A. Köhler and H. Bässler. Triplet states in organic semiconductors. *Materials Science and Engineering R: Reports*, 66(4-6):71–109, 2009.

[136] B. Minaev, G. Baryshnikov, and H. Agren. Principles of phosphorescent organic light emitting devices. *Physical Chemistry Chemical Physics*, 16(5):1719–58, 2014.

[137] A. Köhler and H. Bässler. What controls triplet exciton transfer in organic semiconductors? *Journal of Materials Chemistry*, 21(12):4003, 2011.

[138] L. Lin, H. Meng, J. Shy, S. Horng, L. Yu, C. Chen, H. Liaw, C. Huang, K. Peng, and S. Chen. Triplet-to-Singlet Exciton Formation in poly(p-phenylene-vinylene) Light-Emitting Diodes. *Physical Review Letters*, 90(3):3–6, 2003.

[139] H. Liao, H. Meng, S. Horng, J. Shy, K. Chen, and C. Hsu. Triplet exciton formation and decay in polyfluorene light-emitting diodes. *Physical Review B*, 72(11):113203, 2005.

[140] S. M. King, M. Cass, M. Pintani, C. Coward, F. B. Dias, A. P. Monkman, and M. Roberts. The contribution of triplet-triplet annihilation to the lifetime and efficiency of fluorescent polymer organic light emitting diodes. *Journal of Applied Physics*, 109(7):074502, 2011.

[141] Y. Zhang and S. R. Forrest. Triplets Contribute to Both an Increase and Loss in Fluorescent Yield in Organic Light Emitting Diodes. *Physical Review Letters*, 108(26):1–5, 2012.

[142] A. Endo, K. Sato, K. Yoshimura, T. Kai, A. Kawada, H. Miyazaki, and C. Adachi. Efficient up-conversion of triplet excitons into a singlet state and its application for organic light emitting diodes. *Applied Physics Letters*, 98(8):083302, 2011.

[143] K. Goushi, K. Yoshida, K. Sato, and C. Adachi. Organic light-emitting diodes employing efficient reverse intersystem crossing for triplet-to-singlet state conversion. *Nature Photonics*, 6(4):253–258, 2012.

[144] K. Stegmaier, A. Fleissner, H. Janning, S. Yampolskii, C. Melzer, and H. von Seggern. Influence of electrical fatigue on hole transport in poly(p-phenylenevinylene)-based organic light-emitting diodes. *Journal of Applied Physics*, 110(3):034507, 2011.

[145] F. Laquai, C. Im, A. Kadashchuk, and H. Bässler. Sensitized intrinsic phosphorescence from a poly(phenylene-vinylene) derivative. *Chemical Physics Letters*, 375(3-4):286–291, 2003.

[146] A. Köhler and D. Beljonne. The Singlet-Triplet Exchange Energy in Conjugated Polymers. *Advanced Functional Materials*, 14(1):11–18, 2004.

[147] M. A. Baldo, M. E. Thompson, and S. R. Forrest. Phosphorescent materials for application to organic light emitting devices. *Pure Applied Chemistry*, 71(11):2095–2106, 1999.

[148] E. List, C.-H. Kim, A. Naik, U. Scherf, G. Leising, W. Graupner, and J. Shinar. Interaction of singlet excitons with polarons in wide band-gap organic semiconductors: A quantitative study. *Physical Review B*, 64(15):155204, 2001.

[149] M. Wohlgenannt, W. Graupner, G. Leising, and Z. V. Vardeny. Photogeneration and recombination processes of neutral and charged excitations in films of a ladder-type poly(paraphenylene). *Physical Review B*, 60(8):5321–5330, 1999.

[150] N. F. Colaneri, D. D. C. Bradley, R. H. Friend, P. L. Burns, A. B. Holmes, and C. W. Spangler. Photoexcited states in poly (p-phenylene vinylene): Comparison with trans, trans-distyrylbenzene, a model oligomer. *Physical Review B*, 42(18):670–681, 1990.

[151] W. Graupner, S. Eder, K. Petritsch, G. Leising, and U. Scherf. Origin and Stabilization of Photoexcitations in Conjugated Polymers. *Synthetic Metals*, 84:507–510, 1997.

[152] G. Zerza, M. C. Scharber, C. J. Brabec, N. S. Sariciftci, R. Gómez, L. Segura, N. Martin, and V. I. Srdanov. Photoinduced Charge Transfer between Tetracyano-Anthraquino-Dimethane Derivatives and Conjugated Polymers for Photovoltaics. *J. Phys. Chem A*, 104:8315–8322, 2000.

[153] R. A. J. Janssen, M. P. T. Christiaans, C. Hare, N. Martin, N. S. Sariciftci, A. J. Heeger, and F. Wudl. Photoinduced electron transfer reactions in mixed films of π-conjugated polymers and a homologous series of tetracyano-p-quinodimethane derivatives. *The Journal of Chemical Physics*, 103(20):8840, 1995.

[154] X. Wei, Z. Vardeny, N. S. Sariciftci, and A. J. Heeger. Absorption-detected magnetic-resonance studies of photoexcitations in conjugated-polymer/C60 composites. *Physical Review B*, 53(5):2187–2190, 1996.

[155] H. D. Burrows, J. Seixas de Melo, C. Serpa, L. G. Arnaut, A. P. Monkman, I. Hamblett, and S. Navaratnam. S1->T1 intersystem crossing in π-conjugated organic polymers. *The Journal of Chemical Physics*, 115(20):9601, 2001.

[156] P. F. Barbara, A. J. Gesquiere, Y. J. Lee, and J. Yu. Single molecule modulation spectroscopy of conjugated polymers. *Accounts of Chemical Research*, 38(7):602–610, 2005.

[157] I. D. Parker, Y. Cao, and C. Y. Yang. Lifetime and degradation effects in polymer light-emitting diodes. *Journal of Applied Physics*, 85(4):2441, 1999.

[158] L. Ke, P. Chen, and S. J. Chua. Photoluminescence degradation in organic light-emitting devices. *Applied Physics Letters*, 80(4):697, 2002.

[159] E. Aharon, S. Breuer, F. Jaiser, A. Köhler, and G. L. Frey. Effect of the solvent on the conformation of isolated MEH-PPV chains intercalated into SnS2. *ChemPhysChem*, 9(10):1430–1436, 2008.

[160] Y. Yi, J. E. Lyon, M. M. Beerbom, and R. Schlaf. Orbital alignment at poly[2-methoxy-5-(2'-ethylhexyloxy)-p-phenylene vinylene interfaces. *Journal of Applied Physics*, 102(2):023710, 2007.

[161] X. Yang and D. Neher. Polymer Electrophosphorescence Devices. In K. Müllen and U. Scherf, editors, *Organic Light-Emitting Devices: Synthesis, Properties and Applications*, chapter 11. Wiley-VCH, Weinheim, 2006.

[162] C. A. Amorim, M. R. Cavallari, G. Santos, F. J. Fonseca, A. M. Andrade, and S. Mergulhão. Determination of carrier mobility in MEH-PPV thin-films by stationary and transient current techniques. *Journal of Non-Crystalline Solids*, 358(3):484–491, 2012.

[163] F. Huang and A. K.-Y. Jen. Materials and Interface Engineering in Organic Light-Emitting Diodes. In F. So, editor, *Organic Electronics: Materials, Processing, Devices and Applications*. CRC Press, 2009.

[164] P. W. M. Blom, M. J. M. de Jong, and J. J. M. Vleggaar. Electron and hole transport in poly(p-phenylene vinylene) devices. *Applied Physics Letters*, 68(23):3308, 1996.

[165] S. V. Yampolskii, Y. A. Genenko, C. Melzer, K. Stegmaier, and H. Von Seggern. Bipolar charge-carrier injection in semiconductor/insulator/conductor heterostructures: Self-consistent consideration. *Journal of Applied Physics*, 104(2008), 2008.

[166] H. Heil, J. Steiger, S. Karg, M. Gastel, H. Ortner, H. von Seggern, and M. Stoì^ßel. Mechanisms of injection enhancement in organic light-emitting diodes through an Al/LiF electrode. *Journal of Applied Physics*, 89(1):420, 2001.

[167] H. Antoniadis, M. A. Abkowitz, and B. R. Hsieh. Carrier deep-trapping mobility-lifetime products in poly(p-phenylene vinylene). *Applied Physics Letters*, 65(16):2030, 1994.

[168] J. C. Scott, J. H. Kaufman, P. J. Brock, R. DiPietro, J. Salem, and J. a. Goitia. Degradation and failure of MEH-PPV light-emitting diodes. *Journal of Applied Physics*, 79(5):2745, 1996.

[169] A. A. Zakhidov, S. Reineke, B. Lüssem, and K. Leo. Hydrofluoroethers as heat-transfer fluids for OLEDs: Operational range, stability, and efficiency improvement. *Organic Electronics: physics, materials, applications*, 13(3):356–360, 2012.

[170] P. R. F. Rocha, H. L. Gomes, K. Asadi, I. Katsouras, B. Bory, F. Verbakel, P. van de Weijer, D. M. de Leeuw, and S. C. J. Meskers. Sudden death of organic light-emitting diodes. *Organic Electronics*, 20:89–96, 2015.

[171] C. Gärditz, A. Winnacker, F. Schindler, and R. Paetzold. Impact of Joule heating on the brightness homogeneity of organic light emitting devices. *Applied Physics Letters*, 90(10):103506, 2007.

[172] J. R. Sheats, H. Antoniadis, M. Hueschen, W. Leonard, J. Miller, R. Moon, D. Roitman, and A. Stocking. Organic electroluminescent devices. *Science*, 273:884–888, 1996.

[173] X. Zhou, J. He, L. S. Liao, M. Lu, X. M. Ding, X. Y. Hou, X. M. Zhang, X. Q. He, and S. T. Lee. Real-Time Observation of Temperature Rise and Thermal Breakdown Processes in Organic LEDs Using an IR Imaging and Analysis System. *Advanced Materials*, 12(4):265–269, 2000.

[174] R. F. Cossiello and L. Akcelrud. Solvent and Molecular Weight Effects on Fluorescence Emission of MEH-PPV. *Journal of Brazilian Chemical Society*, 16(1):74–86, 2005.

[175] T.-W. Lee and O O. Park. The Effect of Different Heat Treatments on the Luminescence Efficiency of Polymer Light-Emitting Diodes. *Advanced Materials*, 12(11):801–804, 2000.

[176] Y. Liu, M. S. Liu, X.-C. Li, and A. K-.Y. Jen. Synthesis and Characterization of a Novel Light-Emitting Polymer Containing Highly Efficient Hole-Transporting Aromatic Diamine attracted much attention for their potential applications ported in the literature as potential candidates for poly- meric ligh. *Chemistry of Materials*, 95:3301–3304, 1998.

[177] Xiaoniu Yang, Jeroen K. J. van Duren, René A. J. Janssen, Matthias A. J. Michels, and Joachim Loos. Morphology and Thermal Stability of the Active Layer in Poly(p-phenylenevinylene) / Methanofullerene Plastic Photovoltaic Devices. *Macromolecules*, 37(6):2151–2158, mar 2004.

[178] S. Y. Ni, X. R. Wang, Y. Z. Wu, H. Y. Chen, W. Q. Zhu, X. Y. Jiang, Z. L. Zhang, and R. G. Sun. Decay mechanisms of a blue organic light emitting diode. *Applied Physics Letters*, 85(6):878, 2004.

[179] G. Juška, N. Nekrašas, K. Arlauskas, J. Stuchlik, A. Fejfar, and J. Kočka. Photogenerated carriers in μc-Si:H/a-Si:H multi-layers. *Journal of Non-Crystalline Solids*, 338-340:353–356, 2004.

Curriculum Vitae

Personal details

Name	Oili Johanna Pekkola

Schooling

1991 - 1997	Rajamäen ala-aste, Rajamäki, Finnland
1997 - 2000	Rajamäen yläaste, Rajamäki, Finnland
2000 - 2003	Hyvinkään yhteiskoulun lukio, Hyvinkää, Finland

University education

2003 - 2010	Master of Science (Technology), Major Subject: Chemistry. Environmental and Energy Engineering Degree Programme, Tampere University of Technology, Tampere, Finland
2007 - 2008	Exchange student, Technische Universität Darmstadt.
2009 - 2010	Masters Thesis: *The Influence of Molecular Doping on Organic Semiconductor Interfaces: A Synchrotron Induced Photoemiddion Study*. Surface Science Division, Faculty of Materials Science, Technische Universität Darmstadt.
2011 - 2015	Doctorate candidate. Electronic Materials Division, Faculty of Materials Science, Technische Universität Darmstadt.

Publications

P. Vivo, A. S. Alekseev, K. Kaunisto, O. Pekkola, A. Tolkki, V. Chukarev, A. Efimov, P. Ihalainen, J. Peltonen, H. Lemmetyinen: *Photoinduced electron transfer in thin films of porphyrin-fullerene dyad and perylenetetracarboxiimide.* Physical Chemistry Chemical Physics 12 (2010) 12525-12532.

P. Vivo, K. Kaunisto, A. S. Alekseev, O. Pekkola, A. Tolkki, V. Chukarev, H. Lemmetyinen: *Vectorial photoinduced electron transfer in multicomponent film systems of poly(3-hexylthiophene), porpyrin-*

fullerene dyad, and perylenetetracarboxiimide. Photochemical and Photobiological Sciences 9 (2010) 1212-1217.

O. Pekkola, A. Gassmann, F. Etzold, F. Laquai, and H. von Seggern, *Influence of triplet excitons on the lifetime of polymer-based organic light-emitting diodes.* Phys. Status Solidi (A), 211(9), 2035-3029 (2014)

A. Gassmann, S. V. Yampolskii, A. Klein, K. Albe, N. Vilbrandt, O. Pekkola, Y. A. Genenko, M. Rehahn, and H. von Seggern, *Study of electrical fatigue by defect engineering in organic light-emitting diodes*. Materials Science and Engineering B, 192, 26-51 (2015)

Conference Contributions

O. Pekkola, A. Gassmann, F. Etzold, F. Laquai, and H. von Seggern
Influence of triplet excitons on the performance and lifetime of polymer-based organic light-emitting diodes
Spring meeting of the German Physical Society, Berlin 2012.

O. Pekkola, A. Gassmann, C. Melzer, and H. von Seggern
Influence of triplet excitons on the performance and lifetime of polymer-based organic light-emitting diodes
Materials Science Engineering, Darmstadt 2012.

O. Pekkola, A. Gassmann, C. Melzer, and H. von Seggern:
Influence of triplet excitons on the performance and lifetime of polymer-based organic light-emitting diodes
Spring meeting of the German Physical Society, Regensburg 2013.

O. Pekkola, A. Gassmann, and H. von Seggern:
Influence of triplet excitons on the lifetime of polymer-based organic light-emitting diodes
6^{th} International Symposium on Flexible Organic Electronics (ISFOE13), Thessaloniki, Greece 2013.

O. Pekkola, A. Gassmann, and H. von Seggern:
The harmful influence of triplet excitons on the lifetime of polymer light-emitting diodes
International Symposium on Electrical Fatigue in Functional Materials, Sellin 2014.

Acknowledgements

First of all, I am very grateful to Prof. Dr. Heinz von Seggern for offering me the possibility to pursue a PhD in his group, for the interesting topic, the fruitful discussions and guidance.

I want to thank Prof. Dr. Matthias Rehahn for being the coreferee of this thesis as well as for the excellent cooperation within the SFB 595.

Dr. Andrea Gassmann deserves a huge thank-you for her help during this thesis, for the countless discussions we had and for giving me new ideas. Additionally, I'll always remember our cosy knitting evenings and of course the legendary ESC parties!

For the whole e-mat group: Thank you all for the excellent atmosphere, for the help one could always rely on, for the visits to Kuhle and, very importantly, for the yearly ESC spectacles. I could not have asked for a better group! In no particular order, thanks go to Paul, Riitta, Elmar, Benedikt, Dan, Lorenz, Eva, Tobi, Oli, Jörg, Corinna, Yogi and Christian. Our technicians Helga, Gabi, Berndt and Sabine deserve very special thanks for their help in the labs: you were always ready to help with all possible and impossible problems! Of course, big thanks go to my HiWis Stefan and Hans for your help in the lab. And the e-mat group cannot be mentioned without our Brazilian guests Manu, Lucas, Ivan and Juliana as well as Gabi, the best secretary one can imagine.

There are many people I want to thank for their scientific help: Dr. Nicole Vilbrandt for providing me with OC_3C_8-PPV and for the excellent cooperation within the SFB 595, Dr. Frédéric Laquai and Dr. Fabian Etzold for the PIA measurements and Dr. Stefan Flege for the SIMS measurements. This thesis was funded by the collaborative research center SFB 595, for which I am very grateful. Within the SFB I would especially like to thank Gila, the secretary, for organizing everything, and Mareike for the peer support and for sharing a room during various SFB-related trips.

I want to thank my family for the support they have given me and for encouraging me to make the choices that felt right for me. Finally, the most important people for the finalization of this thesis are my husband and my son. Thank you for being there for me and giving a meaning to all this! Rakastan teitä!